Modelling, control and analysis of moderate electric field in food processing

OLUWOLE-OJO, Oluwaloba

Modelling, Control and Analysis of Moderate Electric Field in Food Processing

Oluwaloba Oluwole-Ojo

A thesis submitted in partial fulfilment of the requirements of
Sheffield Hallam University
for the degree of Doctor of Philosophy

June 2023

Candidate Declaration

I hereby declare that:

1. I have not been enrolled for another award of the University, or other academic or professional organisation, whilst undertaking my research degree.

2. None of the material contained in the thesis has been used in any other submission for an academic award.

3. I am aware of and understand the University's policy on plagiarism and certify that this thesis is my own work. The use of all published or other sources of material consulted have been properly and fully acknowledged.

4. The work undertaken towards the thesis has been conducted in accordance with the SHU Principles of Integrity in Research and the SHU Research Ethics Policy.

5. The word count of the thesis is 28209.

Name	Oluwaloba Oluwole-ojo
Award	PhD
Date of Submission	June 2023
Faculty	Materials Engineering Research Institute (MERI)
Director(s) of Studies	Dr Hongwei Zhang

Abstract

Ohmic heating (OH) is a Moderate Electric Field (MEF) processing technique in which electric current is applied to food products. The food product acts as a resistor and heat is generated and dissipated within the food volumetrically. OH is a very energy-efficient form of heating compared to conventional methods such as conduction and convection. The advantages of OH include rapid heating, reduced food processing times, bacterial inactivation, electroporation, and elimination of unwanted temperature peaks. Compared to other conventional methods of food processing, ohmic heating is over 95% energy efficient and high in energy saving.

This research is majorly focused on the modelling, control and industrial application, and analysis of MEF in food processing. Firstly, the development of the batch ohmic heater model presents three distinct modelling approaches which are the first principle partial differential equation (PDE), lumped ordinary differential equation (ODE) model and regression models using system identification technique. The validation of the developed batch ohmic heater model is done using a commercially available batch ohmic heater and experimental data. Following this, collaboration with industrial partners and technicians led to the design and construction of a continuous flow ohmic heater (CFOH) pilot plant. Consequently, a novel approach to model the CFOH using the state space approach was developed. This work presents the quantitative results which demonstrate significant improvements in modelling the OH process with regard to food of varying conductivities, flow rates and initial temperatures.

The results from the model development led to the application of classical to advanced model-based process control which include Proportional, Integral and Derivative (PID) control, Model Predictive Control (MPC) and adaptive model predictive control on the continuous flow ohmic heater pilot plant. These controllers are implemented on the CFOH pilot plant from MATLAB using Open Platform Communications (OPC). With OPC, server and client protocol are used to exchange data in real-time between the Programmable Logic Controller (PLC) and a stand-alone lab-based computer so that simple and advanced model-based control (e.g., Model

Predictive Control) designed in MATLAB/Simulink can be applied on the continuous flow Ohmic Heater. This research demonstrates the following:

- model-based design and validation of OH in the food industry
- advantages of OH compared to conventional methods
- the benefits advanced process control compared to simple control in food engineering
- the technique of implementing advanced process control on a PLC based hardware.

Industrial heating trial of tomato basil sauce was carried out to present a case study for the pilot scale heating of tomato basil sauce with advanced process control with applications in the food industry. The performances and energy efficiencies of the different control techniques implemented are compared.

Acknowledgements

To God, the giver of life, my source and my all, you alone deserve the glory and honour. Thank you for daily loading me with benefits from the beginning of my existence through the course of the PhD, this very moment and beyond.

My sincere gratitude goes to my principal supervisor Dr Hongwei Zhang, whose immense support was always timely and invaluable. You took interest in my PhD and my career as a whole from the start, thank you for being a teacher and a mentor. Also to the rest of the supervision team, Dr Xu Xu thank you for being my guardian angel throughout my post graduate journey I couldn't have done this without you (literally!) and Prof Martin Howarth, thank you for your inputs, feedbacks and comments from the start of this PhD. Your contributions ensured that even when there were bottlenecks during this research journey, they were resolved and I made progress. Thank you.

To my fiancée – Erioluwa, thanks for your love, patience and understanding, even when it was difficult. Your presence gave me the resolve to overcome the challenges I faced. To my parents, thank you for your constant love and prayers. I could never reach this far without your support and encouragement. I am very grateful for the many sacrifices you made for me and I am so proud to be your son.

To the NCEFE team at Sheffield Hallam University, the staff in the Food Sciences department as well thank you for your support at various times during the course of this research. Special gratitude to Jonny Shepherd, thank you for all the technical support during experiments.

Publications

The work from the following publications produced during this PhD contribute to the content of the thesis as follows: (i) forms the basis of chapter 3, (ii) forms the basis of chapter 5. All papers are freely and legally available online at this time of writing, permission has been gained from the publishers to reuse content from these publications within this thesis, with appropriate referencing.

(i) Oluwole-Ojo, O., Zhang, H., Howarth, M., & Xu, X. (2021). Model based design and validation of a batch ohmic heating system. Modelling, 2 (4), 641-658. http://doi.org/10.3390/modelling2040034

(ii) Oluwole-Ojo, O.N., Zhang, H., Howarth, M., & Xu, X. (2023). Energy Consumption Analysis of a Continuous Flow Ohmic Heater with Advanced Process Controls. Energies, 16 (2). http://doi.org/10.3390/en16020868

The following are currently being prepared:

(i) Oluwole-Ojo, O., Zhang, H., Howarth, M., & Xu, X. (2023). Application of Advanced Process Control to a Continuous Flow Ohmic Heater: A case study of tomato basil sauce. Unpublished.

(ii) Oluwole-Ojo, O., Zhang, H., Howarth, M., & Xu, X. (2023). Model validation and real-time process control of a continuous flow ohmic heater. Unpublished.

Conference presentation

- International Congress on Engineering and Food (ICEF14) 2023 Poster: " Energy consumption of a continuous flow ohmic heater with advanced process controls"
- The European Federation of Food Science and Technology (EFFOST) 2022 Short-Presentation: "Model validation, design, implementation and real-time process control of a continuous flow ohmic heater"
- Conference of Food Engineering (CoFE) 2022 Short-Presentation: " Implementation of Advanced Real-time Process Control on a Continuous Flow Ohmic Heater"

Oral presentation

Oluwole-Ojo, O.N., Zhang, H., Howarth, M., & Xu, X. (2021). Model validation, design, implementation and real-time process control of a continuous flow ohmic heater. MERI seminar series. Sheffield Hallam University.

Posters

Oluwole-Ojo, O.N., Zhang, H., Howarth, M., & Xu, X. (2022). Model Based Design and Validation of a Batch Ohmic Heating System. Winter poster event. Sheffield Hallam University.

Oluwole-Ojo, O.N., Zhang, H., Howarth, M., & Xu, X. (2020). Modelling, Control and Analysis of Moderate Electric Field (MEF) in Food Processing. Winter poster event. Sheffield Hallam University.

Table of Contents

Chapter 1. Introduction

1.1 Background

Most food products consumers eat necessitate thermal processing for various purposes including ensuring safety by eliminating harmful microorganisms, preserving food by extending its shelf life, cooking food to improve its taste and texture, enhancing the nutritional value of certain food items, and inducing physical and chemical changes that can enhance the flavour, colour, and aroma of the food. The most common conventional thermal processing methods for food require heat energy to be generated externally and then transferred to food samples. This is done either by convection, radiation, or conduction heating. These conventional methods require excessive heat processing that can lead to the degradation of the outer portion of food substance especially when food substance is of a large size ratio (Zhao et al 2000).

In addition, the efficiency of the heat transfer mechanisms is limited by the rate of heat transfer from an external medium to the food and by the thermal conductivity of the food, which might result in over processed products due to the lengthy processing time required to reach the target temperature, unwanted temperature peaks, and compromised product quality (Goullieux and Pain, 2005).

Ohmic heating (OH) is a superior alternative to conventional heating methods. Compared to other conventional methods of food processing, OH is over 90% energy efficient and offers significant energy savings. This research outlines the efforts to model the OH process, implement advanced real-time process control on a continuous flow ohmic heater (CFOH) pilot plant and demonstrate substantial improvements in controlling the CFOH process regarding food materials and the industrial practicality of using the CFOH.

1.2 Motivation

While progress has been made in recent years, the food and drinks industry in the United Kingdom (U.K.) still relies heavily on low-energy efficiency processes based on fossil fuel energy sources, leading to high levels of CO2 emissions. In 2019, the U.K.'s food and drink sector accounted for 165 million tons of carbon emissions, contributing to approximately 17%

of the U.K.'s total carbon footprint (Food and drink federation, 2021). Consequently, one of the priorities is to reduce the cost of food processing and energy footprint, while striving to maintain or improve food product quality.

The author's focus on OH in food processing aligns with the Food and Drinks Federation (FDF)'s ambition for the food and drink sector to reach Net Zero emissions by 2040 (Food and drink federation, 2021). The direct application of electrical fields, harnessed from renewable resources, can enhance process sustainability. Furthermore, OH processes can lead to milder processing and reduced temperature peaks, resulting in higher food product quality. Since the energy efficiency of OH is over 90%, significant reduction in cost of energy would be achieved. Therefore, one motivation for this research is the necessity of OH in transitioning towards greener and more sustainable food processing methods.

Another motivation behind this research is the author's aspiration to apply advanced process control to the OH process. Automation of the OH process has proven more energy efficient compared to "human in the loop" processes. The task of heating food products in a CFOH presents several challenges such as changing electrical conductivity as the temperature increases, homogeneity, and heterogeneity of food products, variations in thermophysical properties of food with temperature, fluctuating infeed temperatures, and diverse desired output temperatures. The author's research into the application of advanced process control to OH led to the development of a model-based controller. This controller anticipates the changing dynamics of food products based on the validated model, rendering the OH process of different food products autonomous and energy efficient.

Studying at Sheffield Hallam University afforded the author the opportunity to learn from leading researcher in control and food engineering while conducting his research. The guidance received fuelled the author's desire to apply advanced process control and OH to practical industrial applications. While researching at the National Centre of Excellence for Food Engineering (NCEFE) at Sheffield Hallam University the author collaborated with industry partners, technicians, and researchers to design and build a CFOH pilot plant. This full-cycle process from conceptualisation to implementation broadened the author's knowledge of applying advanced process control to OH to address real-world challenges.

1.3 Research Aims and Objectives

The broad aims and contributions of this research centre around the application of ohmic heating - a technique of moderate electric field - and advanced process control to industrial food processing. This effort supports smart processing for 'Food system sustainability'. The objectives of this work can be categorised as follows:

1. Development and validation of a batch ohmic heater model.
    - This first objective involves developing a first principle PDE model, a lumped ODE model, and a regression model using system identification technique. These models were validated using experimental data from a commercially available batch ohmic heater.
2. Design and construction of a continuous flow ohmic heater (CFOH).
    - The next objective involves commissioning a pilot scale plant. The CFOH was designed and constructed in collaboration with industrial partners.
3. Model development and validation of the CFOH.
    - This entails the development of a mathematical model incorporating the state space representation of the CFOH. The developed model also integrates the mass flowrate of food products, electrical conductivity, infeed temperature and other thermo-physical properties of food.
4. Development and implementation of advanced process controller for the CFOH.
    - Firstly, a Proportional, Integral and Derivative (PID) controller was designed and implemented on the CFOH. The PID controller represents the most common classical control strategy and is widely used in the process industry.
    - With a validated model in hand, a Model Predictive Controller (MPC) was designed and implemented. The MPC controller represents a more advanced control strategy aimed at improving the performance of the CFOH. With the MPC developed and implemented, the performance of the CFOH is evaluated when process parameters, such as product's infeed electrical conductivity and inlet temperature, vary.
    - An Adaptive Model Predictive Controller (AMPC) was developed. The AMPC employs a dynamic optimisation function, unlike the MPC, which is fixed. The

performance of the AMPC is evaluated when critical process parameters in the OH process vary more rapidly.

5. Evaluation of the energy efficiency and performance of implemented controllers.
    - The performance of the different controllers is evaluated based on set criteria, such as the steady state error, rise time and temperature overshoots.
    - The energy consumption analysis of the CFOH under different controllers is evaluated. This is done to select the most energy efficient controller.
6. Conducting experimental trials and case studies.
    - To CFOH is utilised to conduct real-life experimental trials, such as the heating of tomato basil sauces, orange juice, and saline solutions. These experimental trials demonstrate the capability and practicality of the CFOH and the developed advanced controllers in real-world setting.

1.4 Contributions to the research field

The MEF models developed in this study are applicable to both the batch ohmic heater and the continuous flow ohmic heater. For the batch ohmic heater model, first principle PDE modelling, lumped ODE modelling, and system identification technique was employed. These models were subsequently validated with experimental data. As for the continuous flow ohmic heater model, a novel approach that combines physical modelling with state space determination was utilised. The resulting model of the CFOH was also experimentally validated.

In the implementation of advanced process control on the CFOH, a novel approach of communication between MATLAB/Simulink and the onboard Programmable Logic Controller (PLC) was achieved using Open Platform Communication (OPC) servers.

Furthermore, the PID, MPC and AMPC were developed and implemented on an onboard PLC-based hardware using MATLAB/Simulink. This work opens opportunities for the research community to apply this technique in implementing various advanced controllers.

1.5 Research challenges

The predominant issue lies in the dearth of scientific paper concerning continuous flow ohmic heater models and the energy analysis of the CFOH. While this research has contributed to progress in the development of CFOH models and energy efficiency analysis, the author advocates for increased scientific involvement. The major research challenges involve the modelling of time and temperature varying thermophysical properties during ohmic heating. These varying properties include varying input temperatures, mass flow rates and food electrical conductivity.

This research also presented a range of challenges that were addressed. These included:

- Design of time varying models of the batch ohmic heater and the continuous flow ohmic heater with different structure, electrode number and applied voltage.
- Model validation of state-space model of the continuous flow ohmic heater.
- Design of advanced controller specifications using model-in-the-loop technique
- Online estimation of the electrical conductivity of food product as a function of the output temperature.
- Implementing advanced process control on PLC-based hardware.
- Interfacing the MATLAB/Simulink environment with a Mitsubishi PLC.
- Performing real-time controller analysis and fine-tuning.
- Conducting online measurements of electrical conductivity.

1.6 Outline of thesis

This research is divided into seven chapters. The first chapter provides a brief introduction to the subject of ohmic heating, moderate electric field and advanced process control. It follows with an explanation of the author's motivations behind the research, the research aims and objectives, the contribution of this work and the research challenges. The chapter concludes with an outline of the thesis structures and a summary of the chapter.

Chapter 2 offers a comprehensive literature review on ohmic heating, moderate electric field, batch ohmic heater, continuous flow ohmic heater, and advanced process control, with their applications in the food industry. This section identifies the gaps existing in existing literature and how this thesis contributes to addressing these gaps.

Chapter 3 extends the published work by Oluwole-Ojo, Zhang, Howarth, & Xu. (2021), presenting the model-based design and validation of a batch ohmic heating system. This work develops first principle PDE models, lumped ODE models, and regression models for the MEF process, using COMSOL and MATLAB/Simulink software for simulations. A systematic approach is used to validate the developed models, with experimental data derived from a commercially available batch Ohmic heater. The chapter concludes with validation, analysis, and model comparison as well as an exploration of the effect of different critical process parameters of foods under a range of initial conditions.

In Chapter 4, the design and development of the CFOH are presented, along with a discussion of its hazards, and safety mechanisms. The layout of the CFOH and detailed descriptions of the ohmic heater's main components are also provided.

Chapter 5 extends the published work by Oluwole-Ojo, Zhang, Howarth, & Xu. (2023), presenting an analysis of the energy consumption of a continuous flow ohmic heater (CFOH) with advanced process controls for heating operations in the food and drinks industry. This study uses operational data from a CFOH pilot plant designed and constructed at NCEFE, Sheffield Hallam University, and shows significant energy savings compared with conventional heating methods. The analysis presented in this chapter describes the energy consumption of the CFOH and compares the efficiency of the CFOH when different advanced process control techniques are used. Experimental results and analysis demonstrate an energy efficiency conversion of at least 87.9%, which can be further increased by applying advanced controllers such as model predictive control (MPC) or adaptive model predictive control (AMPC).

Chapter 6 presents a case study of pilot scale heating of tomato basil sauce with advanced process control comparing the performance and energy efficiencies of different control techniques. It presents quantitative results that demonstrate significant improvements in controlling the CFOH process for different food materials, underscoring the industrial practicality of using the CFOH.

The final chapter provides general conclusions and discussions, as well as potential avenues for future work.

Chapter 2. Literature Review

2.1 Main Principles of ohmic heating

Ohmic heating (OH) is a moderate electric field (MEF) process in which the applied electric field is less than or equal to 1k V/cm which is considerably lower than the field strength used in the high voltage pulsed electric fields technology (PEF) (Sastry, 2008). OH involves the passing of electric current through food products, heat is generated within the food substance and dissipated directly in the medium with very high efficiency (>90%) by Joule effect, eliminating the heat-transfer step from the surroundings to the medium by means of temperature gradients or hot surfaces (Silva et al. 2017). Singh and Heldman (2009) explained that the collision of ions within the food substance creates resistance to their movement and increases their kinetic energy, thereby heat is produced. As a result, heat is generated instantly and volumetrically within the food substance due to the ionic motion. (Kumar 2018).

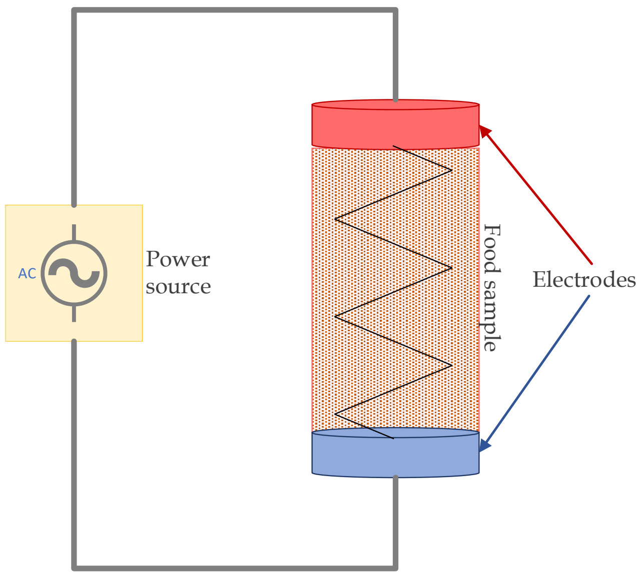

Figure 2.1. Schematic of the ohmic heating process

OH concept dates to the 18th century, James Prescott Joule discovered that heat is released when electric current is passed through a material, hence OH is also known as Joule heating (Kumar 2018). Industrial application of OH was implemented in the early 19th century in the sterilization of milk in a process tagged “electro pure”. (Kaur & Singh, 2015). Carbon electrodes and alternating current at 60 Hz were applied following that the process got approved in six

US states (Jaeger et al., 2016). However, due to the high cost of electricity and production cost, the industrial application of OH left the limelight. Also, due to the short supply of inert materials needed for electrodes the interest in the industrial application waned (Mizrahi et al 1975).

2.1.2 Ohmic heating vs Conventional heating vs other methods

Gavahian and Farahnaky (2018), describes the conventional heat treatment methods of radiation, convection, and conduction as the commonest, time consuming and energy wasting. These inefficiencies in conventional heating methods may present cold spots within the food leading to non-uniform heating or overheated food samples leading to burns. Jaeger et al., (2016) highlighted that these inefficiencies are significant in particulate and viscous foods. In contrast, ohmic heating heats up food samples volumetrically therefore rapid heating is achieved with high efficiency (Sastry, 2008). cappato et al, (2017) explains that the food material acts as a resistor in an ohmic process and converts electrical energy to thermal energy directly and quickly shortening the heating time.

Other heating methods apart from conventional heating methods are microwave heating and inductive heating. The figure below is adapted from Silva, Santos, Luis & Silva, (2017). It shows the different heating methods and their peculiarities. For microwave heating (MH), the heat within the food molecule is generated by the agitation of water molecules within the food (Chandra, 2011). Therefore, for MH heating the food substance must contain water molecule. Inductive heating (IH) in food processing is non-contact however, the heat generated from the ferromagnetic containing vessel is transferred to the food substance by conduction. The heat generated from IH is achieved when current is generated as a result of magnetic field across a ferromagnetic conductor resulting in joule effect. (El-Mashad & Pan 2017).

Conventional heating (CH)	Microwave heating (MH)	Inductive heating (IH)	Ohmic heating
		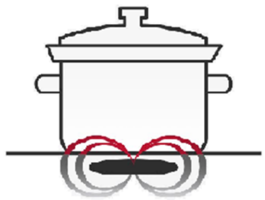	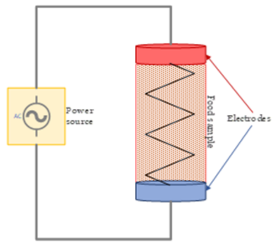
The energy is transferred through the walls of the reaction vessel and then dissipated into the reaction mixture.	Direct and internal absorption of microwave radiation by the molecules present in the reaction mixture.	Joule effect resulting from induced electric current in the medium. Continuous or alternating field.	Joule effect resulting from the passage of alternating electric current. Electrodes in contact with the medium.

Figure 2.2. Different heating methods and peculiarities (Silva, Santos, Luis, & Silva, 2017).

2.1.3 Advantages of ohmic heating

I. Different authors have presented rapid and volumetric heating of ohmic heating compared to other heating methods as its major advantage (Aydin, Kurt, & Kaya, 2020; Zell, Lyng, Cronin, & Morgan, 2010).

II. Marcotte (1999) explains that the simplicity of ohmic heating by comparing it to an electric circuit, that is comprised of a voltage source, current and resistance is an advantage. The food product between the electrode acts as the resistance.

III. Marcotte (1999) pointed out that unlike MW heating, there is no intermediate step in ohmic heating to convert electricity to microwaves or any other form of electromagnetic radiation through a magnetron. Hence a higher efficiency (Silva, Santos, Luis & Silva, 2017),

IV. Uniform heating is achieved within the food. (Sastry, 2008, Sofi'i, Arifin, & Oktafrina, 2022)

V. The heating process is quiet and less noisy due to the absence of moving mechanical parts.

VI. The heating depth of ohmic heating in foods is unlimited unlike microwave heating or other conventional methods (Marcotte, 1999).

VII. Heating system is scalable to account for batch process and continuous flow process.

VIII. Highly suited for industrial and domestic use (Varghese, Pandey, Radhakrishna, & Bawa, 2014).

2.1.4 Disadvantages of ohmic heating

The ohmic heater (OH) can be designed as a batch system or a continuous flow system. In the batch ohmic heating system, there is constant contact between a specific quantity of food sample and the electrodes during heating. For the continuous flow ohmic heater (CFOH), food products flow through the heating chamber where the electrodes are housed. For industrial applications that require long holding times during cooking such as evaporation, the batch ohmic heating system is used (Lima & Sastry, 1999). A drawback of the batch ohmic heating system observed by Maloney & Harrison (2016) is that without some form of mixing apparatus uneven heating of the food is observed. This uneven heating is termed thermal stratification. The CFOH has wider industrial applications compared to the batch and conventional heating systems because of the increased processing speed (Stirling, 1993). The general design of the CFOH which includes an infeed pump to transport the food and holding tubes to attain desired lethality adds to the complexity (Ruan, Ye, Chen, Doona, & Taub, 2001).

2.1.5 The commercialisation of ohmic heating

The examples of commissioned commercial ohmic heating units are shown below.

Table 2.1. Examples of commissioned commercial ohmic heating units.

Company	Year	Location	Power	Product functions
Sous Chef Ltd (H.J.Heinz division)	1989	UK	75KW	Prepared meals of meat and vegetables
Advanced Food Science (AFS) Land O' Lakes Minneapolis. IL	1992	US	5KW	R & D assistance for product development. a continuous system
NCFST/FDA/APV Bedford Park. IL	1994	US	5KW	Dynamic batch ohmic heating unit for research tests.
Nestlé Food Service Division (Chef Mate brand) Trenton, MO	NA	US	300KW	Shelf stable Low acid beef stew and ravioli in 10cm packaging
Agriculture Canada Food Res. Centre	1999	Canada	5KW	Continuous liquid and solid food
Center di Tramariglio	2001	Italy	50KW	Continuous aseptic ohmic heating system

Source: Updated data of Marcotte (1999), Revised in Ohmic Heating in Food Processing (2014).

2.1.6 Application of moderate electric field (MEF) in ohmic heating

The use of MEF in ohmic heating spans the thermal processing such as heating and pasteurization. Also, MEF is applicable in the non-thermal processing of food such as electroporation and blanching. Thamkaew & Galindo, (2020) explains that non-thermal effect of ohmic heating of food is achieved easier and quicker with MEF because it involves the direct application of electric current and no pulse forming network. Thamkaew & Galindo went further to explain that cell permeabilization or electroporation achieved can either be reversible or non-reversible. Palaniappan and Sastry, (1991a) explained that the application of MEF causes electro-osmotic dehydration leading to the softening of food tissues causing the internal cell membranes to rupture.

Below is a table describing the applications of MEF in food processing.

Table 2.2 Applications of MEF in ohmic heating

Applications of MEF in ohmic heating	
Thermal processing • Heating • Pasteurization	Non-thermal processing • Electroporation • Blanching • Extraction

2.2 Design of an ohmic heater

2.2.1 Physical structure

Several researchers have proposed different physical models for ohmic heater (OH) system, but a fundamental design structure of OH systems is such that two or more electrodes are used to pass current into food substance (Sakr & Liu, 2014). Icier and Ilicali (2005b) explained that ohmic heater can be designed to be a containing vessel or a continuous flow system depending on the location and position of the electrodes. Kamonpatana et al. presented a continuous flow OH system for solid-liquid mixture (Kamonpatana et al., 2013). This model consists of a mixing tank with a variable mixer, displacement pump, a magnetic flow meter, OH chamber consisting of two spaced stainless-steel electrodes separated by a plastic spacer, aseptic tank to provide back pressure, laminar flow hood for product flow and two independent OH chamber with constant electric field perpendicular to the product flow. Pesso & Piva (2017) described another collinear cylindrical ohmic heater system in laminar flow. Unlike the model described by Kamonpatana et al, the heating chamber is a cylindrical circular electrically insulated glass pipe with two electrodes at the pipe ends and the electric field applied to the electrodes is parallel to the product flow. A design flaw of Pesso & Piva's physical model is the presence of live electrodes at the pipe inlet and exit will cause current leakage through the product to earth Shiby Varghese et al (2014).

Sastry et al (2009) developed batch ohmic heaters equipped with foil electrodes inside V-shaped pouches. Somavat et al (2012a) redesigned the pouch from V-shaped to rectangular with 2 flat foil electrodes to facilitate more uniform heating, this corrects a drawback of that design which led to the occurrence of cold zones at the non-electrode sides. A similar batch OH system described by Kanogchaipramot, et al (2016) which is an upgrade of the work of Sastry et al is an electrically conductive food package using polymer film integrated with an electrically conductive film to form a conductive package for orange juice. This design increases the possibility of different geometric shapes for OH systems based on the temperature distribution, power, input voltage and heating time.

A batch OH system described by Choi, Kim, Park, Ahn, & Kang, (2020) consist of a rectangular heating chamber with two titanium electrodes installed at the inner wall opposite to one another. An electric field of 25.6 V/cm at a waveform of 20kHz is applied to the electrodes. A batch ohmic heater does not necessarily have to be rectangular. Sagita, Darmajana, Hidayat, Novrinaldi, & Sitorus, (2020) presented a cylindrical batch ohmic heater used in the fermentation of soya beans. The heating chamber is made of PET plastic and the electrode are the closed ends of the cylinder.

Table of some physical structural designs of an ohmic heater in literature are presented.

Table 2.3. Review some physical structural design of an ohmic heater by authors.

Author	Design
Icier and Ilicali (2005b)	• Continuous flow heater • Variable electrode position
Kamonpatana et al., (2013)	• Continuous flow • Parallel spaced electrodes • constant electric field perpendicular to the product flow
Pesso & Piva (2017)	• collinear cylindrical ohmic heater system • two electrodes at the pipe • electric field applied to the electrodes is parallel to the product flow.
Sastry et al (2009)	• batch ohmic heater • foil electrodes inside V-shaped pouches
Somavat et al (2012a)	• batch ohmic heater • 2 flat foil rectangular electrodes
Kanogchaipramot et al (2016)	• Batch ohmic heater • electrically conductive food package using polymer film
Choi, Kim, Park, Ahn, & Kang, (2020)	• Batch ohmic heater • rectangular heating chamber

	• two titanium electrodes installed at the inner wall opposite to one another
Sagita, Darmajana, Hidayat, Novrinaldi, & Sitorus, (2020)	• cylindrical batch ohmic heater • electrodes are the closed ends of the cylinder

2.3 Process parameter

The process parameters are process variables that influences the performance of the ohmic heating system. The various process parameters are correlated and cannot be singled out in the ohmic heating process. Hence, the influences of the process parameters are studied generally.

2.3.1 Modelling the electrical conductivity.

Different techniques have been used to model the electrical conductivity of food substance. In available literature, electrical conductivity models which are based on the linear temperature function, finite difference technique, electrical circuit model and Artificial neural networks have been used. Sastry and Palaniappan, (1992) showed that the rate of ohmic heating is directly proportional to the square of the electric field strength and the electrical conductivity and therefore showed that the electrical conductivity can be modelled as linear function of temperature. Icier & Ilicali, (2004) described the finite difference technique in modelling the electrical conductivity as very accurate. According to Icier & Ilicali, this mathematical modelling method of the electrical conductivity is an iterative procedure to establish the time-temperature profile within a particle and of the fluid during ohmic heating and accurately predicts the ohmic heating times of fruit juices having different concentrations. Guo et al (2017) applied the series and parallel impedance and resistance component to predict electrical conductivities of foods, the electrical conductivity was estimated from the geometry of the electrodes and the resistance. Therdthai & Zhou (2001) presented an artificial neural network model, this method models a non-linear relationship that accounts for the effect of milk constituent and the temperature on the electrical conductivity of recombined milk.

2.3.2 The effect of electrical conductivity on heating rate

Stirling (1987) made a simple classification of the electrical conductivity values of common foods to show their heating rates. Stirling's classification showed that the electrical conductivities of food can fall into rapid heating (1-5 °C /s), very rapid heating (7-50°C /s) and unsuitable for heating.

The work of Assiry, A et al (2010) to generate ohmic heating in seawater also showed that the heating rate is dependent on the electrical conductivity.

2.3.3 The electrical conductivity in solids and liquids

Solid food particles will exhibit lower electrical conductivities than liquid ones. The method of soaking the solid food in a known concentration of saline solution to increase the electrical conductivity is described as the best approach by Palaniappan and Sastry (1991a).

Palaniappan and Sastry (1991a) measured the electrical conductivities of untreated samples of potato, yam and carrot and compared the electrical conductivity with samples soaked in water and saline solution with various concentration. The samples soaked in water had lower electrical conductivity than the untreated sample while the sample soaked in saline had increased electrical conductivity in relation to the saline concentration.

Another method employed is to pre-heat the solid food to raise its temperature before ohmic heating. Wang and Sastry (1997a) showed that this method increased the electrical conductivity and heating rate of solid food potato, yam, and carrot samples but the thermal effect was different.

Palaniappan and Sastry (1991b) showed that the electrical conductivity of liquid food decreases with the increasing presence of dispersed solid constituents. Palaniappan and Sastry explained that this is to be expected because solid foods have a lower conductivity compared to liquid ones.

2.3.4 Electric field in the OH system

The electric field in a system where the electrical conductivity varies with temperature can be modelled according to De Alwis and Fryer (1990b) by solving the Laplace equation given the appropriate boundary conditions. The electric field equation is represented using the Laplace representation to describe the electric field as

$$\nabla [\boldsymbol{\sigma} (T)\nabla V] =0 \tag{2.1}$$

Kanogchaipramot et al (2016), Salengke & Sastry (2007) explained that the boundary conditions and initial condition for the OH are given as follows:

- Electrode with a ground: V=0
- Electrode with an electric potential: V=V0
- Electrical insulation at the walls: $n\cdot (\boldsymbol{\sigma}(T)\nabla V) =0$

where n is the unit vector perpendicular to the boundary, $\boldsymbol{\sigma}$ is the electrical conductivity and V is the applied voltage.

Another approach by Sastry and Palaniappan (1992c) to model the electric field is to use the circuity analogy approach where a set of equivalent resistances for the liquid and particles in the heating cell were computed for each incremental section consisting of two resistances in parallel for the liquid and the particles and one resistance in series for the liquid. Initial work by Robertson & Gross. (1958) describes this model by relating the Fourier equation of heat conduction, the equation for a series resistance and shunt capacitance of a transmission line together using analogous relationship between thermal and electrical quantities. Zhang and Fryer, (1995) compared the Laplace approach and electrical circuit approach of electric field modelling in the determination of OH heating rates and reached a conclusion that the predicted OH heating rates using circuit analogy was not appropriate.

2.3.5 Effect of electric field gradient in ohmic heating

The following table presents the effect of the electric field gradient presented by different authors.

Table 2.4. The effect of electric field gradient in ohmic heating

Author	Electric field gradient on food	Food type	Effect
Palaniappan and Sastry, (1991a)	• decreasing the electric field gradient to 0 V/cm	• Solid food	• Sigmoid temperature curve • Electrical conductivity decreases
Palaniappan and Sastry, (1991b)	• Electric field of 30-60 V/cm	• Liquid (orange juice)	• No effect on the electrical conductivity
Icier,F. (2009)	• Increase in electric field. • Increase from 10V/cm to 60 V/cm	• Liquid (Milk) • Liquid (Ice cream)	• Reduced ohmic heating times. • 50 to 31 times faster heating
Yildiz, Bozkurt, & Icier, (2009)	• Increased electric field	• Liquid • Solid	• Increased blanching • Increased electroporation

2.3.6 Product temperature

The electrical conductivity of food and the temperature are closely related therefore, the ohmic heating times of different food product depends on the initial temperature and the respective conductivity (Sastry, 2008)

2.3.7 Residence time distribution for a continuous flow ohmic heater

The movement of liquid and solid particulate food in a pipe will result to residence time distribution (RTD) (Manson and Cullen,1974). Marcotte (1999) describes the RTD as the amount of time food products spends in the ohmic heating system. Sarang et al (2009) explained further that the residence times of food products helps in evaluating quality degradation as it passes through the ohmic heater. Variables that can affect the RTD include the dimension of the pipe, the orientation, product flow rate, food density.

Chandrarana and Unverferth (1996) presented a technique to determine the RTD which involves tagging food particles with small magnets. The theory behind this technique is based on the law of electromotive induction. As the magnet tagged food passes through a stainless-steel tubing of diameter 34.8mm with varnished 24-gauge copper coil of 800 turns, emf is induced. Therefore, for this method the magnitude of the emf induced is proportional to the relative motion of the food particles. The limitation of this method is the inability for multiple tagged particles to pass through the detector at once therefore, a tagged particle must exit before a new one enters (Sastry and Cornelius, 2002).

Tulsiyan et al (2009) developed a new technique to measure the RTD using radio frequency identification (RFID) for RTD measurement of chicken particles. Sarang et al (2009) explains that the RFID method makes it possible to track multiple particles and alleviate waiting times.

2.4 Ohmic heating modelling

2.4.1 Modelling the ohmic heating process.

In modelling the ohmic heating (OH) process, the temperature of the food substance must be known to ascertain the efficiency of the process. Considering a continuous flow OH system, a lot of thermo-physical complexities like fluid flow dynamics, viscosity, density, and mass flow rate arise and makes it difficult to adequately predict the temperature. Therefore, a suitable OH model will require the simultaneous solution of the thermal differential equation, electrical equation, and fluid flow in the spatial geometry of the OH cell. If a batch OH system is considered, the model developed will represent a static thermal system. Therefore, the solution for fluid flow will be ignored thereby reducing the complexity to just the coupled electrical and thermal partial differential equations (PDE) to determine the temperature distribution in the OH cell.

2.4.2 Modelling the general energy transfer.

The temperature is the primary objective therefore, the energy transfer equation needs to be solved. The governing equations of the OH system therefore consists of the thermal and electrical equation. Marcotte (1999), Somavat et al (2012a) presented the thermal conduction and internal energy generation equation as:

$$\rho c\frac{\partial T}{\partial t} = \nabla\cdot(k\cdot\nabla T) + Q_h - \rho\nabla .\, v - \nabla .q_r \quad (2.2)$$

$$Q_h = \boldsymbol{\sigma}|\nabla E|^2 \quad (2.3)$$

$$\boldsymbol{\sigma}\,(T) = \boldsymbol{\sigma}\,(1+k_o(T-T_o)) \quad (2.4)$$

Q_h is the volumetric heat (W/m^3) generated by the applied electric field (E)

T is the temperature term in K, T_o is the initial temperature.

where k, ρ, c and $\boldsymbol{\sigma}$ are the temperature-dependent thermophysical properties of the food: the thermal conductivity (W/mK), the density (kg/m^3), the specific heat capacity (J/kgK) and the electrical conductivity (S/m) respectively.

$\nabla\cdot(k\cdot\nabla T)$ of equation 2.2 on the right-hand side represent the heat transferred by conduction through the fluid and the term Q_h represents the volumetric heat generation which is important in ohmic heating but negligible in conventional heating processes. The predicted temperature is described by equation 2.4 where k_o is the temperature coefficient (1/K). The addition of the fourth term ($\rho\nabla .\, v$) is the work done by the fluid on its surrounding which is zero for an incompressible fluid, fifth term (q_r) is the radiative heat transfer (Marcotte, 1999).

2.4.3 Ohmic heater electrical circuit model

Researchers have applied various modelling techniques to the OH process for different type of food products. Chávez-Campos et al (2019) studied the modelling of OH processes using the thermal circuit method by evaluating thermal resistance and capacitance as steady-state and transient analogue parameters. Lawson & McGuire (1953) explained that the flow of heat in materials not maintained at a uniform temperature obeys laws similar to those that govern the flow of charge in suitably designed electrical networks. Early work by Lawson & McGuire showed the rapid determination of the temperatures inside materials and composite structures using a derived lumped RC circuit network that relates the equivalent length of the structure, the varying distance from the source of heat and the electrical transient to repetitively solve the heat problem. The complexity and time-consuming nature of determining the analytic or approximate numerical solution to complex thermo-fluid dynamic system resulted in the use of this intuitive electrical-analogue technique (Robertson & Gross 1958).

Robertson & Gross (1958) describe this model by relating the Fourier equation of heat conduction, the equation for a series resistance and shunt capacitance of a transmission line together using analogous relationship between thermal and electrical quantities. Chávez-Campos et al (2019) showed that the batch ohmic heating system is modelled based on the analogous relationship between thermal and electrical quantities and each one of the three terms involved is replaced by an electrical component. Chávez-Campos et al further explained that the energy input is modelled as a current source, the differential term in function of the temperature is modelled as a capacitance, the voltage in the circuit is related to the temperature in the ohmic heating system therefore, the linear term is modelled as a resistance device.

A major advantage described by Chávez-Campos et al is that the system transfer function of the ohmic heater system which links a variable response to an excitation signal can be determined using the Laplace transform for understanding of the system’s response and to design a suitable controller for the system. Steere (1971) also showed that it is possible to construct a simple analogue network which can solve quite complicated heat transfer problems with low computation cost. This modelling technique is however not immune to errors, Robertson & Gross (1958) explained that errors due to the boundary and initial condition, the number of lumps of R-C circuit and the ratio of the time constant in which the measurement of the R-C(resistance-capacitance) product in the model are present.

2.5 Control techniques used in ohmic heater applications.

Several authors have shown that the process variable to have the most significant impact of the OH system is the applied voltage. The ohmic heating rate is directly proportional to the square of the electric field strength and the electrical conductivity as reported by Sastry and Palaniappan (1992), Silva et al (2017) further showed that the increasing value of the applied electric field strength increases the food electrical conductivity and the heating rate and that the field strength can be varied by adjusting the gaps between the electrodes or by varying the applied voltage.

2.5.1 Early control

Richardson (2001) pointed out that Gethchell was the first to emphasize the control and regulation of the ohmic heating process in the early 1930s. From then on, different types of controllers are being implemented in the control of the applied voltage to the ohmic heating/resistive heating/joule heating system, these controllers range from simple open loop controller to closed loop feedback controller. Goeltenboth et al (2010) patented a continuous flow heater for open loop control, the invention relates to a continuous flow heater for liquids, particularly for water or milk in beverage machines. The heating device comprises an electrically conductive bare wire, the heating channel is formed regionally by the heating device, wherein the heating device is in direct contact with the liquid to be heated in the said region forming the heating channel. A drawback of this controller is that a single control signal which is the voltage in the case of Goeltenboth's heater is applied, the output result is assumed to be desirable without verification this is because there is no comparison between the actual and desired values (Vandoren 1998). Vandoren went further to explain that with open loop control, there is accuracy loss as there is no guarantee that the control input applied will have the desired output.

2.5.2 Control and automation in ohmic heating

The control and automation in ohmic heating is based on the system desired performance and response such as in any other engineering system. Stirling (1987) describes the following control requirement of an ohmic heating system:

i. The control of the heater outlet temperature against the flow rate, initial product temperature and heater power.

ii. Detecting temperature overshoot and applying the appropriate control strategies such as stopping flow, shutting down power.

iii. Scheduling specific ohmic heating operations such as warm up and start-up routines

iv. Data collection, report generation, and energy observation.

2.6 Feedback control

Pidhayny (1972) explained that the first major use of feedback control was in the development of the float control mechanism in the early Greek civilization in the development of water clock and oil lamps. In the modern control system, a microprocessor acquires the process variables and continuously computes the electrical power required to heat the product and compares the set value with the signal from a power transducer on the output side of the transformer. (Skudder and Stirling, 1992). Li & Li (2019) showed that with temperature feedback control, the applied control voltage can be effectively regulated by a control gain. Tatem (1955) patented a simple bang-bang temperature control apparatus for electrode type boilers. The invention provides a simple feedback temperature control apparatus for electrode type water boilers by means a hydraulic motor, thermo-sensitive switch, a pump, and a magnetically operated valve for shifting insulating shields between the electrodes and their neutrals to expose a greater length of electrodes to the fluid. As the Water temperature falls below a value set by a first thermo-sensitive switch, the hydraulic mechanism increases the exposure of the electrode as the temperature approaches a value set by a second thermo-sensitive switch the hydraulic mechanism reduces the electrode exposure at the length to which it is momentarily set as the water temperature falls once more below the value set by the second switch. The insulating shields reduces the exposed length of the electrodes and thus the heating Silva et al (2017). As the heating rate is reduced, naturally the Water temperature will be reduced as soon as it falls below 185 F (85 degC) the magnetic valve will close and prevent any further reduction in heating. (Tatem,1955)

This control is either on or off if the temperature is within a set limit, an advantage is that if the water within the boiler is set to boil at 100 degrees Celsius full heating can be achieved since maximum voltage and electrode contact is used. A downside is that the boiler is restricted to a lower and upper bound tolerance temperature therefore accurate temperature cannot be achieved. Liberzon, & Trenn (2013) showed that this type of controller exhibits oscillating output error which is not totally restricted to the physical bounds the bang-bang control set points.

2.6.1 Proportional, integral, and derivative control

Sellers (2007) explained that implementing proportional, integral, and derivative (PID) control in heating, ventilating and air conditioning (HVAC) system improves the system response by compensating the offset or error between the setpoint (SP) and the system response to the open-loop control. The equation of the PID controller is expressed as:

$$R(t) = K_p . x(t) + K_i \int_0^t x(t)dt + K_d \frac{dx(t)}{dt}. \qquad (2.5)$$

The term $K_p . x(t)$ is known as the proportional term and it is proportional of the difference between the set point (desired output temperature) and actual value (recorded temperature), i.e., in this case it represents a temperature error which is $x(t)$. The integral term, $K_i \int_0^t x(t)dt$ is the summation of the error values and $K_d \frac{dx(t)}{dt}$ is the derivative of the proportional error, it determines if the error is diminishing. Therefore, the proportional term K_p decreases the rise time, the integral term K_i reduces the steady state error while the derivative term K_d reduces the settling time and overshoot. The C-Joule 100 batch ohmic heater developed by C-Tech innovation UK employs the use of a PID controller with feedback using four thermocouple sensors. (https://www.ctechinnovation.com/product/c-joule-lab-100/). The control gains are tuned by the user intuitively in response to the output process variable (temperature), the manipulated control output by the PID controller is a dimensionless scale of 0 to 100% of the maximum voltage value of the power thyristor, the control output is then translated to voltage level across the heating electrodes which in turn determines the heating rate. Inoue et al (2008) also designed a reaction heating vessel consisting of a temperature detection part configured to detect a temperature of the processing region; and a control part configured to control the heating unit by an automatically adjusting PID control. A rule table is prepared such that selected target temperature value corresponds to a change ratio of PID gains. A performance unit constantly calculate the difference between actual measured value and target value of the temperature property item based on the temperature profile (Inoue et al 2008).

2.6.2 Multivariable control

Multivariable control explained by Airikka (2004) is a control method capable of handling several processes input and output simultaneously which can be based on several PID controllers combined with a compensator placed between the unit controllers for decoupling the unit controller's output and process variables. Stephen, & Michael. (2011) used multivariable control technique in the development of a heating tank of conductive liquid used in devices such as residential and commercial water heaters and dishwashers. Stephen & Michael explained that when heating the water, the changing chemical property of the liquid makes it to react to the pre-tap liquid, and to adhere to the surface of the electrode, forming a lime coating on it. The first controller adjusts the conductivity of the liquid through feedback by measuring the current flow in the liquid, between the electrodes. The second controller supplies full wave or half-wave current alternatively to each set of electrodes. Until the temperature set point is reached, the temperature controller provides an output of square wave to the switches of each set of electrodes, allowing control of the duty cycle of the sets of electrodes for each connection and disconnection.

Stirling (1987) highlighted the flaws of the feedback control in ohmic heating applications given that step changes do occur at the ohmic heater inlet and are not detected by the outfeed feedback sensor until the food product has passed through the heater. Stirling further explained that a given volume of food product is processed incorrectly. To correct this flaw, Stirling proposed a feedback control with slow rates of change of heater input parameter.

2.7 Feedforward control

The application of feedforward control in heating dates to the early 1930s when it is applied as three-element control in boilers to control the water level, feed flow and the flow of steam (Seborg, 2011). In ohmic heating processing, Stirling (1987) describes the feedforward control to mean the continuous scanning of input parameters and process variables to calculate in advance the require heater power to be applied. In feedforward control in ohmic heating applications the process set-point temperature is entered, and the appropriate heating power is applied. The measured value is then compared to the setpoint value to evaluate the error signal which is used to increase or decrease the heating power delivered (Stirling, 1987).

Richardson (2001) examined the works of Biss, Coombes and Skudder in the control of the APV Baker (Baker Perkins UK) ohmic system and showed that pure feedback control is not suitable due to large time constants in the system and therefore, presented a feedforward control technique. Earlier works by Elliott & Sutton (1996) in examining the performance of both feedforward and feedback controllers regarding their variation with delays in a plant buttresses Richardson's point when it was found at that the potential performance of the feedback control system was better than that of the feedforward system if the plant delay was smaller than about 1.5ms. Richardson (2001) went forward to explain that for the feedforward processes, the control depends on the process parameters as well as the control loops. Therefore, when a feedforward control system is implemented in a system it makes it adaptive so that it can adjust its response to the changing statistical properties of the primary disturbance due to prior knowledge of the disturbance to be controlled (Elliott & Sutton 1996).

Li et al (2013) described a feedforward temperature control method for heating cleaning fluids, this system consists of 3 temperature sensors one placed in the heating tank to determine a set temperature point, one at the outlet of the electric heater to control the heating power, and one at the outlet of the liquid feed to regulate the supply of cleaning fluid into the tank. This method effectively overcome the disturbance of liquid feed temperature at the outlet of liquid feed as a result of the replacement of the cleaning liquid and the fluctuation of liquid flow on liquid temperature at the outlet of the heater due to the factors such as changes in pipeline pressure. Therefore, the feedforward control measure important disturbance variables and take corrective action before they upset the process which contrasts with a feedback controller that takes corrective action only after the disturbance has upset the process and generated a nonzero error signal (Seborg, 2011).

Stirling (1987) explained that a weakness of the feedforward control in ohmic heating is the control action being too fast in applying corrective actions. Stirling went further to show that the accuracy of the feedforward control depends on the performance of the temperature sensors and input transducers.

Tao et all (1994) implemented a feedforward learning control technique applied to the rapid thermal processing reactor of semiconductor wafers, the control algorithm involved measures the real time feedback loop and therefore makes the tuning of feedforward controller easier because it can learn from the past on-site control circulation. Liu et al (2019) explained that one of the limitations of the classical feedforward control algorithm is the limitation with the system nonlinearities, plant model uncertainties and time delay. Therefore, a combined strategy which involves feedforward neural network and fuzzy logic control can be considered Chen (1992).

2.7.1 Model predictive control

Model-based predictive control (MPC) refers to a class of sophisticated control techniques that use a process model to predict the future behaviour of the controlled system. (Schwenzer, Ay, Bergs, & Abel, 2021). At each time step, the MPC determines an optimal solution for the control output using the prediction model by solving a constrained optimization problem using predictions of future costs, disturbances, and constraints over a moving time horizon. Hence, the MPC is referred to as a “receding horizon” control (Mattingley, Wang, & Boyd, 2011). In essence, the idea is that a short-term (predictive) optimization achieves optimality over a long time.

Short-term prediction over a long time achieves optimal results since the error forecast is small compared to a distant prediction. The combination of prediction and optimization is the main difference from conventional control approaches, which use precomputed control laws (Mayne, Rawlings, Rao, & Scokaert, 2000). The main disadvantage of MPC is that the optimization problem must be solved at each time step, which lead control engineers to think that it can only be used for systems with slow sampling typically less than one Hz (Mattingley, Wang, & Boyd, 2011). Several techniques have recently been developed to get around this problem. In one approach, called explicit MPC, the optimization problem is solved analytically and explicitly, so evaluating the control policy requires only a lookup table search (Bemporad & Filippi, 2003).

2.8 Summary

The literature explored the main principles of OH technology, the progress of OH over the years when compared to other conventional heating methods, the advantages and disadvantages of OH and the commercialisation of OH. This section also identified the application of MEF in the food industry.

The subject of commercialisation of OH technology will be difficult without the application of advanced process control. This is because food samples vary in various thermophysical and chemical properties. The strategies developed in the design of the advanced process control include the modelling and validation of the OH process with regards to the changes of thermophysical and chemical properties of foods. In the next chapters the work done in the development of advanced process control with the CFOH are presented.

Chapter 3. Model based design and validation of a batch ohmic heating system.

This section is focused on the dynamic modelling and validation of MEF in food processing and was aimed to address the gap in the literature as follows:

- Model the predicted temperature output of different foods under the MEF heating process with variable process parameters.
- Present a range of modelling techniques, illustrate their advantages and disadvantages, and validate the simulated models using experimental data.
- Compare MEF processes with other alternative emerging processing methods.

In this section, the modelling of the MEF Ohmic heating process was based on the data gathered and equations derived from the available literature. The Ohmic heating process model was built using a combination of MATLAB/Simulink and COMSOL Multiphysics software. The derived model was then validated against published works and experimentation. The objectives to be achieved and methods used in this work are described in Figure 3.1

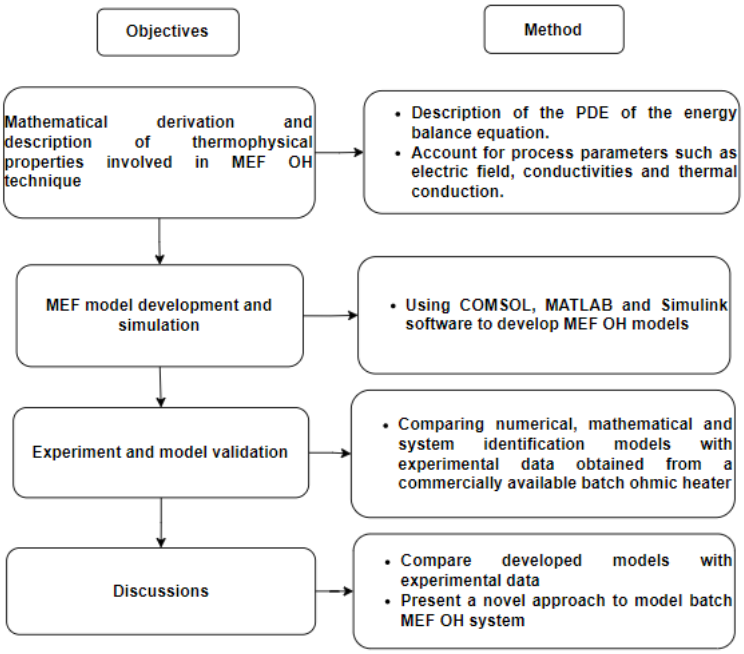

Figure 3.1 Methodology flow path between the objectives and the method used in this work.

3.1 Modelling the batch ohmic heating process.

During modelling, the temperature of the food substance must be known to ascertain the efficiency of the OH process. If a batch OH system is considered, the developed model represents a static thermal system. Therefore, the solution for fluid flow dynamics is ignored, thereby reducing the complexity to only the coupled electrical and thermal partial differential equations.

3.2 Modelling the general energy transfer.

The temperature was our primary objective, so the energy transfer equation needed to be solved. The governing equations of the OH system consist of the thermal and electrical equations.

The simultaneous solution of the general heat transfer described earlier in section 2.4.2 yields:

- The equation describing the electrical potential within the food product.
- The heat balance equation relating to the electric potential within the food.
- The electrical conductivity relating to the temperature.

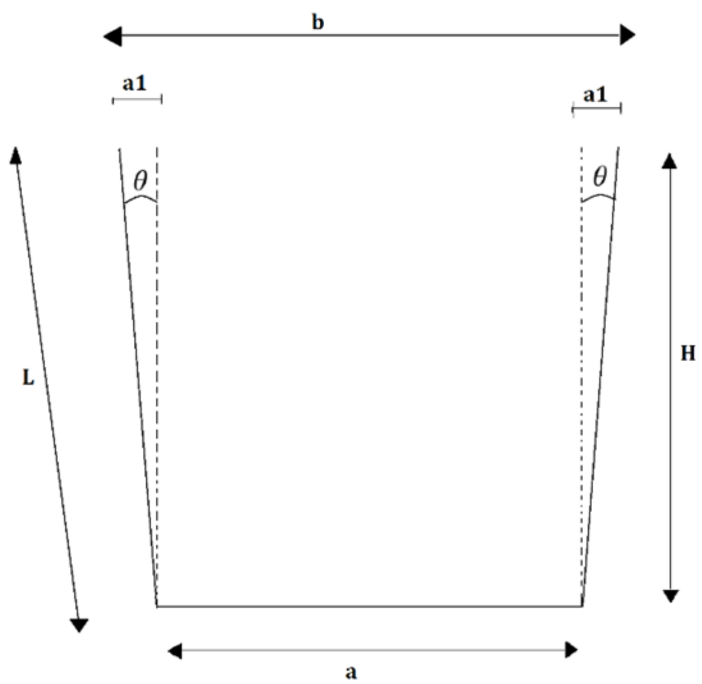

Figure 3.2. Modelling of the electric field between the slant electrodes of the batch ohmic heater

From Figure 3.2 above, the electric field E is modelled as follows:

Assume the electric field is given as:

$\mathrm{E} = \frac{\mathrm{V}}{a+2a1}$, where a1 = Lsinθ for $0 \leq \theta \leq 90^0$

Therefore:

$$\mathrm{E} = \frac{\mathrm{V}}{a+2\mathrm{L}\sin\theta} \text{ (V/m)} \tag{3.1}$$

When θ = 0, $\mathrm{E} = \frac{\mathrm{V}}{a}$. The electric field E is calculated as a resultant of the overall electrode gap $a + 2\mathrm{L}\sin\theta$.

3.3 Model simulation.

General model simulations can be based on three levels of spatial details to which models of materials can be organised. The microscopic level is concerned with the properties and arrangement of large numbers of atoms and molecules. The macroscopic level deals with the overall structure averages and is the domain of mechanics and thermodynamics. The mesoscopic level is intermediate to the other two. The macroscopic level requires that the materials' properties are generally represented by a set of partial differential equations that express energy, mass, and momentum conservation and are formulated to represent the symmetry of the material to which they are applied to National Research Council (1993).

Regarding MEF as an ohmic heating technique, there is no sharp boundary between the macroscopic level and the mesoscopic level. Different food types have varying process parameters (conductivities, viscosity, density and heat capacity etc.) and these process parameters respond nonlinearly to factors such as applied electric field or initial temperature. Therefore, the modelling approach applied span the first principle to the data-driven model techniques. Ghosh et al (2019) described the first-principles or mechanistic modelling as the type of modelling where explicit knowledge of the process mechanism was present and utilized. In this type of modelling, the developed models invoke fundamental physical and chemical laws that describe the system being considered or use partial differential equations. Whilst in comparison, the data-driven modelling approach involves mathematical equations that are not derived from physical processes in the catchment but from analysis of time series data (Solomatine, See, & Abrahart, 2008).

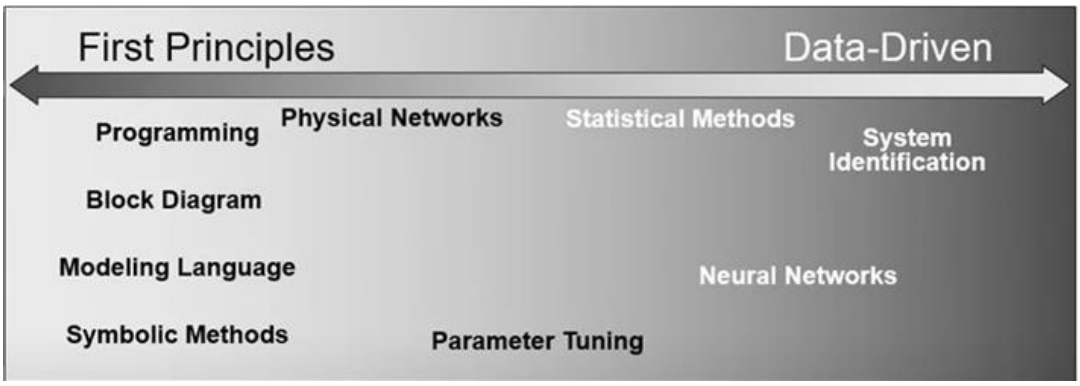

Figure 3.3: An overview of the modelling approaches (Matlab. Converter Modeling and Efficiency Considerations [MATLAB]. Retrieved August 04, 2021, from https://www.youtube.com/watch?v=0uvWtWMYin4&t=31s)

The ohmic heating system model is developed using three techniques. These techniques are:

- First principle partial differential equation model (Using COMSOL)
- Lumped ordinary differential equation model (block diagram using SIMULINK)
- Regression models using system identification technique (Using MATLAB).

The energy balance heat equation of the MEF process is the same for both the First principle partial differential equation (PDE) and lumped ordinary differential equation (ODE) model. However, the lumped ordinary differential equation (ODE) model provides an analytic method to its solution. The lumped ODE model using Simulink blocks do not follow any defined algorithm but solves the balance equation in a closed form described by the individual Simulink blocks. This provides a fast and exact solution (Applied mathematics for science and engineering, 2014). Unlike the First principle PDE model, where a robust solution using the Backward Differential Formula (BDF) algorithm is used. However, first principle PDE model increases the computation requirements.

3.3.1 First principle PDE model

The governing equation, ohmic heater dimensions and initial conditions were solved using COMSOL Multiphysics version 5.6 and the electromagnetic heating module (emh). The analysis ran on a PC with Intel core i5 8th Gen CPU at 2.3 GHz with 4 Gb RAM, 8 processors, with Windows 10 operating system. The electromagnetic heating couples the electric current (ec) system and the heat transfer (ht) in a solid system into one equation describing the time-dependent equation problem, given in Eq. (3.2.1) above. A BDF solver using a time-stepping scheme was used to solve the time-dependent problem for 5108 degrees of freedom (including 2560 internal DOFs). The maximum time constraint was set to automatic such that at each time step, the software might need to solve a set of nonlinear equations. Where a nonlinear system was encountered, the BDF method event tolerance was set to 0.001. An arbitrary linear system solver was then used for the final solution. A flowchart showing general procedure for first principle PDE modelling and solution of PDEs is presented in Figure 3.4

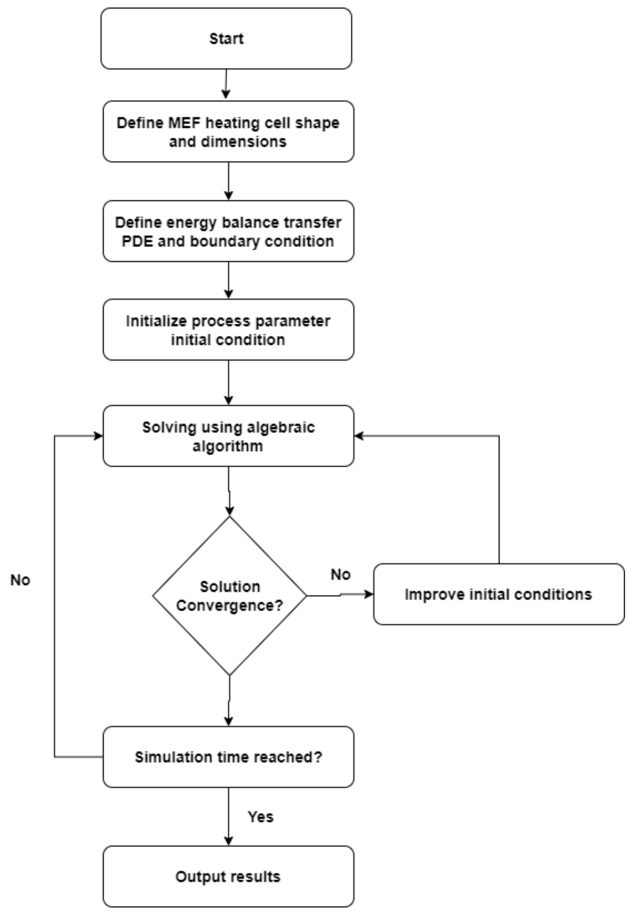

Figure 3.4. General procedure for First principle PDE model and solution of PDEs

3.3.2 Lumped ODE model

The lumped ODE model was developed using SIMULINK and the governing equations were defined using Simulink blocks. The model defines the ohmic heater geometry, specifies the thermophysical properties of the food substance, calculates the electrical conductivity as a function of temperature, calculates the volumetric heat within the food as a function of the electric field and evaluates the final temperature. The Simulink structure and the corresponding subsystems are presented in Figures 3.5 -3.7.

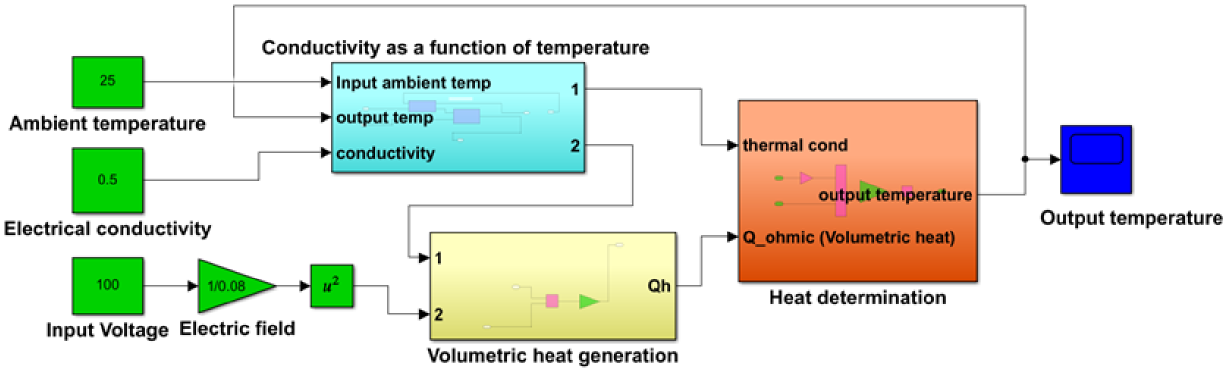

Figure 3.5. A snapshot of the developed lumped ODE model showing different blocks representing terms of the energy balance equation.

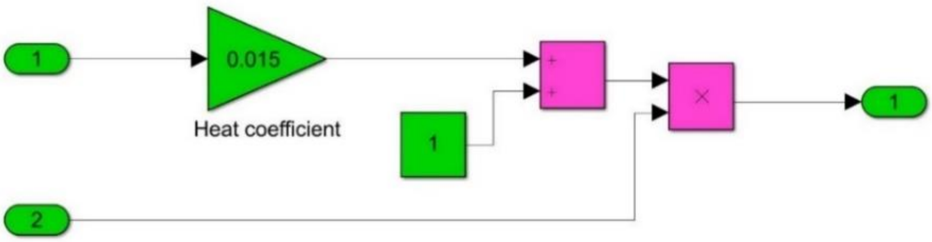

Figure 3.6. A snapshot of the block subsystem representing the electrical conductivity (σ(T)=σ(1+k_o(T-T_o)) as a function of temperature. Here, k_o = 0.015.

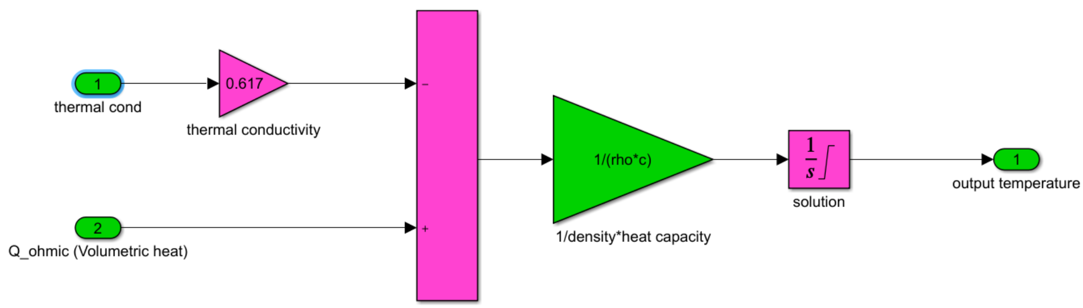

Figure 3.7.A snapshot of the heat determination block subsystem showing the energy balance equation ($\rho c\frac{\partial T}{\partial t} = \nabla\cdot(k\cdot\nabla T) + Q_h$) and the integral to determine its solution.

The resulting term $\frac{\partial T}{\partial t}$ gives the rate of change of the food temperature which can be represented by $\frac{\partial T}{\partial t} = \frac{1}{\rho c}\nabla\cdot(k\cdot\nabla T) + Q_h$. The output temperature is the integral of the signal $\frac{\partial T}{\partial t}$.

3.3.3 Regression models using system identification technique.

The MATLAB system identification toolbox was used to determine a nonlinear model of the ohmic heating system. Three regression models were developed:

- Nonlinear ARX model (nlarx)
- Process model (P1D)
- ARX model (arx728)

The system identification toolbox of MATLAB was used to develop the models listed above, based on the input-output experimental data. This approach does not require mathematical formulae of process dynamics from the user. It is based on empirical data only and the user is not required to have complete understanding of the process dynamics.

'British fresh whole milk' purchased at a local supermarket at initial temperature of 15^0C was heated to a setpoint of 80^0C. The experimental data set is split into test and validation data. The validation process is discussed in section 3.4 below. The steps taken in training the models involves selecting the regression model and specifically preparing a data set of a time span of 2.5 minutes. The data set is a single run of 17^0C to 80^0C. The justification for selecting this data set is because the data points (150) are spread across different temperature ranges. Also, it was observed during experimentation that a linear correlation exists between the applied voltage and the output temperature.

A. Nonlinear ARX model (nlarx)

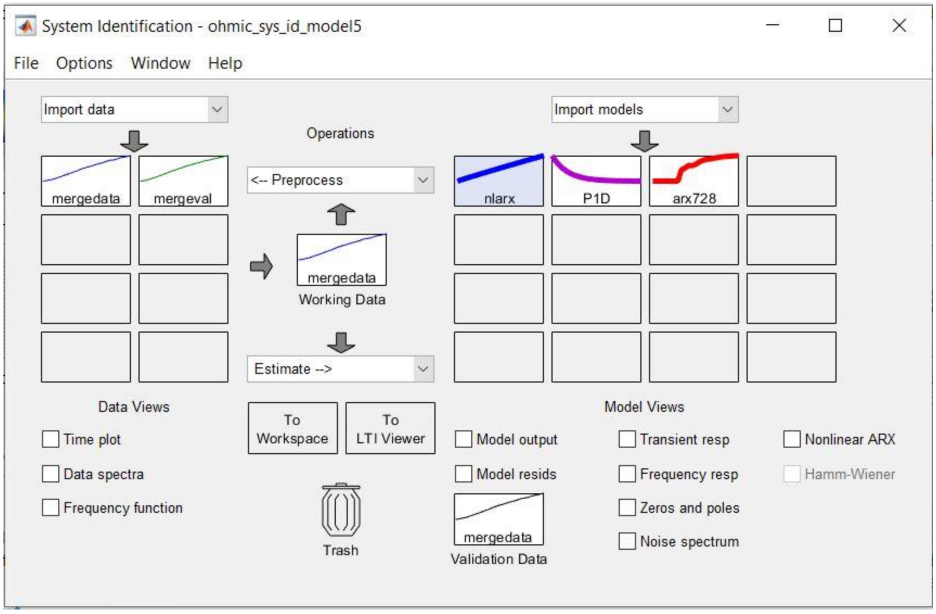

Figure 3.8. A snapshot of the system identification interface showing the imported experimental data on the left plane and the developed system identification model on the right plane.

The nonlinear ARX model consists of model regressors and a nonlinearity estimator. The nonlinearity estimator comprises both linear and nonlinear functions that act on the model regressors to give the model output.

Given a single input (Voltage) single output (temperature) system, a maximum delay in the input is set to 2 samples, the maximum delay in output is set to 2 samples and the wavenet is set to 1 unit. Therefore, this model has a total of 4 states given as:

$$X(t) = [temp(t-1), temp(t-2), voltage(t), voltage(t-1)] \quad (3.2)$$

B. Process model (P1D)

The process model (P1D) are simple continuous time models that are described in terms of the main time constants, the static gain, a possible dead-time, and a possible process zero (non-constant numerator).

A typical such model is a 1st order transfer function.

$$G(s) = K \exp(-T_d s) / (1 + s T_p 1), \tag{3.3}$$

where $K = 4.1975$, $T_p1 = 805.14$ and $T_d = 0$

C. ARX model (arx728)

The ARX model is a linear difference equation that relates the input u(t) to the output y(t) (where t represents the time step), as follows:

$$y(t) + a_1 y(t-1) + ... + a_{na} y(t-n_a) = b_1 u(t-n_k) + ... + b_{nb} u(t-n_k-n_b+1). \tag{3.4}$$

The structure is thus entirely defined by the three integers na, nb, and nk. na is the number of poles, nb+1 is the number of zeros, and n_k is the pure time delay (the dead time) in the system. The parameterization used here are $n_a = 7$, $n_b = 2$, $n_k = 8$ and the number of free coefficients is set to 9.

3.3.4 Regression models results

The performances of the developed regression models are based on the best fit estimation and the performance of the residual analysis. The best fit estimation describes the closeness of the predicted output to the experimental data. The residual analysis determines the error between the model's predicted output and validation data from the experiment. If the autocorrelation function falls between the two straight lines this indicates a very good model.

1. Nonlinear ARX model (nlarx)

Figure 3.9 shows that the percent best fit of the simulated output to the measured validation data was 97.25 when heating from 17 ◦C to a set point of 80 ◦C. This shows that the model predicted the MEF process with a very high accuracy. Additionally, Figure 3.10

shows that the residual lay mostly within a very confident region (from 0.12 to −0.12), with a tolerance of +−2%, and the cross-correlation function lay between −0.9 and 0.9. Hence, this model was able to represent the MEF process at a high level of confidence.

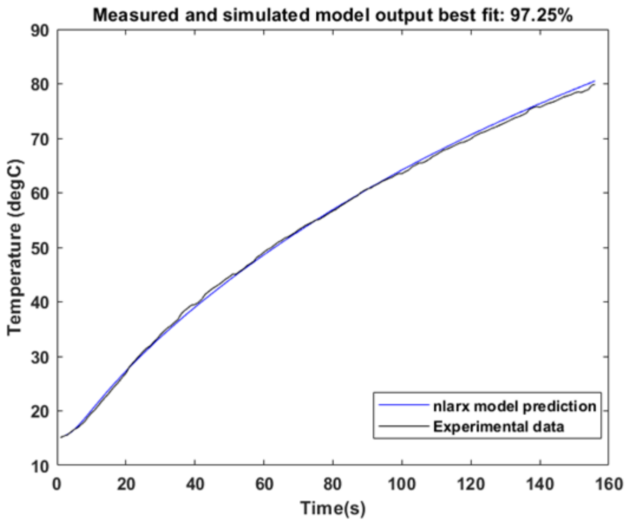

Figure 3.9 The % best fit plot of the nlarx model between the simulated and measured output

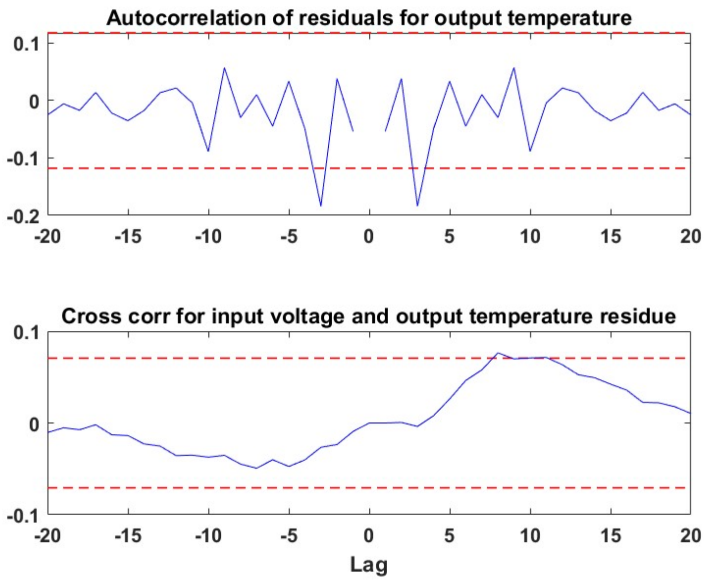

Figure 3.10 Plot of the co-relation and residual analysis of the nlarx model

2. Process model (P1D)

From Figure 3.11 belowthe % best fit of the simulated output to the validation data is 97.83 when heating from 17^0C to a setpoint of 80^0C. This shows the model predicts with a very high accuracy the MEF process. In Figure 3.12 it is observed that residual lies outside the confident region (0.12 to -0.12) and the cross-correlation function lies within -1.9 and 0.9. This indicates the residuals are not co-related and the confidence of the model's capability of validating actual data is low.

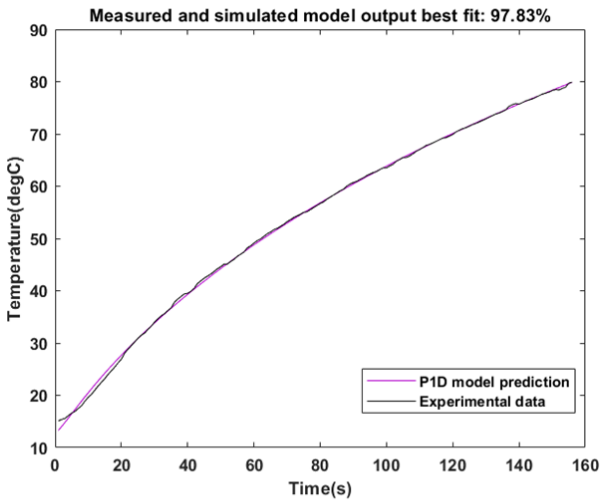

Figure 3.11. The % best fit plot of the process model between the simulated and measured output

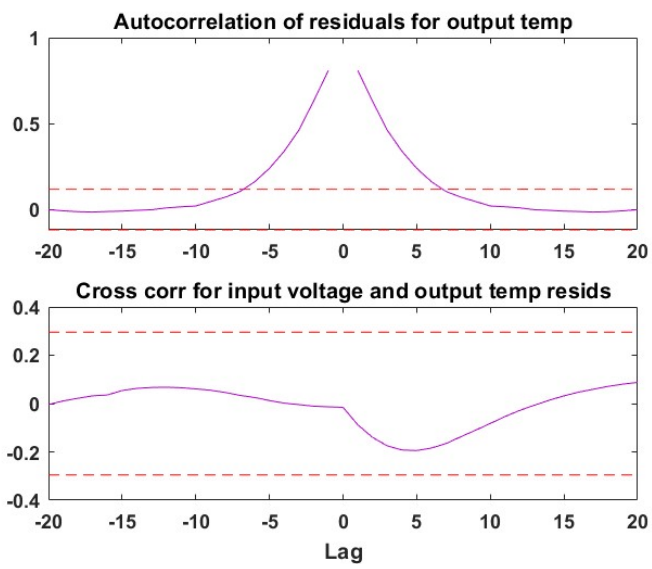

Figure 3.12. Plot of the co-relation and residual analysis of the process model

3. ARX model (arx728)

The % best fit of the simulated output to the validation data of the arx728 model from Figure 3.13 below is 93.78 when heating from 17^0C to a setpoint of 80^0C. This shows the model predicts with a very high accuracy the MEF process. The residual of the arx728 model lies outside the confidence region (0.12 to -0.12) and the cross-correlation function lies outside -0.9 and 0.9 as shown in Figure 3.14. This indicates the residuals are not co-related and the confidence of the model's capability of validating actual data is low.

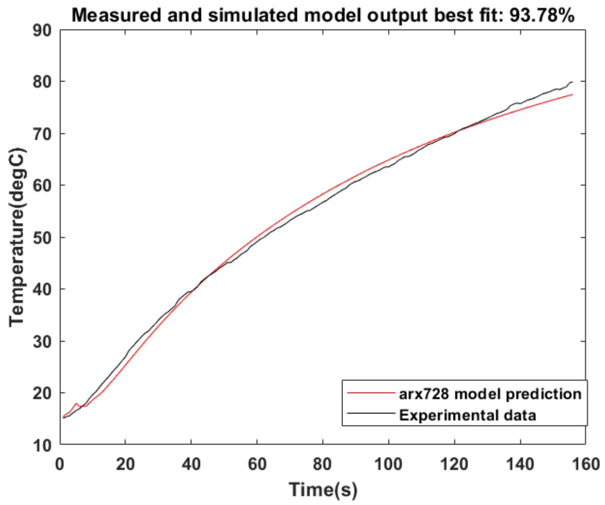

Figure 3.13 The % best fit plot of the Discrete ARX (arx728) model between the simulated and measured output

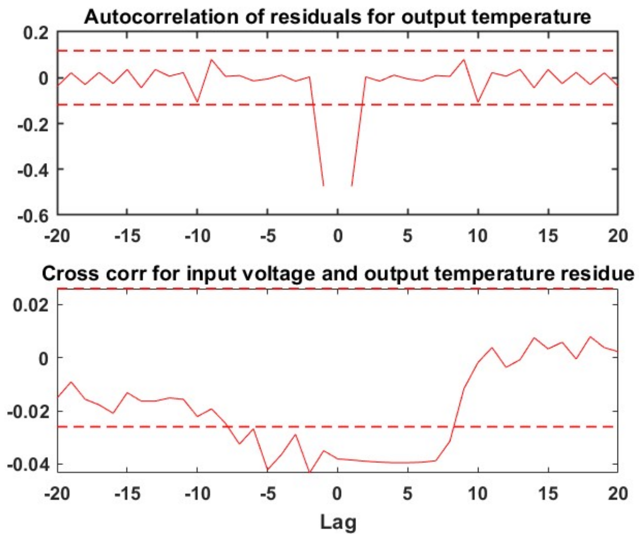

Figure 3.14. Plot of the co-relation and residual analysis of the Discrete ARX (arx728) model.

Based on the performance criteria of the % best fit plot, the confidence given by the residual and co-relation analysis, the nonlinear ARX (nlarx) model was adopted given its high performance. The autocorrelation plot of the nlarx model stays within the confidence region during validation.

3.4 Experiment

3.4.1 Food sample preparation

The food product used is 'British fresh whole milk' purchased at a local supermarket. The initial temperature of the refrigerated milk is between 15^{0}C to 17^{0}C. The initial electrical conductivity of the milk at start-up and at initial product temperature is measured using PC60 Aprea conductivity meter. The volume of milk used for each experiment batch is 500ml.

3.4.2 Batch ohmic heater

The batch Ohmic heater used was the C-Joule LAB 100, which is commercially available through C-Tech Innovation C-Joule LAB 100, accessed 12 November 2021 https://www.ctechinnovation.com/product/c-joule-lab-100/. The batch ohmic heater made by C-Tech Innovation which has been used in model validation is shown in Figure 3.15.

Figure 3.15. Image of the C-Tech Innovation batch ohmic heater used in model validation.

The system was fitted with a control panel and a heating cell with removable titanium (Ti) electrodes. Four thermocouples with variable positions were used to read the temperature. An emergency stop, start/stop/reset switch, and data port for removable flash drives were on the control panel. The set-up and operation of the unit were accessible via the touch screen. The Ti electrode was made of trapezium with a total size 17 × 14.5 × 15.3 × 15 × 0.1 cm (length × length × slant height × height × thickness). Figure 3.16 shows the arrangement of the Ti electrodes in the heating cell.

Figure 3.16 Heating chamber consisting of the heating cell, Ti electrodes and 4 mounted thermocouples.

The total size of the heating cell is 17cm x 15cm x 8cm x 9cm (length x height x width x width). Therefore, the gap between the electrodes was 8cm at the shortest point and 9cm at the longest point. During the experiment given the fixed volume of 500ml which corresponds to a height of 4cm in the heating cell, the shortest gap between the electrodes is 8cm while the largest gap due to the slant profile is 8.3cm. The control panel of the ohmic heater consists of a voltmeter, an ammeter, a timer, a main switch, and functions for manual/automatic operation. The AC power supply is a 3-phase supply at 50 Hz at 415V.

3.5 Model validation and results

Experiments using the batch ohmic heater follow the plan described in Table 3.5. For every batch of product heated, the actions in the table are followed.

Table 3.5. A set of tasks in sequential order in the batch ohmic heater experiments

S/N	**Experiment task**	**Reason**
1	Clean the heating cell and electrodes with distilled water	To remove impurities that can affect the electrical conductivity
2	Serve a measure of 500ml of milk in a beaker	To ensure consistent product quantity
3	Measure the initial product temperature	To confirm the required start temperature
4	Measure the electrical conductivity	To determine the initial electrical conductivity
5	Fill the ohmic cell with the product	
6	Insert the removable flash drive to the control panel	To save temperature, voltage, current and power values
7	Enter a temperature set point	To commence heating
8	Close the heating cell enclosure and start	Prevent spillage and ensure safe operation of the heater
9	Continue to higher temperature setpoints or restart the process.	

To validate the models, temperature data collected from the experiment were compared to the simulated model results. The voltage inputs were also the real-life data measured from the C-Tech Innovation batch Ohmic heater. In the model comparison figures, 'Ohmic' represents the Ohmic heater temperature from experimental data and 'comsol', 'sysid', and 'simulink' represent the first principle COMSOL model, the regressor model, and the lumped Simulink model, respectively. The applied voltage was controlled by a simple PID controller in the C-Tech Innovation batch Ohmic heater. In the following comparison table, 'Ohmic heater' represents the experimental data and heating time that were validated against the developed models.

3.5.1 Validating from 23^0C to 40^0C

The result presented below show the developed model being validated with experimental data and voltage input. The set point is 40^0C from an initial temperature of 23^0C. Table 3.6 also shows the steady state error from the set point within a total time of 26s.

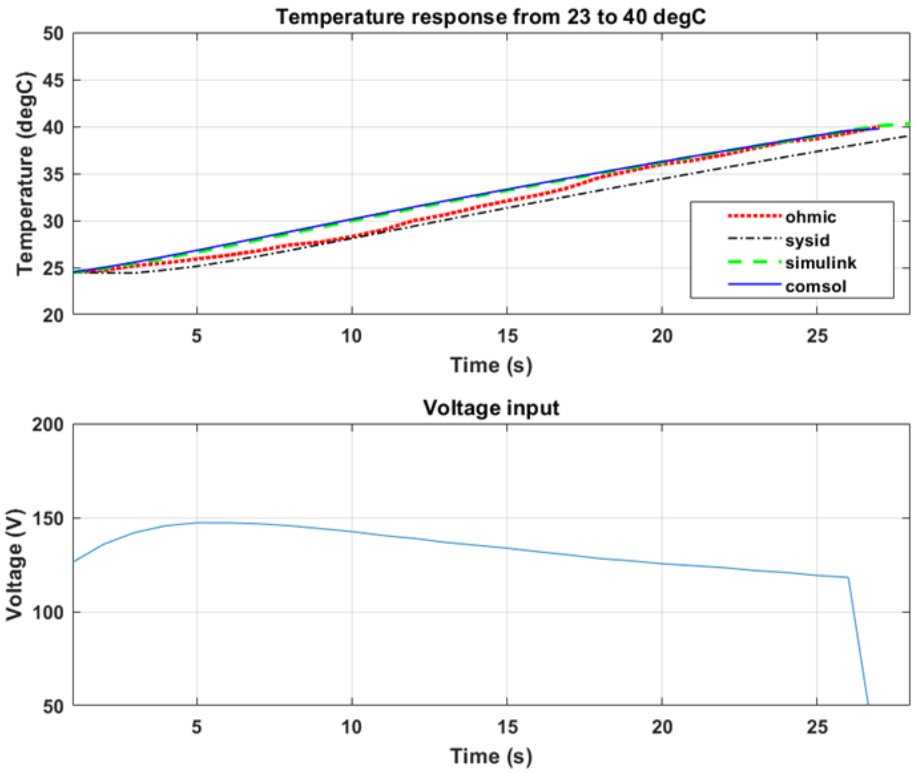

Figure 3.17. Model comparison between 23^0C to 40^0C

From Figure 3.17 above, the peak voltage is close to 150V. This agrees to the equation describing the electrical conductivity as a function of temperature in Eq.2.4.2.3 and the volumetric heat produced in Eq.2.4.2.2 The electrical conductivity was modelled as a function of temperature, therefore at a lower temperature higher electric field is required to produce proportional volumetric heat. In Table 3.6 below, the prediction performance of the different models to represent the MEF process was determined using the set point error as a benchmark. The COMSOL model prediction performance is 98%, the SIMULINK model prediction performance is 99% and the regressor model prediction performance is 90%.

Table 3.6. Performance comparison of Figure 3.17

Model	**Set point temperature 40^0C**	**Set point error**
Ohmic heater	40.0	0.0
COMSOL model	39.7	0.3
SIMULINK block model	40.1	0.1
Regressor model	38.4	1.6

3.5.2 Validating from 42^0C to 60^0C

The results presented below show the developed model being validated with experimental data and voltage input. The set point was 60^0C from an initial temperature of 42^0C. Table 3.7 shows the steady state error from the set point within a total time of 37 s.

Table 3.7 Performance comparison of Figure 3.18

Model	**Set point temperature 60^0C**	**Set point error**
Ohmic heater	59.1	0.9
COMSOL model	59.6	0.4
SIMULINK block model	59.6	0.4
Regressor model	57.6	2.4

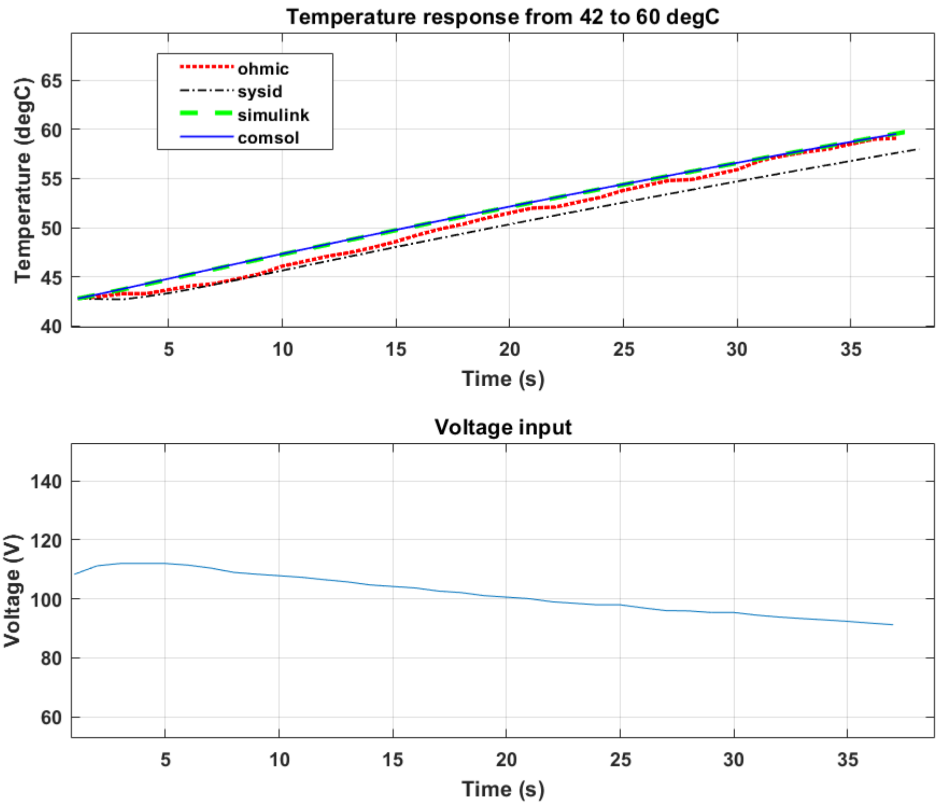

Figure 3.18. Model comparison between 42 and 60 ◦C

Figure 3.18 shows that the peak voltage was about 125 V. This shows that with the increased food temperature, a proportional increase in the food conductance was achieved. Therefore, the magnitude of the electric field to raise the food temperature was reduced compared to the results presented Figure 3.17. The heating time shown in Figure 3.18 was longer than that in Figure 3.17 because of the reduced electric field. Table 3.7 shows an increase in the set point error in comparison to Table 3.6. The increase in set point error could be attributed to an increase in the temperature range of validation. The prediction performance of the COMSOL and SIMULINK models was 97%, while the prediction performance of the regressor model was 86%.

3.5.3 Validating from 61^0C to 80^0C

The results presented below show the developed model being validated with experimental data and voltage input. The set point was 80^0C from an initial temperature of 61^0C. Table 3.8 shows the steady state error from the set point within a total time of 55 s.

Table 3.8. Performance comparison of Figure 3.19.

Model	**Set point temperature 80^0C**	**Set point error**
Ohmic heater	80.2	0.2
COMSOL model	81.0	1.0
SIMULINK block model	82.0	2.0
Regressor model	79.6	0.4

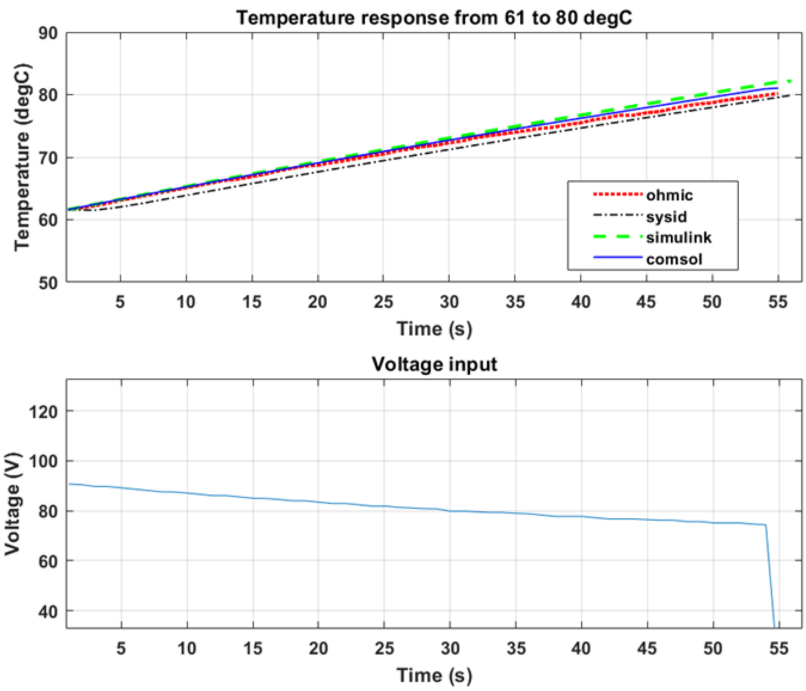

Figure 3.19. Model comparison between 61^0C to 80^0C

From Figure 3.19 above, the peak voltage from the ohmic heater is 87V. The heating time seen in Figure 3.19 is longer than that of Figure 3.17 -3.18. This shows that the heating time is proportional to the magnitude of the electric field. Table 4 shows that COMSOL model had a prediction performance of 94%, the SIMULINK model had a prediction performance of 89% and the regressor model had a prediction performance of 97%.

3.5.4 Validating from 17^0C to 80^0C

The results presented below show the developed model being validated with experimental data and voltage input. The set point was 80^0C from an initial temperature of 17^0C. Table 3.9 shows the steady state error from the set point within a total time of 141 s.

Table 3.9. Performance comparison of Figure 3.20.

Model	**Set point temperature 80^0C**	**Set point error**
Ohmic heater	79.1	0.9
COMSOL model	73.3	6.7
SIMULINK block model	73.0	7.0
Regressor model	77.8	2.2

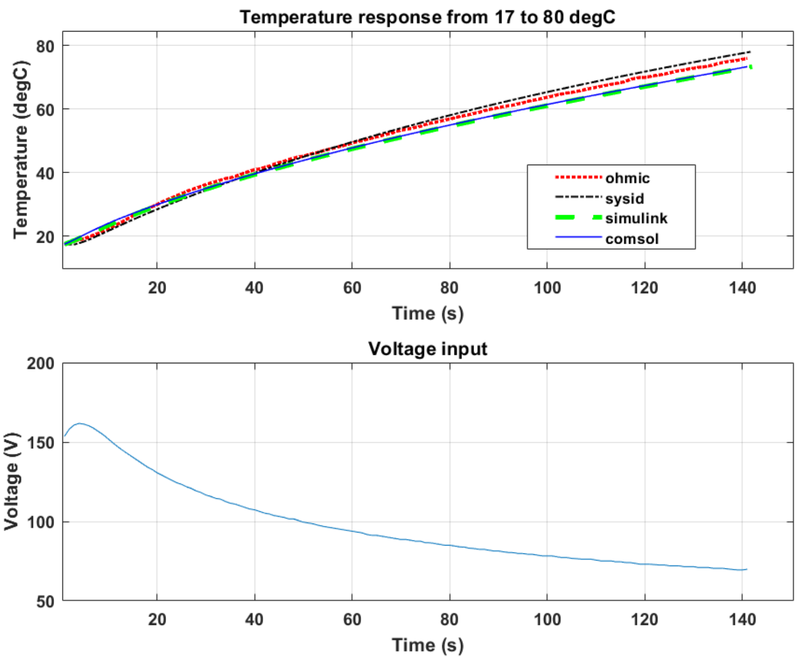

Figure 3.20 Model comparison between 17^0C to 80^0C

Figure 3.20 shows that due to the low electrical conductivity at 17 ◦C, very high electric field was needed to volumetrically raise the temperature of the food. After about 60 s of heating to prevent uncontrolled temperature, the in-built PID controller in the batch Ohmic heater regulated the applied voltage with regard to the set point temperature. Table 3.9 shows an increase in the set point error value for a large temperature set point value for both the COMSOL and SIMULINK models. The COMSOL model had a prediction performance of 89%, the SIMULINK block model had a prediction performance of 88%, and the regressor model had a prediction performance of 96%

3.6 Summary

In this chapter, a novel approach in modelling and validation of the MEF and OH process using a range of techniques was presented. Comparisons between a first principle PDE model, a lumped ODE model and a regression model using system identification have been made. The lumped ODE model illustrates a simpler and 'close to the real thing' representation for software requiring lower computational power. The analytical solution obtained from lumped ODE model offers a clear view into how the food process variables interact and affect the result.

The error seen from these models could also be attributed to the errors from the real life PID-produced voltage profile. Given that the PID controller of the batch Ohmic heater was tuned according to the user, errors were transferred to the models being validated by the voltage inputs. These models showed robustness and tolerable error values given that they were validated by a simple PID voltage input from a real-life machine. The first principle PDE model using COMSOL shows that any OH operation using MEF could be designed and validated using an iterative solution based on the BDF algorithm. The regressor model using system identification is a data-driven model based on experimental data. The system identification technique is useful when modelling a highly complex system that cannot be easily represented mathematically. However, the system identification technique can also add intrinsic system experimental errors into the regression model, so the experimental data must be accurate and post-processed to remove noise. Future work will model a continuous MEF system that accounts for flow dynamics, including the viscosity and laminar flows of different foods, and relationships with temperature change.

Chapter 4. Design and development of the continuous flow ohmic heater

The designed continuous flow ohmic heater shown in Figure 4.1 consists of the following parts:

A: Infeed tank

B: Infeed pump

C: Applicators/electrodes and applicator/electrode housing

D: Outfeed tank

E: Control panel

F: PC control

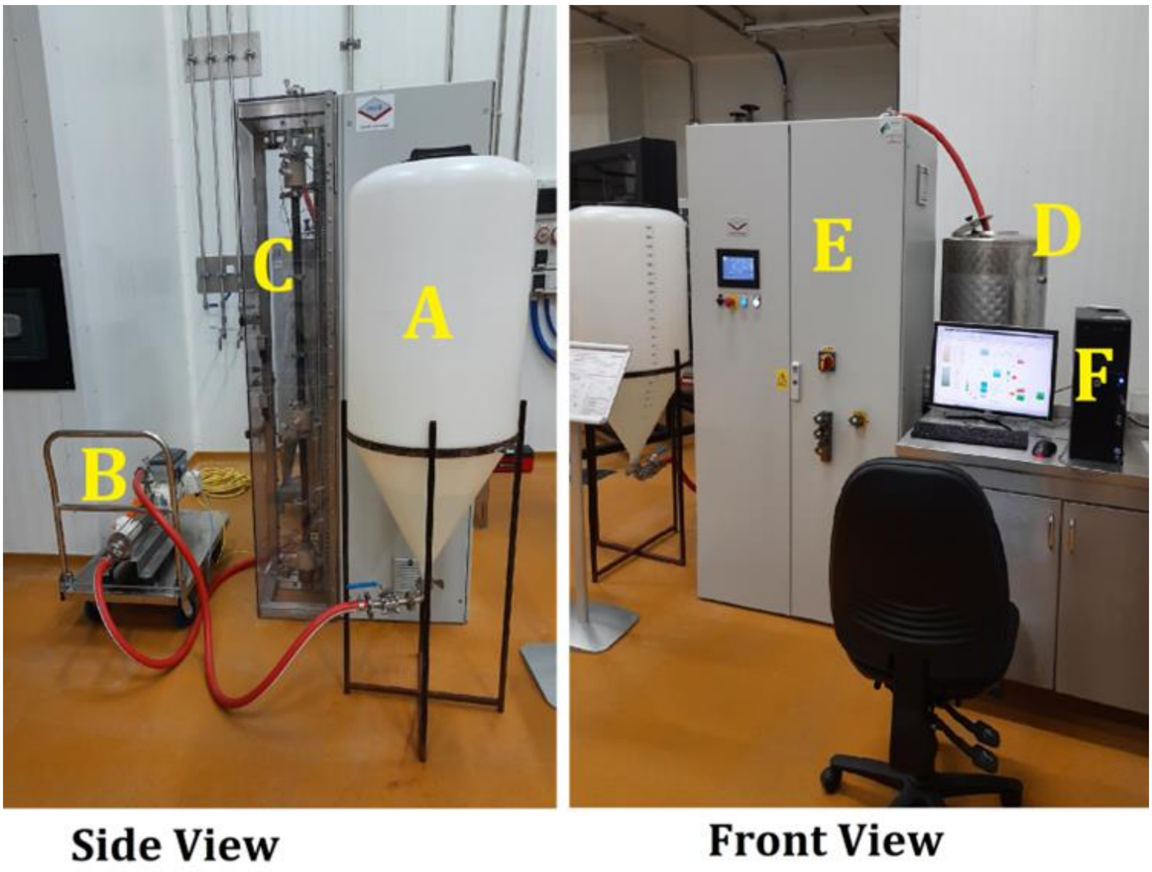

Figure 4.1. Continuous flow ohmic heating system pilot plant designed at NCEFE in collaboration with Ohm-E technology (UK)

From the CFOH unit in Figure 4.1 above, the pilot plant has the following features:

- delivering nominally 10 KW into a wide range of product conductivities from 0.15S/m to 0.9 S/m (infeed).
- comprising a continuous process applicator with three electrodes operating at voltages up to 4.2 kV.
- being integrated with and being controlled from a PC- MATLAB or LabVIEW platform.
- driving a suitable pump with pump speed control for product flow rate control of up to 60L/hr

In addition, the power supply to the unit is from a 3 phase 32A N +E supply to operate at 10kW but can deliver 5kW when powered from a 240 V single phase supply. The applicator, power and control system can be scaled up to higher power levels of up to 15 kW from a 63A supply and over a wider range of conductivities 0.11S/m to 1.1 S/m (infeed) as a pilot process with further development/upgrade of some components.

4.1 Hazards of the CFOH

Comprehensive risk assessment was carried out at the beginning of your PhD project and health and safety procedures have been followed during all experiments (The risk assessment documents are attached at the appendix). The equipment operates at high voltage up to 4.2kV therefore, contact with high voltage can be lethal. The applicator enclosure, materials of construction and safety systems guard against contact with high voltage. The safety mechanisms in place will be discussed in section 4.2.

Another hazard present during the use of the CFOH is contact with hot products. Since food products can be heated to over 90 ◦C in seconds the risk of burns from contact with heated product or pipework is present. In this regard, the product outfeed material, discharge pipe and outfeed tank were designed to be secure to prevent unwanted movement and isolated from physical contact when the CFOH is in operation.

Arcing within the applicator could occur due to turbulent flow of product within the applicator or due to intermittent contact with the electrodes. Arcing within the applicator does not present any immediate hazard to the operator. Arcing within the applicator can be observed by smell of burnt food products. This can be corrected by ensuring that food flow is not intermittent and the electrode surface in contact with the food products are clear of fouling.

4.2 Safety mechanism of the CFOH

The safety mechanism designed for the CFOH consists of trapped key isolator-interlock system that prevent unauthorised access to the applicator and electrodes and prevents the CFOH to be in operation when physical access to the applicator is possible. The applicator and control panel are fitted with a trapped key mechanical-electrical interlock system which guards against and prevents access to the applicator enclosure without the HV having been electrically disabled back in the control panel. The applicator doors can only be opened when their mechanical lock keys are released from a key exchange on the control panel door shown below in figure 4.2. The door keys can only be released from the key exchange when a separate master key trapped in an isolator switch is turned disabling powering of the HV and in doing so releasing this key to be used in the key exchange. The master isolator switch in releasing the door keys is trapped in the key exchange until released by reinsertion and turning of both door keys. The door keys when opening the door locks on the applicator become trapped in the lock and cannot be released until the doors are locked.

Figure 4.2. Highlighted in red is the electromechanical trap door key located on the control panel.

4.3 Applicator and control panel description

The applicator comprises three electrodes contained in insulating housings arranged in a vertical column with insulating pipe spool sections between the electrodes. High voltage is applied to the centre electrode relative to the infeed and outfeed electrode creating two heating sections/lengths one between the infeed and middle electrode and a second between the middle and outfeed electrode.

Power delivered to the product for heating is controlled by varying and controlling the voltage applied to the HV transformer primary using a thyristor operating in phase angle control mode (as opposed to burst firing). The thyristor setting is controlled by the PLC and via the lab-based PC control system.

The high voltage applied between the electrodes is derived from a step-up transformer which can be powered at 230V or 415V on its primary side. Turns ratios are provided which can realise different high voltages on the secondary of the transformer, 10.1 turns ratio will generate 4.2kV from a typical UK supply.

The electrode separations can be altered by combining different spool lengths to suit the product conductivity being processed. Four basic length configurations are provided for to cover the power delivery (10 kW) into the range of conductivities (0.11 to 1.1 S/m) using a voltage range up to 4.2kV. Other voltages and configurations can be configured with appropriate design and calculation to extend the operation outside the present scope.

The applicator and the electrical design incorporate a degree of flexibility and several different configurable options to fit with the development and research purposed intended for the CFOH. With this configurable and alterable arrangement potential comes a critical responsibility for informed and guided and approved only interventions.

i. The applicator enclosure has been designed to give very open and easy access to the applicator for assemble and configuration with large doors opening two sides of the framework.
ii. Protection and guarding from HV whilst having easy access by doors are achieved using dual circuit electrical safety door switches and a mechanical-lock/electrical-interlock trapped key interlock system fitted on the applicator doors and on control panel. These

systems ensure that the applicator enclosure cannot be opened without having disabled the generation of any HV in the control panel.

iii. The electrode housings can be easily repositioned, and different applicator lengths configured using easily adjustable electrode housing support shoes mounted on a support column.

iv. The electrode connections are via HV plugs mating with a HV receptacle board. High Voltage is generated within the control cabinet and is connected to the applicator electrodes using HV cable routed directly from/through the rear of the control panel into the applicator enclosure to ensure isolation from this. No HV cables are routed to the applicator other than via the defined connections on this HV lead-through path.

v. The enclosure polymer panels are secured using tamper proof fasteners. The trapped key locks and safety switches are secured using tamper proof fasteners so that they cannot easily be removed or defeated.

In figure 4.5 below, the applicator and control panel schematic are shown. The image on the left shows the top view while the side view is shown on the right-hand side.

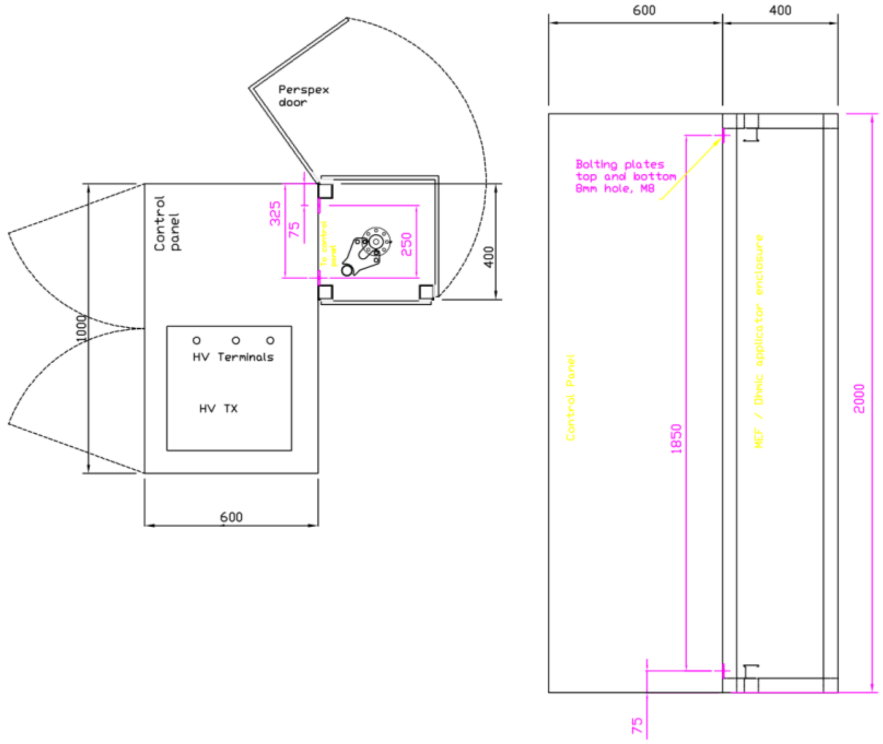

Figure 4.5. Applicator and control panel schematic measurements are in mm.

In figure 4.6 below, the internal layout of the CFOH control panel showing the different electrical components highlighted.

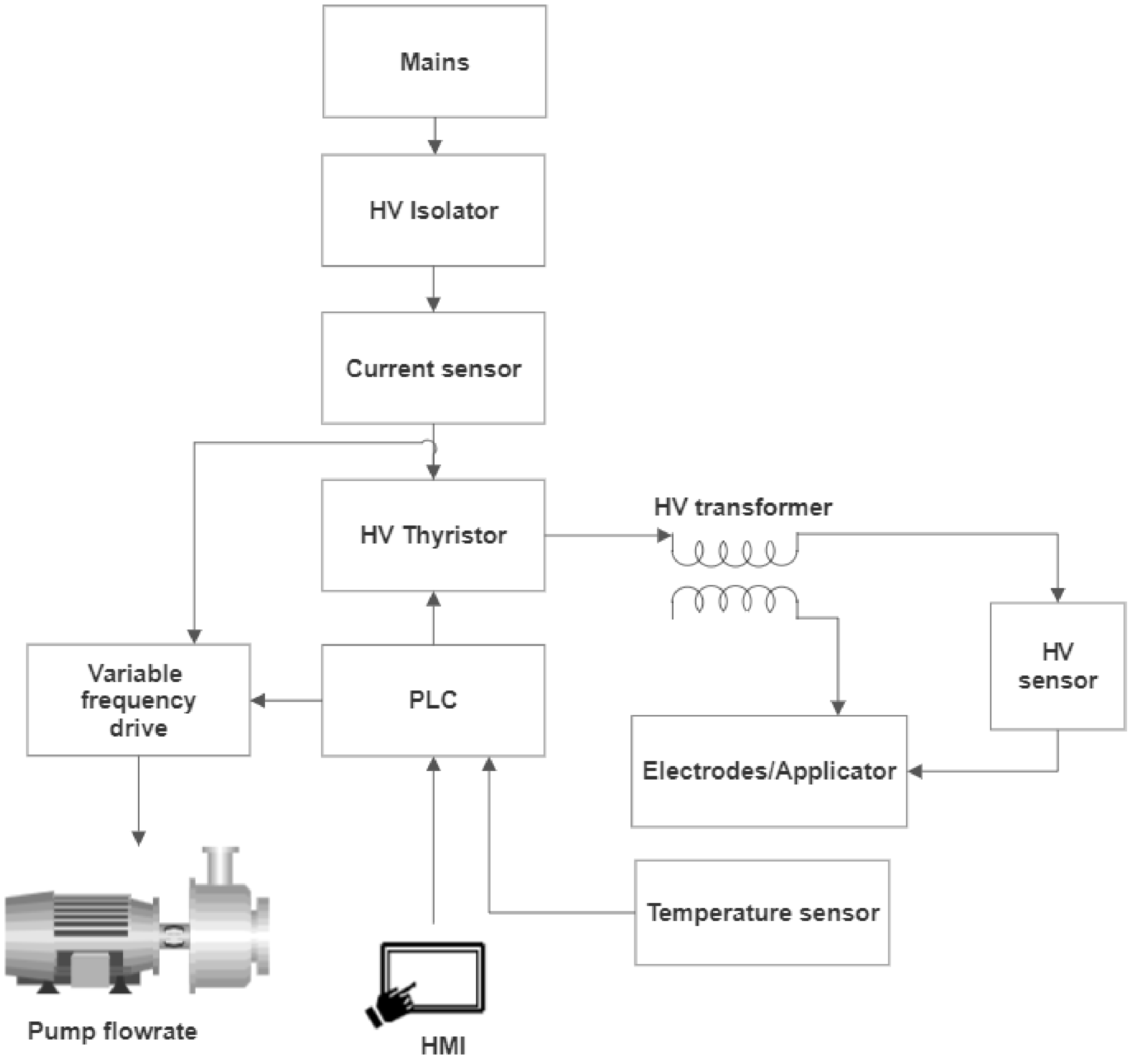

Figure 4.6 Internal structure of the CFOH control panel.

The main components of the CFOH which are:

1. HV transformer
2. HV thyristor
3. Current sensor
4. Isolator
5. Variable frequency drive

6. Ethernet switch
7. Voltage converter
8. PLC and I/O cards
9. HMI
10. HV zone consisting of HV sensor and applicator contacts.

Other components in the control panel includes contactors, circuit breakers, safety relay, safety interlock switches, HV fuse and holders and signal conditioners for analogue inputs.

4.4 Heater assembly

The heater is assembled in the applicator enclosure in a vertical column comprising three electrode housings with insulating spacing spools between the housings shown in figure 4.7.

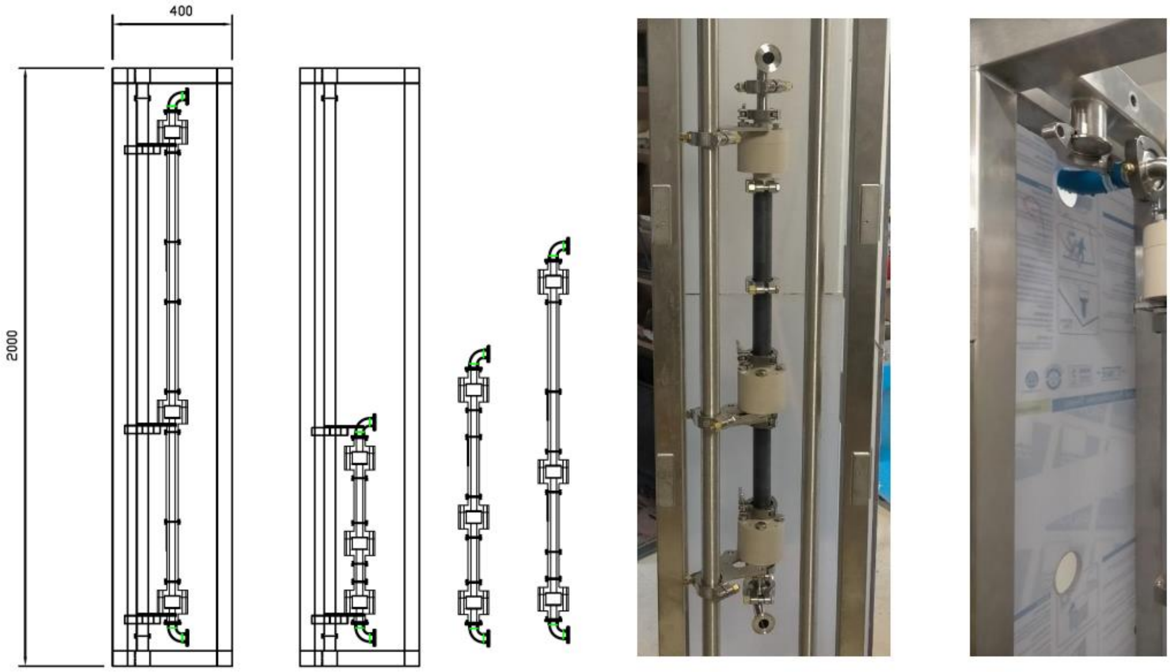

Figure 4.7. Applicator arrangements and pipework layout.

Each electrode housing is supported using a support shoe which is clamped to the vertical tubular stainless steel column. The support shoes are positioned on the column to suit the applicator length being configured. The assembly can also be removed intact attached to the tubular stainless steel support column disassembled or assembled outside the applicator and then inserted into the framework attached to the support column.

There are four basic configurations as shown in figure 4.7. The applicator enclosure has openings to admit infeed pipework at the bottom and four outfeed openings corresponding to these basic configuration lengths. Other lengths can be configured with an appropriate connection to the column inside the applicator enclosure, for example by inserting another elbow to attach to a vertical tube or hose.

4.5 PLC-HMI and PC control

The control panel contains an integral Mitsubishi PLC which is in effect locally driving the thyristor. The control is designed then to integrate with a PC based control system which is integrated using OPC server (the OPC server will be discussed in chapter 5) which will generate an output value/setting for the thyristor. This setting might originate from a conventional PID control loop running on the PC, a bespoke mathematically calculated value or a manually input value input from the PC. This setting is communicated to the PLC over an ethernet connection. The PLC does not have any PID, or control loop programmed on it.

The applicator and pumping can also be controlled locally at the control panel using the HMI on the door. All instrumentation is processed by the PLC with the data communicated to the PC over the ethernet connection for processing or logging.

The thyristor and a motor inverter in the panel are controlled by the PLC via ethernet connections inside the panel. The motor inverter fitted in the panel and is sized to drive pump motors up to 1.5kW, connected for 230V three phase control.

Table 4.1 below shows the parameters which are measured by the PLC or estimated by the PLC from measured variables and shown on the HMI.

Process parameter	**Name**
Thyristor measured output voltage V rms (via ethernet from thyristor)	V rms
Thyristor measured output current I rms (via ethernet from thyristor)	I rms
Primary current measured separately	CT3
Secondary current applicator infeed section	CT1
Secondary current applicator outfeed section	CT2
Infeed temperature T1 (thermocouple)	T1
Outfeed temperature T2 (thermocouple)	T2
Fibre optic probe temperature 1	FT1
Fibre optic probe temperature 2	FT2
Fibre optic probe temperature 3	FT3
Fibre optic probe temperature 4	FT4
High voltage supply	HV
Calculated parameters	
Applicator power P Watts. Product of V rms x I rms	P

Table 4.1 CFOH parameters

The HMI screens showing the different operational settings of the CFOH are shown below.

Figure 4.9 below shows the default HMI home page of the plant control. On this page, the power supply to the CFOH can be switched on/off by pushing the ‘power start’ button. The setpoint of the thyristor which is a number ranging from 0 to 100 needs to be entered in the ‘Setpoint (%)’ section. The number entered scales the HV supply in percentage, e.g if 100 is entered the maximum voltage of 4.2kV will be supplied if 50 is entered 2.1kV will be supplied and 0 gives 0V. The infeed pump can be turned on/off by pushing the ‘pump start’ button also, the appropriate frequency related to the product mass flow rate will be entered in the ‘speed (Hz)’ section. If the pump is turned on, and the flowrate in Hz is set to zero the pump will operate in idle mode.

Figure 4.9. The default home screen of the CFOH

Also shown in figure 4.9 is the emergency button that cuts out power entirely to the unit when it is pressed. When the emergency button is pressed a combined action of resetting the emergency switch and pressing the reset button returns the unit back in normal work mode.

Figure 4.10 shows the analogue outputs screen of the CFOH. The screen is accessible by clicking the ‘Analogue outputs’ button on the default screen.

Figure 4.10. Analogue output screen.

The analogue output screen shows the information that describes the PLC tags attached to the process parameters for analogue outputs. Currently they are not used but the tags are provided for future upgrades to the CFOH.

The next screen shown in figure 4.11 is the analogue input screen. The screen shows the process parameters highlighted in table 4.1.

Figure 4.11. The analogue inputs screen.

The power control screen is shown in figure 4.12. The power control screen contains the setting to turn on/off the power for heating, settings to set the mode of operation of the voltage whether in continuous mode or pulsed mode. For this research continuous mode (MEF mode) is used to explore the effect of pulsed electric field (PEF) in future research the PEF mode would be selected. The ability to select the preferred mode makes the CFOH advanced for specific application regarding the applied electric field.

Figure 4.12. Power control mode.

Also, in the power control mode in figure 4.12 other information such as the magnitude of the supplied voltage, the frequency of the alternating current (AC), electrical power, voltage and current from the mains are provided. An option to calculate the power factor of the CFOH plant in future use is provided but it was not used during this research. The secondary tap is set to 100% to ensure the maximum HV from the HV transformer is supplied. The secondary tap value is the same variable as the thyristor setpoint on the default home page.

The pump control page is shown in figure 4.13. The page expands on the pump control settings on the default home page.

Figure 4.13 The pump control page.

On the pump control page, the operator can input the desired flowrate frequency value which corresponds to an experimentally calibrated mass flowrate. The pump can be turned on/off on this page. The torque parameter is not used in this experiment, but it is a feature that can be used in future experiments to determine the specific power consumed by the pump when products of different viscosity are pumped.

The last screen is the alarm threshold screen shown in figure 4.14. The screen contains parameter values to keep the CFOH in safe operation.

Figure 4.14 Alarm threshold screen.

Shown in the alarm threshold screen above, an alarm is triggered when the infeed temperature is greater than or equal to 60^{0}C and the alarm cuts the power to the CFOH when the inlet temperature reaches 80^{0}C. For the outfeed thermocouple and four temperature fibre probes, a cut out temperature of 125^{0}C is set. The alarm setting for the temperature measured is to prevent overheating within the CFOH. This is necessary because temperature within the heating chamber can rise from 220^{0}C to 90^{0}C in seconds. The other alarm set for CT1+CT2 set a cutout limit to the current drawn within the two sections. The current cutout limit is to protect the CFOH from foods that have high electrical conductivities or when the electrical conductivities of heated food rises far above the recommended limit. The flexibility of the alarms makes the CFOH robust such that it can be upgraded to heat foods within a certain conductivity range/temperature range. The alarm will be displayed along the bottom of all screens and the cutout turns the applicator power off by switching of the enable/run command to the thyristor.

4.6 General operation procedures

Experimental planning is crucial to safely and reliably operate the CFOH system. Heating can be so rapid that it must/should be known in advance what will happen when the unit is switched on. Experiments and processing should not be undertaken without prior assessment and calculation of expected performance (in simulation or theoretically). With prior knowledge of the product infeed conductivity applicator power and current vs applied voltage can easily be determined and from that heating and temperature rise vs flowrate. In the absence of other an assumption of 2% / °C increase in conductivity will be reasonable for predicting performance.

Below are the general safe operating procedures:

1. Inspect the unit physically to check for lose probes, unconnected piping, and closed valves.
2. Connect the unit to the mains and ensure the connections are tightly secured.
3. Turn on the unit and clear any errors by pressing the reset button.
4. Do not turn on the thyristor and pump control yet.
5. Have sufficient product in the infeed tank so as not to run out and/or have a following solution or water to follow if needed. Have facilities to empty the applicator flush it and clean it afterwards on hand.
6. Measure the infeed product conductivity (S/m) and infeed temperature and confirm that it is as expected. Adjust the calculated performance to match the measured value (i.e., set a max thyristor value to prevent overheating).
7. Ensure proper connection of the outfeed pipework to check that the product discharge is secured and suitable for discharge of hot liquids and steam should this occur.
8. Enter the desired flowrate and start the pump.
9. Turn on the mains isolator switch. (Before turning ON, ensure the thyristor setpoint is 0 and establish that product has filled the applicator past the outfeed electrode.)
10. Enter a lower-than-expected thyristor setpoint initially, the value can be increased later to give a desired output temperature.
11. Adjust the pump speed if required.

12. Observe that the expected voltage is reached and that the expected power and current is drawn. Prepare to switch the unit off if conditions are not as predicted. If temperature rises, then for a given voltage the current drawn should increase and the power drawn should increase with temperature rise.
13. Poor or intermittent contact with the electrodes or air entrainment will lead to unstable operation.
14. Boiling of the product in the applicator will lead to unstable operation and the unit should be switched off if the product boils.
15. Be alert for any incidence of arcing with intermittent electrode contact and boiling.
16. The applicator should not be operated unsupervised or left under automatic control unsupervised.
17. The heater should not be operated in manual control setting mode unsupervised.

The operator must monitor the heater current and applied voltage (primary or secondary) and power drawn while heating. A falling current with the same applied voltage is often a signal that fouling, or a problem is developing which is leading to an increase in the electrical resistance in the applicator. Thyristor may generate an alarm if a load failure is detected. The CFOH processing should be completely predictable and follow prior calculation very well. If the electrodes and the applicator are staying clean and not becoming fouled, then operation should remain consistent and stable-steady. The operator should be looking for deviation from expected or recent operating conditions as this is generally indicative of something starting to impact on performance. Air, gas, or vapour pockets passing between the electrodes can cause instability and can result in arcing in the applicator.

When processing is complete the CFOH should be shutdown using the following procedures:

1. Switch off the power by re-pressing the red “Power Stop” button on the HMI, or by the associated command from the PC. The power on indicator will turn red.
2. Turn off the product pump.
3. Empty and flush the applicator by pumping through a cleaning solution for at least 5mins at 1L/min.
4. Do not leave product in the heater to dry and adhere to surfaces.

When operating in manual control, start with a LOW initial setting, incrementing this upward, should be used until experience is gained with the CFOH performance, and dynamics across different conductivities, with different flowrates and different voltages applied.

4.7 Summary

In chapter 4, the design and development of the CFOH was presented. The parts, layout and structure of the CFOH was presented. Different parts of the CFOH were described including the specification of the CFOH in terms of the maximum product flowrate, electrical power and output temperature. The voltage rating of the ohmic heater, maximum current rating and the maximum allowed electrical conductivity of food products through the ohmic heater were discussed.

The potential hazards of the CFOH which includes HV, and hot products discharge were discussed. Also, the risk assessments done before operating the ohmic heater are affixed to the appendix. Safety mechanisms incorporated to the CFOH to eliminate the risk of accidents were discussed. The safety mechanisms such as the HV protection that isolates the operator from contact with HV connection leads were presented. The CFOH was designed with a trap door mechanism to cut the supply of power when the control panel or any other safter doors are open. The trap door mechanism also ensures that unless all enclosures are closed with their keys in them, power is not supplied to the ohmic heater.

The use of heat resistant piping at the outfeed tank ensures the safe discharge of hot food products. The outfeed discharge pipe is securely fixed into the outfeed tank to ensure that at higher flow rate and temperature, the discharge pipe does not wobble and spray hot products. To prevent overheating and uncontrollable temperatures, series of alarms have been added. These alarms either alert the operator to high temperature or/and cut out power to the ohmic heater.

The applicators, electrodes, heater assembly and electrode housing were presented. The assembly describing the heating sections and the position of the electrodes were described. The component lists were presented, and the control panel design layout were shown. The interface between the control panel and the lab-based PC using OPC server communication protocol were discussed.

The operational guideline and the duties of the operator at start up and shut down operation of the CFOH were described. The duties include manual (not controlled) or automatic (controlled) heating and cleaning procedures. The operational guide ensures the safe and efficient use of the CFOH.

Chapter 5. Model validation and real-time control of a continuous flow ohmic heater

The research work presented in this chapter is conducted on the continuous flow ohmic heater. Having discussed the batch ohmic heater model development and validation in the previous chapter, this chapter presents an extension of the published work Oluwole-Ojo, Zhang, Howarth, & Xu. (2023) that addresses the following gaps in the literature as follows:

i. Model the continuous flow ohmic heater using a linear model represented in state-space or transfer function forms.

ii. Validate the linear model with experimental data.

iii. Apply advanced process control with the aid of the validated model on the physical plant.

iv. Evaluate the performance of different controllers on a continuous ohmic heater plant.

The linear model also aims to be used as a benchmark for testing and validating different continuous flow ohmic heater models in education and research. Furthermore, it presents a reduced algorithm with fewer process parameters but the same input-output dynamics of a physical system.

5.1 Continuous flow ohmic heater modelling and validation

5.1.1 Modelling the continuous flow ohmic heater

The transfer function (TF) model of the continuous flow ohmic heater has been developed. The TF model relates the change in the inlet temperature, applied electrical power, electrical conductivity as a function of temperature, product mass flowrate, thermophysical properties and the resulting change in the output temperature. The novel technique used to model the CFOH is to describe the 1st and 2nd stage shown in figure 5.1 as an independent reactor. This reactor mimics the continuous stirred heater reactor. This technique is a new technique compared to the work of previous authors.

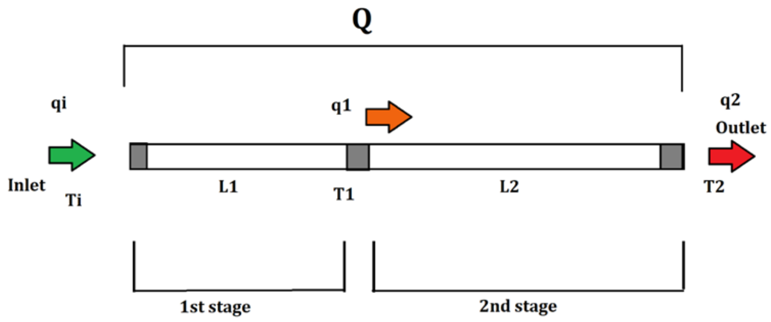

Figure 5.1. The ohmic heater diagram shows the different heating stages separated by electrodes.

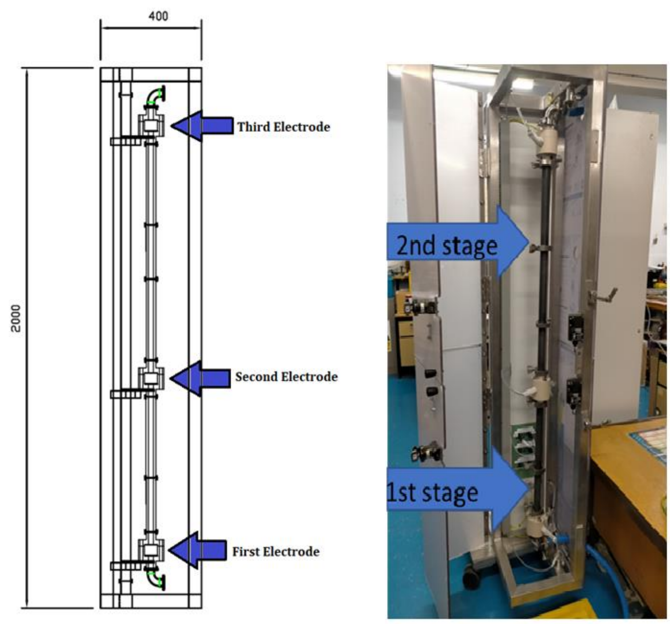

Figure 5.2. The ohmic heater cross section showing the different heating stages.

The first stage is examined for simplicity, with the electrical heating and fluid flow being the two dynamics involved. The balance equation of the heating stage can be described as:

Rate of energy into the chamber – rate of energy out of the chamber + rate of energy from electrical heating = rate of accumulation of energy.

This can be written as $\frac{dE}{dt} = \dot{m}_{in}H_{in} - \dot{m}_{out}H_{out} + Q$, (5.1)

where $\dot{m}$ is the mass flowrate, E is the accumulation of energy, Q is the rate of electrical heating and H is the enthalpy and is defined as:

$H = \frac{Energy}{mass}$.

Therefore:

$\frac{dE}{dt} = \frac{\rho v dH_{chamber}}{dt}$.

where ρ is the density and v is the volume. From the above equations above, we have:

$$\rho v \frac{dH_{chamber}}{dt} = \dot{m}_{in}H_{in} - \dot{m}_{out}H_{out} + Q$$

The enthalpy can also be represented as H = C (T-T_{ref}) where C is the heat capacity

Then:

$$\rho v C \frac{d\,(T-T_{ref})}{dt} = \dot{m}_{in}C\,(T_{in} - T_{ref}) - \dot{m}_{out}C\left(T - T_{ref}\right) + Q$$

The following conditions are assumed:

- The chamber is well mixed.
- The reference temperature is constant. T_{ref} = 0.
- Volumetric heating is achieved from the applied Q
- The same mass flowrate throughout. $\dot{M}_{in} = \dot{m}_{out} = \dot{m}$

Where T is the output temperature, T_{in} is the inlet temperature, T_{ref} represents the surrounding reference room temperature.

The total energy balance can therefore be written as:

$$\rho vC\frac{dT}{dt} = \dot{m}C\,(T_{in} - T) + Q \tag{5.2}$$

The energy balance in equation (5.1) has two inputs ΔT_{in} and ΔQ letting Q be constant.

Since the electrical heating Q is constant, therefore the rate of change of electrical $\Delta Q = 0$.

$$\rho vC\frac{dT}{dt} = \dot{m}C\,(T_{in} - T) \tag{5.3}$$

Taking the Laplace transform of equation 4.2. We obtain the following:

$\dot{m}\,C[T_{in}(s) - T(s)] = \rho vC\,sT(s)$

$\dot{m} = \dot{m}$ taking the flowrate constant and not a time dependent function.

$\frac{T(s)}{T_{in}(s)} = \frac{1}{\frac{\rho vs}{\dot{m}}+1}$

Let $\frac{\rho v}{\dot{m}} = \Psi$

$$\frac{T(s)}{T_{in}(s)} = \frac{1}{\Psi s+1} \tag{5.4}$$

For the effect of Q, set T_{in} =0.

$$\rho vC\frac{dT}{dt} = -\dot{m}CT + Q \tag{5.5}$$

The Laplace transform of equation 4.4 is then given by:

$\frac{T(s)}{Q(s)} = \frac{\frac{1}{\dot{m}C}}{\frac{\rho vs}{\dot{m}}+1}$

Let $\frac{1}{\dot{m}C} = k$, then the equation above can be simplified to:

$$\frac{T(s)}{Q(s)} = \frac{k}{\Psi s+1} \tag{5.6}$$

From equation (4.4) and equation (4.5), we have:

$$\mathrm{T(s)} = \frac{1}{\Psi s+1} T_{in}(\mathrm{s}) + \frac{k}{\Psi s+1} Q(\mathrm{s})$$

Given no change in the inlet temperature conditions $T_{in}(\mathrm{s}) = 0$.

The transfer function of the first section of the continuous ohmic heater is given by:

$$\frac{\mathrm{T_1(s)}}{Q(\mathrm{s})} = \frac{k}{\Psi_1 s+1} \tag{5.7}$$

Similarly, for the second heating stage of the ohmic heater the transfer function is given by:

$$\frac{\mathrm{T_2(s)}}{Q(\mathrm{s})} = \frac{k}{\Psi_2 s+1} \tag{5.8}$$

To determine the transfer function of the combined heating stages figure 5.3 below shows their interactions.

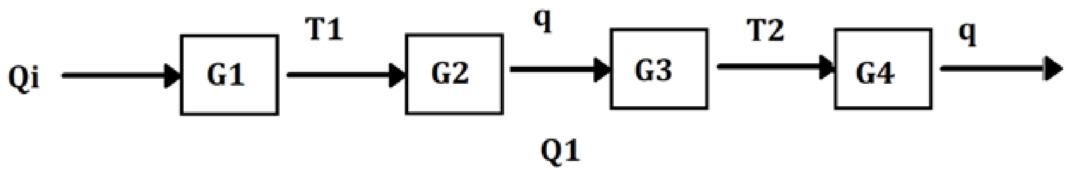

Figure 5.3 Block diagram showing the combined heating stages.

$\mathrm{Q_1 = Q}$

q = $\dot{\mathrm{m}}\mathrm{CT}$

The Laplace transform is given as q(s) = $\dot{\mathrm{m}}\mathrm{CT(s)}$

G(s) = $\frac{\mathrm{T_1}}{\mathrm{Q}_i} \cdot \frac{\mathrm{q(s)}}{\mathrm{T_1}} \cdot \frac{\mathrm{T_2}}{\mathrm{Q_1}} \cdot \frac{\mathrm{q(s)}}{\mathrm{T_2}}$

$\frac{\mathrm{q(s)}}{\mathrm{T_1}} = \frac{\mathrm{q(s)}}{\mathrm{T_2}} = \dot{\mathrm{m}}\mathrm{C} = \frac{1}{\mathrm{k}}$

Therefore, the second order overall transfer function describing the continuous flow ohmic heater is given by:

$$\mathrm{G(s)} = \frac{1}{(\Psi_1 s+1)(\Psi_2 s+1)}$$

where $\Psi_1 = \frac{\rho V_1}{\dot{m}}$ and $\Psi_2 = \frac{\rho V_2}{\dot{m}}$

and V_1 and V_2 represents the volume of each chamber while $Q = \frac{{V_e}^2 A\sigma}{L}$ .Here, V_e is the applied voltage, A is the area of the heating section, σ is the electrical conductivity as a function of temperature and L is the gap between the electrodes.

The developed state space model is given below as:

$A = \begin{bmatrix} 0 & 1 \\ -(1/(\Psi_1 * \Psi_2)) & -((\Psi_1 + \Psi_2)/\Psi_1 * \Psi_2) \end{bmatrix}$, $B = \begin{bmatrix} 0 \\ 1/(\Psi_1 * \Psi_2) \end{bmatrix} Q$, $C = [1\ 0]$, $D = 0$

The governing equations represented by the state space equation describes the dynamics of the CFOH. The state variable $1/(\Psi_1 * \Psi_2)$, represents the energy stored as temperature individually in each heating cell in series when electrical power is applied. The $((\Psi_1 + \Psi_2)/\Psi_1 * \Psi_2)$ state represents the rate of energy stored as a resultant effect of both the first and second heating chamber. The control vector is the applied electrical power Q.

The physical parameters of the CFOH used to develop the CFOH model are given in table 5.1.

Table 5.1 Physical parameters of the CFOH model

Parameters	Description	Unit
E	Energy	W
$\frac{dE}{dt}$	Rate of accumulation of energy	W/s
$\dot{m}_{in}$	Infeed mass flowrate	Kg/s
H_{in}	Infeed enthalpy	W/kg
$\dot{m}_{out}$	Outfeed mass flowrate	Kg/s
H_{out}	Outfeed enthalpy	W/kg
Q	Rate of electrical heating	W
ρ	Density	Kg/m^3
v	Volume	m^3
$H_{chamber}$	Enthalpy in the heating chamber	W/kg

C	Heat capacity	$Jkg^{-1}k^{-1}$
T	Output temperature	◦C
T_{in}	Input temperature	◦C
V_e	Voltage	V
A	Area	m^2
σ	Electrical conductivity	S/m
L	Length	m

The developed model in MATLAB/Simulink is described next.

In figure 5.4 below, the overall open loop model structure is shown. In the open loop model, the model is not controlled by a controller but by varying only the inputs and the temperature output is observed.

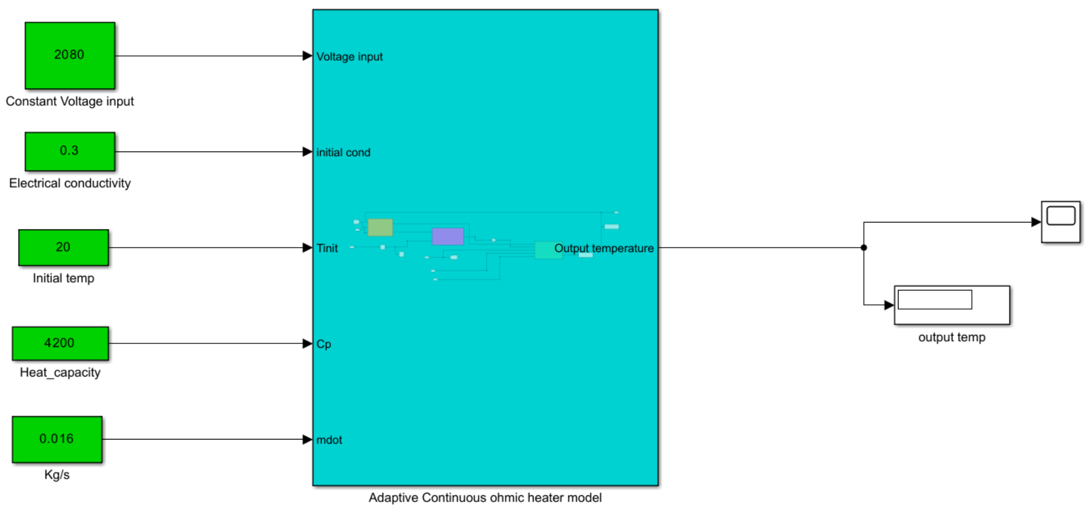

Figure 5.4 Overview of the CFOH model in Simulink

In figure 5.4 above, the inputs to the CFOH model are the Voltage (V), initial electrical conductivity (S/m), initial temperature (°C), heat capacity (J/kg°C) and the mass flowrate in kg/s. The output of the model is the output temperature of the heated product in ◦C.

Figure 5.5 below shows the next level model structure inside the adaptive Continuous ohmic heater model subsystem.

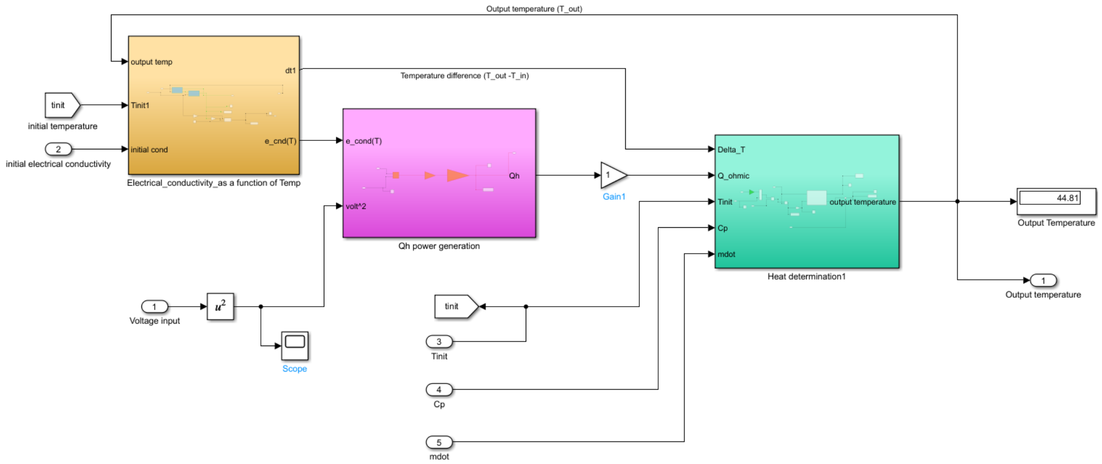

Figure 5.5 Internal subsystem structure of the CFOH model.

In figure 5.5, the main blocks which models the MEF process are shown. The orange block determines the electrical conductivity of the food product as a function of temperature. The inputs to the orange block are the output temperature, the initial temperature of the food and the initial electrical conductivity of the food. The outputs of the orange block are the temperature difference and the electrical conductivity as a function of the output temperature. The temperature difference is the constant changing difference between the output temperature and the input temperature. This changing temperature difference influence gives a proportional change in the electrical conductivity values. The orange block represents the following equation σ(T)=σ(1+k_o(T-T_o))

The purple block contains blocks to determine the electrical power generation. The inputs to the purple block are the electrical conductivity as a function of temperature and the square of the input voltage. Within the purple block are blocks that physically represent the length of the electrode gaps and the cross-sectional area of the heating chamber. The output of the purple block is the electrical power Qh. The block represents the following equation $\mathrm{Q} = \frac{\mathrm{V_e}^2\mathrm{A}\sigma}{\mathrm{L}}$

The green block in figure 5.5 is the 'Heat determination' block. This block contains the developed state space model of the CFOH. From this block the output temperature of the CFOH is determined. The inputs to the block are the change in temperature (Delta_T), the electrical power (Q_ohmic), initial temperature (Tinit), heat capacity (Cp) and the mass flow rate (mdot). The output of this block is the determined output temperature. This block represents the total energy balance equation which is given as $\rho v C \frac{dT}{dt} = \dot{m}C\,(T_{in} - \mathrm{T}) + \mathrm{Q}$.

In figure 5.6 below, the orange block is expanded and the components to determine the electrical conductivity as a function of temperature are explained. The electrical conductivity as a function of temperature is determine using the equation σ(T)=σ(1+k_o(T-T_o)). This block is similar to the batch ohmic heater model described in figure 3.6. The improvement added is the addition of a saturation block that has an electrical conductivity range of 0.1 S/m to 2.5 times the initial electrical conductivity. The addition of the saturation block is to prevent unrealistic temperatures from the model.

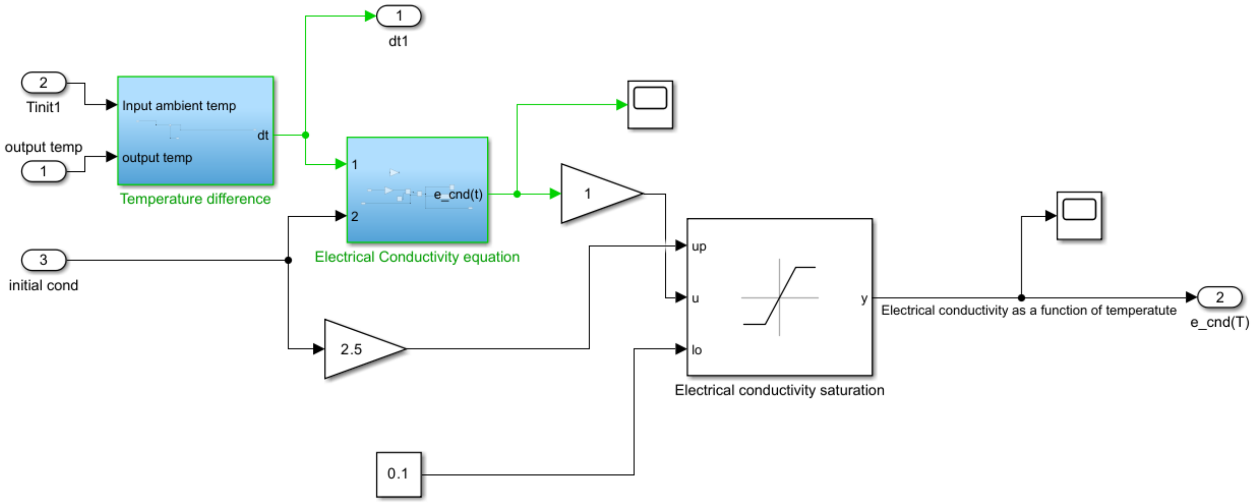

Figure 5.6 Block layout to determine the electrical conductivity as a function of temperature.

The saturation block added conforms with the specification of the CFOH plant which has a minimum infeed electrical conductivity limit of 0.1 S/m and a maximum infeed electrical conductivity of 0.9 S/m.

Figure 5.7 below shows the content of the electrical power generation block (purple block). The electrical power is determined from the $\mathrm{Q} = \frac{{V_e}^2 A\sigma}{L}$. The length L is given as the combination of the two sections of separation of the heating chamber 0.6m and 0.89m.

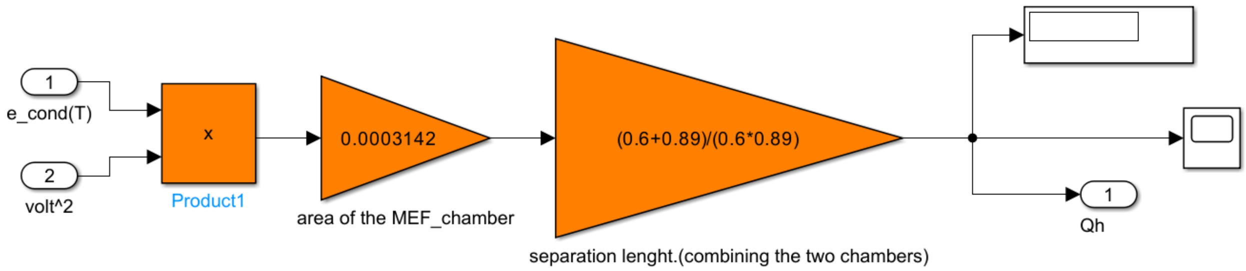

Figure 5.7 Block layout of the electrical power generation block.

Figure 5.8 below shows the content of the heat determination block (green block). The block consists of the state space model and the solution to the energy balance equation $\rho v C \frac{dT}{dt} = \dot{m}C\,(T_{in} - T) + Q$.

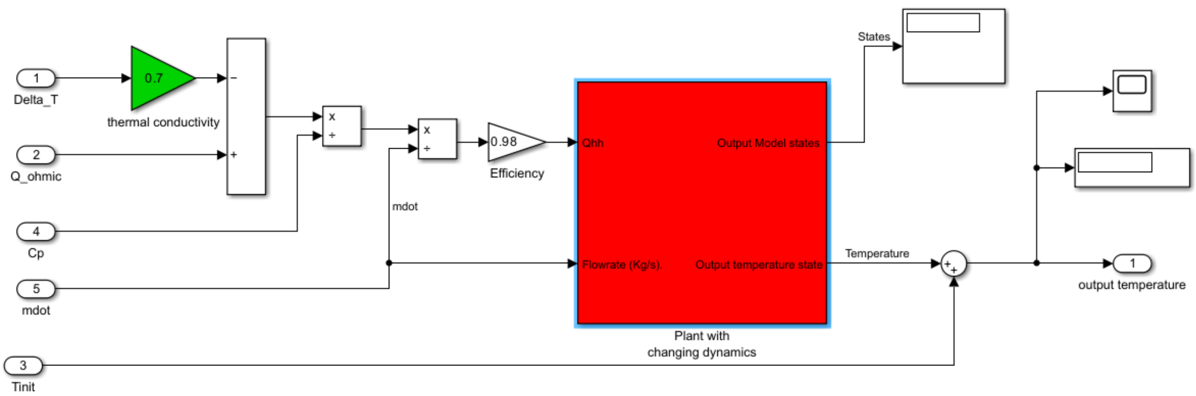

Figure 5.8 Block layout of the heat determination block (green block)

Figure 5.8 above shows the how the output temperature for the CFOH model is determined. The inputs to the red block are the electrical power 'Qhh' and the mass flowrate. The outputs of the red block are the output model states which is directly related to the state of the state space matrix and the output temperature.

Figure 5.9 below shows the layout of the model with changing dynamics (state space model) block.

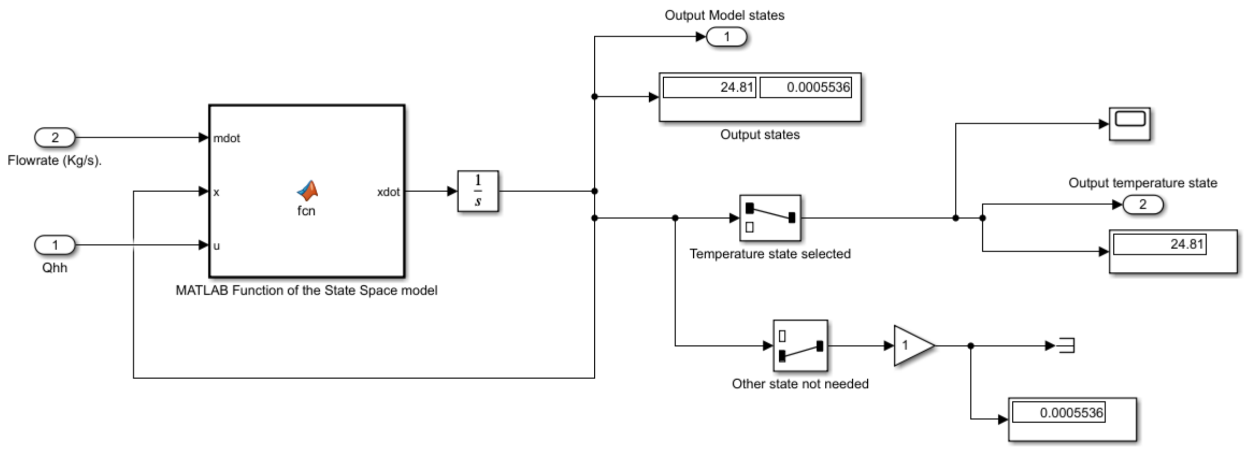

Figure 5.9 Layout showing the output temperature determination from the state space model of the CFOH.

In the figure above the state corresponding to the output response is selected. This state is the state response of the A matrix in the state space representation. The other state not selected is a state that describes the input B and U matrices.

The state space script in the 'MATLAB Function of the State Space model' block describes the state space model described in section 5.2.

5.1.2 Continuous flow ohmic heater model validation

In validating the transfer function model, temperature data collected from the experiment are compared to the simulated model results. The Voltage inputs are also the real-life data measured from the continuous ohmic unit. The product flowrate is set to a constant value during heating. The food product used is a saline solution with an electrical conductivity range between 0.24 S/m or 0.6S/m. The saline solution was prepared by mixing known quantities of table salt and tap water. The infeed electrical conductivity of the saline solution was measured before heating. The validation is achieved using a steadily increasing applied voltage and a step rising applied voltage at the input of the open loop plant. The applied voltage changes and the corresponding output responses are shown in the Figures below.

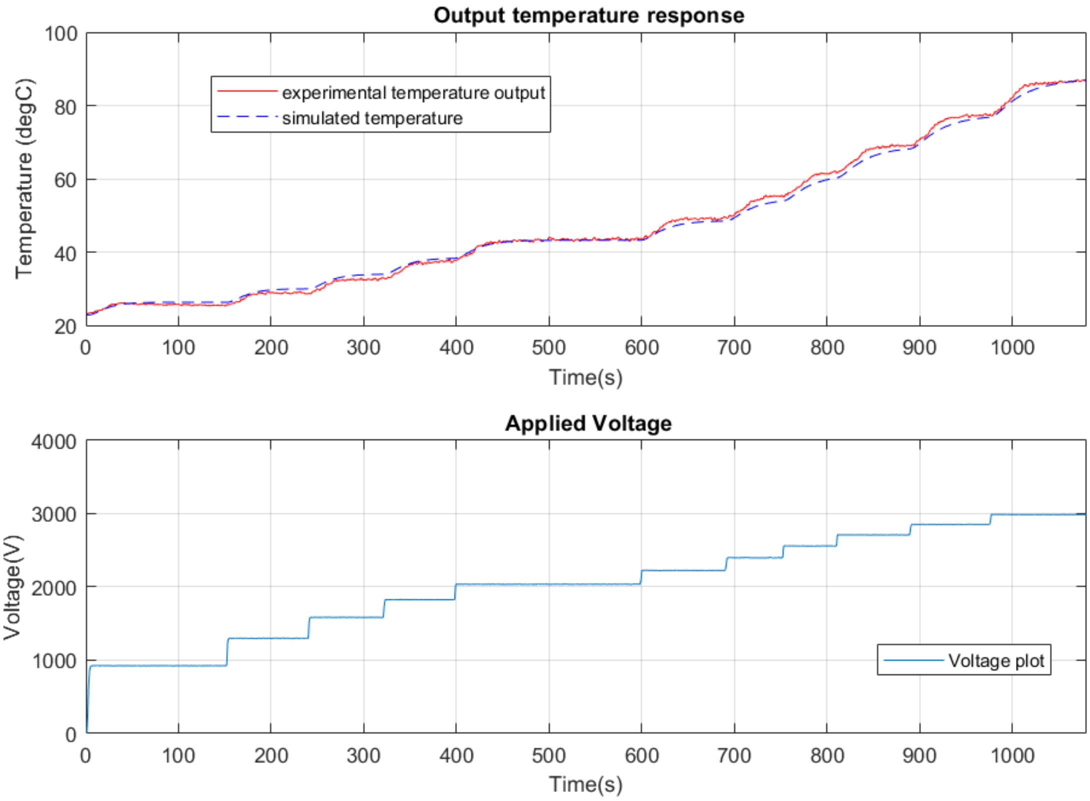

Figure 5.10. Open loop validation when applying a gradual step increase in voltage at 1L/min at 0.3S/m saline solution.

From figure 5.10 above, the simulated temperature output is compared with the experimental temperature output from the CFOH plant. The low electrical conductivity and high flowrate combination of the saline solution used showed close conformity between the simulated and experimental data. Short voltage steps were taken at random so that the performance and behaviour of the CFOH model can be observed.

In figure 5.11 below, a combination of low electrical conductivity and high flowrate of saline was used. The difference between figure 5.10 is that more shorter voltage steps were applied.

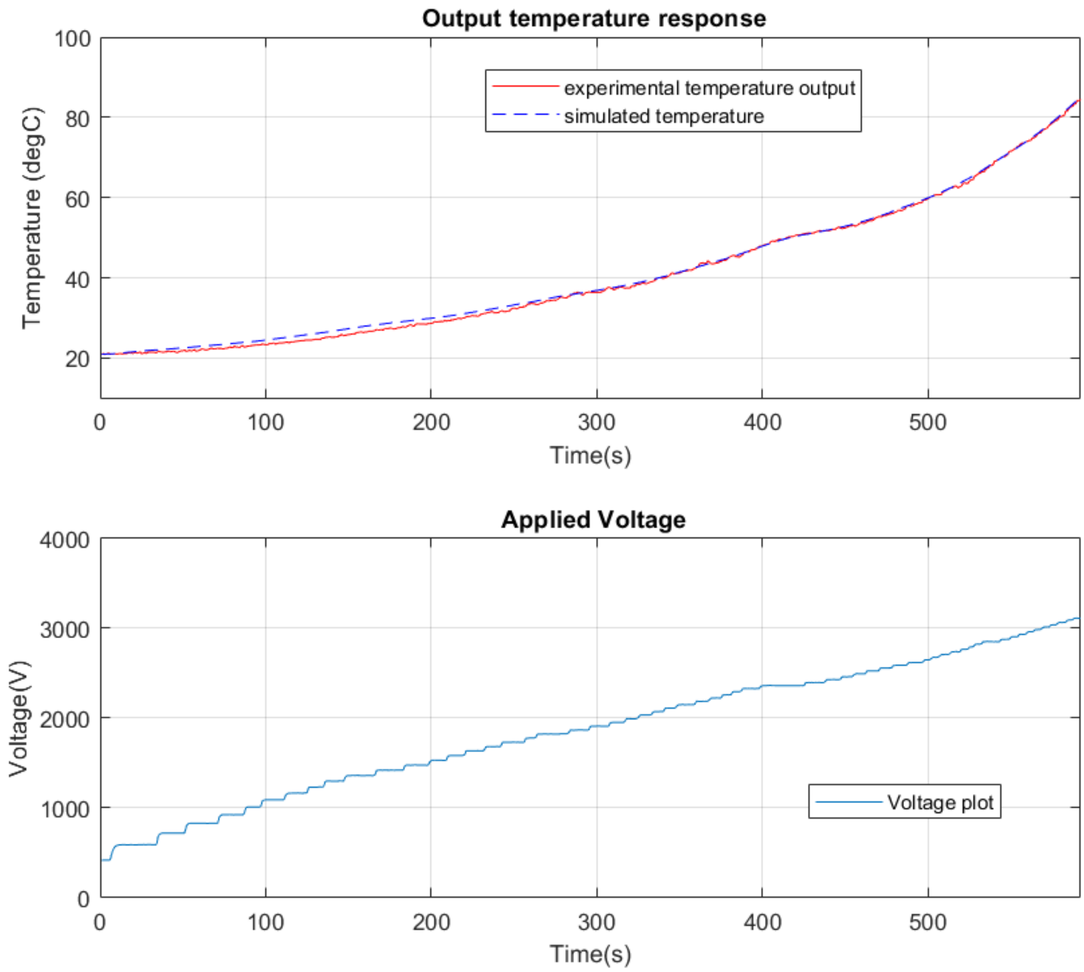

Figure 5.11. open loop validation when applying a rapidly increasing voltage at 1L/min at 0.3S/m saline solution.

In figure 5.11, the response of the model when the real-life voltage is applied to the model is shown. With increasing applied voltage, a corresponding proportional increase in output temperature is observed. During the open loop validation, the flow rate is kept constant.

In figure 5.12 below, a combination of high electrical conductivity and low flowrate of saline solution for model validation is tested. The applied voltage is randomly applied in random steps and the output temperature is compared.

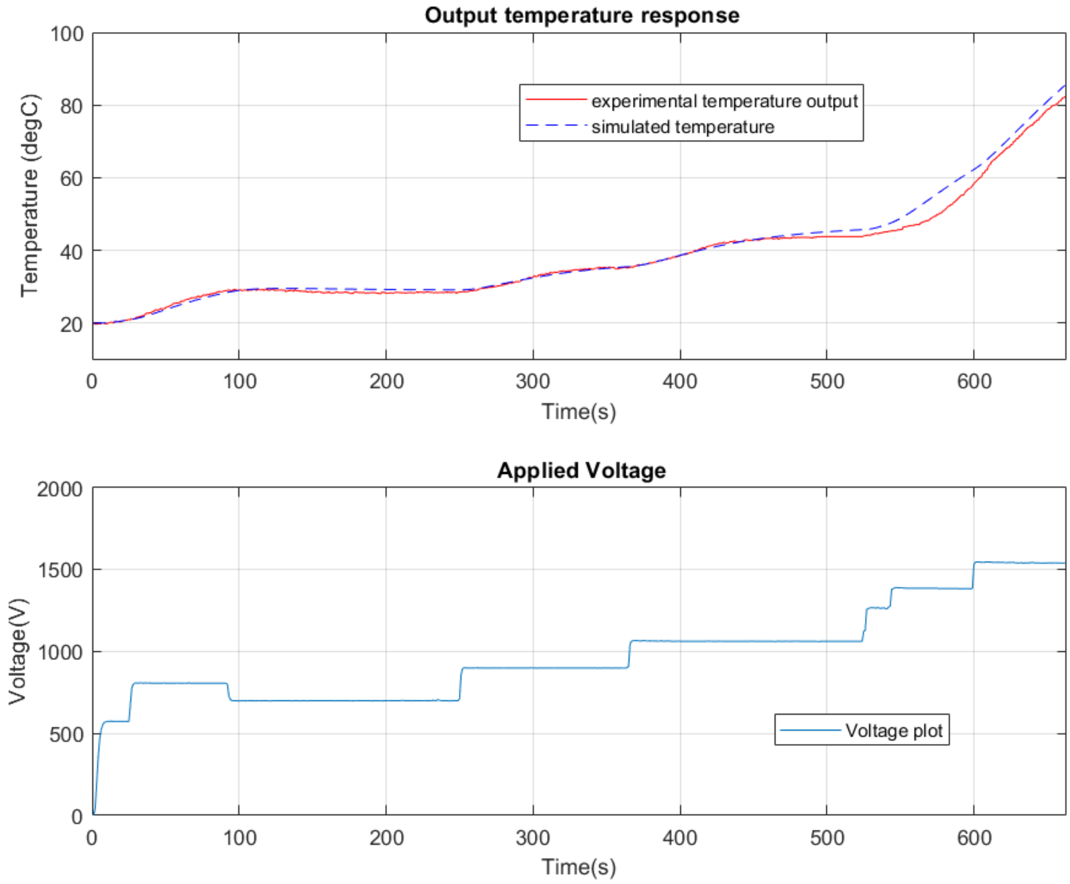

Figure 5.12. Open loop validation at 0.48L/min when applying a step voltage at 0.6S/m saline solution.

From figure 5.12, the model and plant have a high degree of conformity up until 500s. From about 500s to 600s deviations were observed between the CFOH model and the real-life plant. Between 500s-600s three step voltages were applied, ordinarily a proportional increase in the real-life temperature response is expected regarding figure 5.10 and figure 5.11. However, the real-life temperature data appears to dip/lag for about 8°C. This short deviation is unclear to the author and might be attributed to hardware temperature sensor behaviour or the unmodelled non-linearities due to fluid mixing within the heating chamber.

In the figure below, steady increasing step voltage was applied to the low flowrate high electrical conductivity saline solution. The aim of the test is to observe the performance of the CFOH model.

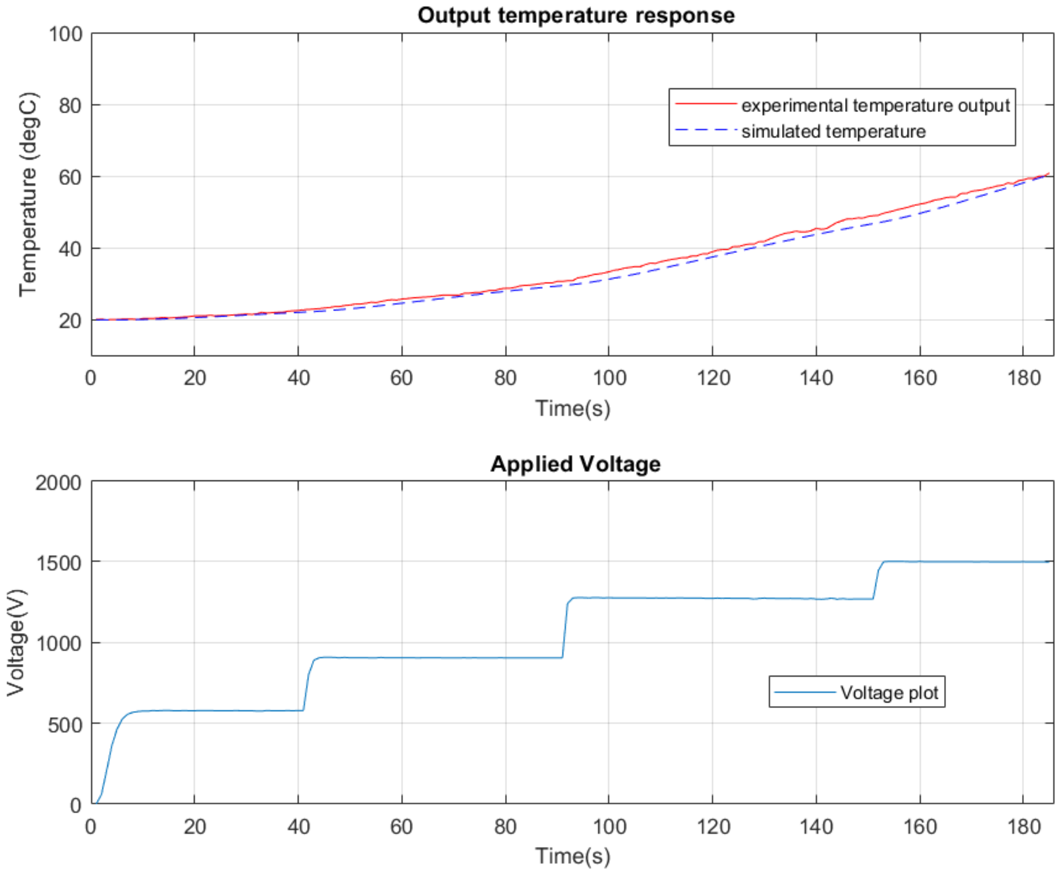

Figure 5.13. Open loop validation at 0.48L/min using a steadily increasing voltage at 0.6S/m saline solution.

From the figure above, the temperature outputs of the CFOH model and CFOH plant are proportional to the applied voltage. The relationship observed is in accordance with the previous results.

In figure 5.14 below, a combination of low electrical conductivity and low flowrate of the saline solution is tested. These combinations are chosen to put to test every possible scenario when the real-life plant is in operation. In addition, the step voltage is decreased at time 450s in order to observe the effect of temperature reduction as to temperature rise.

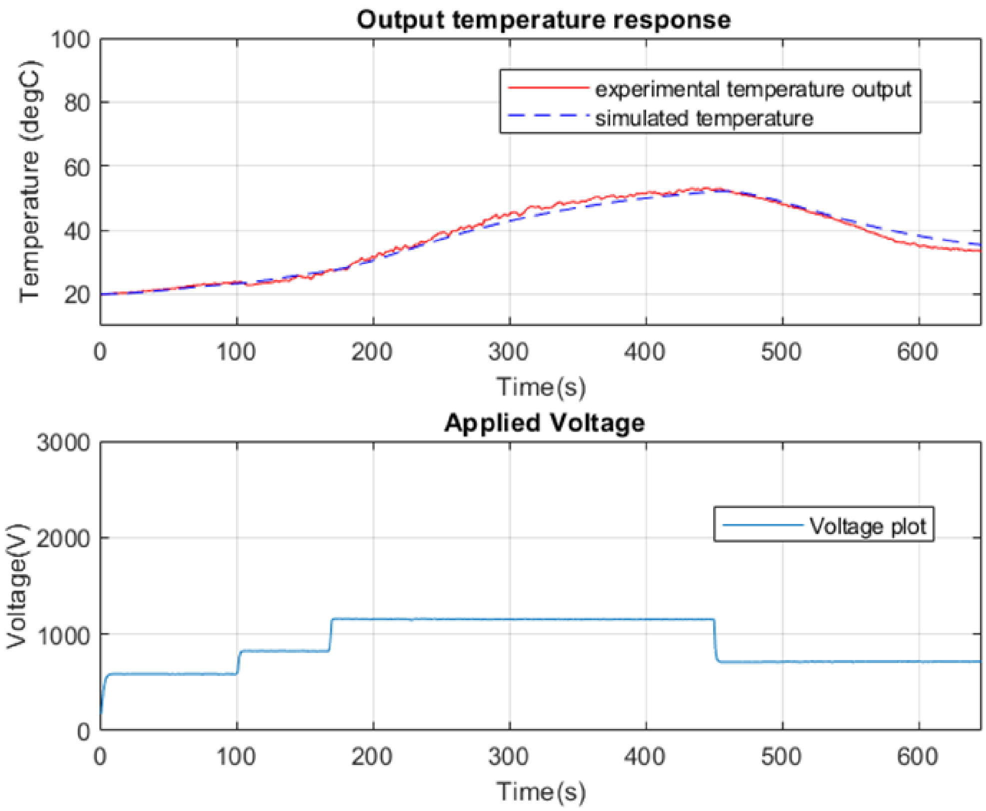

Figure 5.14. Open loop validation at 0.22L/min when applying a step voltage at 0.3S/m saline solution.

In figure 5.14 above, from 0s to about 450s when steady step rise in voltage is applied the temperature response from CFOH model and CFOH real-life plant conform and are proportional to the applied voltage. From time 500s to 650s when a lower step voltage was applied a temperature difference in the output of the CFOH model and CFOH plant of about 7°C was observed. The deviation can be attributed to the CFOH model being developed for output temperature rise only. To remove this deviation the model can be improved to account for temperature reduction by modelling the thermos-physical effect that attributes to temperature reduction.

5.2 Implementation of advanced process control

5.2.1 MATLAB and PLC OPC server/client configuration

The OPC technology is a hardware and software interface standard using Client/Server mode based on COM (Component Object Model)/DCOM (Distributed Component Object Model), which offers a general standard mechanism for the client's and server's data communication and exchange on different platforms (Zhang, Zeng, & Zhang, 2007). OPC Unified Architecture (OPC UA) is an industrial communication standard developed by the OPC foundation. OPC is vendor independent and supports all major industrial automation platforms. Reading data in MATLAB or SIMULINK and writing parameters to industrial devices becomes easy and vendor independent with OPC UA. This approach enables the user to directly benefit from performing data science and other capabilities with MATLAB (MATLAB Documentation 2022).

The OPC server KEPServerEX has been configured to communicate with the MITSUIBISHI FX5U PLC with ethernet module using ethernet communication protocol. The input/output (I/O) tags written to the PLC is sent to the OPC server for MATLAB to read and write to it.

Table 5.2 below shows the I/O tags, address, description, and data types configured for the PLC and OPC server.

Table 5.2. I/O tags description for the PLC and OPC server.

Tag name	**Address**	**Data type**	**Description**
CT1	D132	short	Current at the first stage
CT2	D133	short	Current at the second stage
HV	D130	short	High voltage reading
MEF_pulse_width	D2014	short	MEF application pulse width (not used)
MEF_repeat_time	D2012	short	MEF application repeat time (not used)
ON/OFF	M10	Boolean	Turn on/off the unit
Pump_ON/OFF	Y200	Boolean	Turn on/off the pump
Setpoint	D2011	short	Setpoint for thyristor
T1	D135	short	Fibre temp probe 1
T2	D136	short	Fibre temp probe 2
T3	D137	short	Fibre temp probe 3

T4	D138	short	Fibre temp probe 4
TC1	D111	short	Inlet temp probe
TC2	D112	short	Outlet thermocouple probe
CT3	D134	short	Current through the MEF system
Irms	D61	short	Current rms value
Power	D74	short	Electrical power reading
Vrms	D64	short	Voltage (vrms)
TX1	D117	short	Transformer temp probe 1
TX2	D118	short	Transformer temp probe 2

The OPC server and client protocol enables exchange of data in real-time between the PLC in which the ohmic heater is based on and a stand-alone lab-based computer so that simple and advanced model-based control can be applied. With the OPC established the following tasks are done:

- Read/Write to and from the PLC
- Trend and real-time data collection and storage on the lab-based PC
- Implementation of classical and advanced controllers

5.2.2 Thyristor automatic level safety controller

The classical controller developed is the proportional, integral and derivative controller (PID) while the advanced controller developed are the model predictive controller (MPC) and adaptive model predictive controller (AMPC). Before the implementation of these controllers, a safeguard system was developed to ensure that the ohmic heater regardless of any controller deployed operates in a safe region.

The thyristor automatic level safety controller termed ‘auto leveller’ ensures the safe operation of the continuous flow ohmic heater. The auto leveller sets a bounded limit to the amount of electrical power that can be supplied for heating operations. Technically, it sets the voltage bounds which the thyristor can supply and in turn the electrical power. This is to prevent hazards such as overheating and to generally keep the ohmic heater in safe operation.

Even with a temperature probe registering and being used for any control technique an immediate demand by the control system for 100% power may lead to overheating or overshoot before product reaches and registers on an outfeed temperature probe. Product may boil before power is reduced and temperature is brought under control. Therefore, the 'auto leveller' limits the thyristor value to prevent 100% voltage from being applied.

The structure of the safeguard system (auto leveller) is shown below in Figure 5.15.

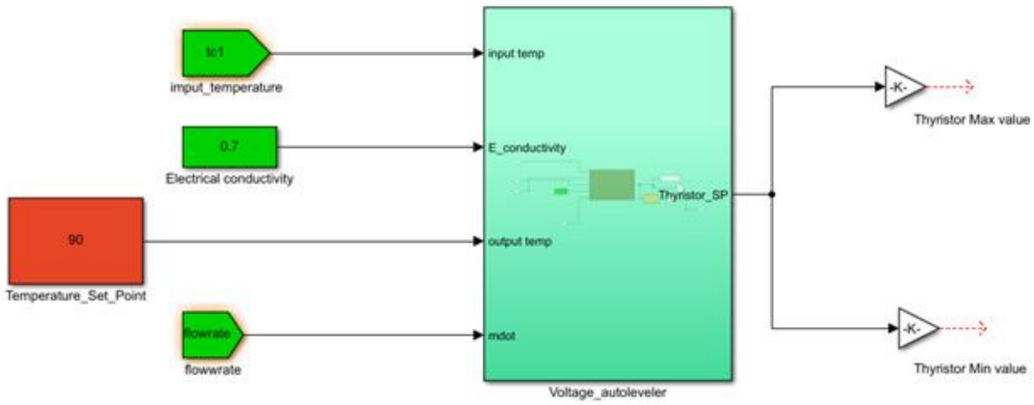

Figure 5.15. The safeguard system implemented with the controllers deployed on the ohmic plant.

The auto leveller system works by calculating the theoretical temperature rise using equation 5.8 below.

The heating rate in a continuous ohmic heater is described by (Marcotte, 1999):

$$(T_{out} - T_{in}) = \frac{dT}{dt} = \frac{V^2 A\sigma}{L\dot{m}C_p} \tag{5.8}$$

Equation 5.8 provides the minimum electrical thermal power to cause a required temperature change. With this information the required maximum and minimum electrode voltage safety range is therefore estimated. The value of the maximum and minimum voltage safety range is 'back calculated' to a maximum and minimum thyristor setpoint using the designed thyristor scaling function which will be discussed subsequently. This auto leveller ensures that any other controller implemented keeps the food product temperature setpoint within a tolerable theoretical range and prevents temperature oscillations.

All codes and block diagrams are provided in the appendix. To select the minimum thyristor value, an intuitive value usually 10% less than the original thyristor value is selected to prevent large oscillations.

The block diagrams to implement real-time process control from the MATLAB environment to the CFOH system are described below.

In figure 5.16 below, the overall open loop block to implement real-time control on the CFOH is presented. The block diagram consists of blocks which will be explained subsequently.

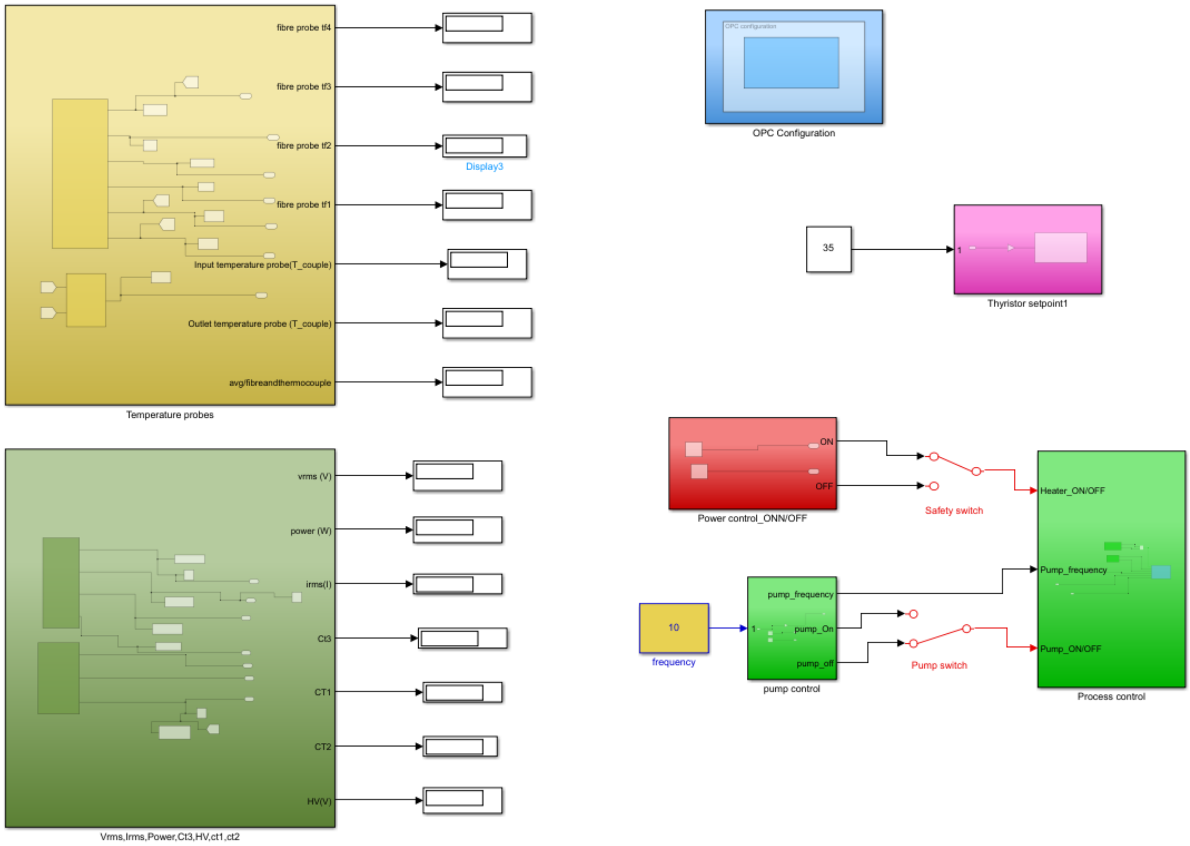

Figure 5.16 Open loop implementation on the CFOH from MATLAB/Simulink environment.

From figure 5.16, different block and subsystem block have different function. The 'Temperature probes' block contains all the blocks to measure the and record real-time temperature data from the optic fibre probes and the thermocouples. Four optic fibre temperature probes were used. With a pair placed side by side along the heating section of the CFOH. 2 sets of thermocouple temperature sensors were used, they are placed at the inlet and outlet of the heating chamber.

The 'Vrms, Irms, Ct3, HV, ct1, ct2' block shown measures and records the real-time root mean square voltage (vrms) and current (irms) which is the voltage and current supplied at the mains. Also, the electrical power during heating is measured and recorded, the current at each section of electrode spacing (ct1 and ct2), the overall current through the electrodes (ct3) and the high voltage (HV) supplied from the HV transformer.

From figure 5.16, the 'Thyristor setpoint1' block contains OPC enabled blocks that allows data to be written to the HV thyristor to supply the corresponding HV. The 'process control' block also contains write enabled OPC blocks to send binary commands to the CFOH to turn on/off the device. The 'process control' block also allows the frequency of the infeed pump to be modified to attain the desired mass flowrate and to turn on/off the infeed pump.

The 'OPC Configuration' block contains the OPC server client configuration that enables read/write functions when the model is running. The OPC server clients links the respective input/output commands to specific tags on the PLC.

5.2.3 Implementation of PID, MPC and AMPC

With the implementation of the OPC technology, reading data in MATLAB/Simulink and writing parameters to the PLC becomes seamless. The OPC approach enables the direct implementation of developed controllers in the MATLAB/Simulink environment on the PLC.

Table 5.3 below shows the different process variables of the continuous ohmic heating plant and the variables that are controlled, manipulated, and fixed.

Table 5.3. A list of variables, manipulation, type of signal and their dependencies

Variable type	**Manipulation**	**Unit**	**Signal type**	**Dependencies**
Flowrate	Fixed value	L/min	Digital	Product flow
Thyristor setpoint	Estimated by the controller	Dimensionless	Digital	Applied High voltage
RMS Voltage	Measured by a voltage sensor	V	Digital	
RMS Current	Measured by a current sensor	A	Digital	
HV	Measured by a high voltage sensor	V	Digital	Heating rate and voltage at the electrodes
Current at the electrodes	Measured by a current sensor	A	Digital	
Power	Estimated from the voltage and current values	W	Digital	Shows the maximum heating rate
Temperature (inlet and outlet)	Measured from a thermocouple	°C	Analog	Temperature change
Temperature (between the electrodes)	Measured from an optic fibre sensor	°C	Digital	Temperature change

From table 5.3 above, the most significant process variable that influences the heat generated is the voltage applied to the electrodes. This can be seen from equation 2.4.2.2 that electrical thermal energy is a function of the applied voltage and the electrical conductivity of the product. The applied voltage can be easily controlled by manipulating the thyristor setpoint while the electrical conductivity of the food product as a function of temperature change can be easily estimated. The resulting temperature rise described by equation 4.8 can therefore be determined.

The first task before implementing the controllers is the calibration of the infeed pump flowrate. The infeed pump is controlled by a motor inverter located in the MEF unit control panel labelled E in figure 4.1. The motor inverter varies the flowrate of the pump by varying the frequency of the voltage applied to the pump. To calibrate the infeed pump speed the following steps were taken:

- Set the frequency on the control panel to a fixed value (e.g., 30Hz)
- Measure the quantity of product flow into a measuring beaker for 1 minute.
- Repeat for a different value of frequency.

Using the steps above, the result of the infeed pump calibration is shown in figure 5.17 below.

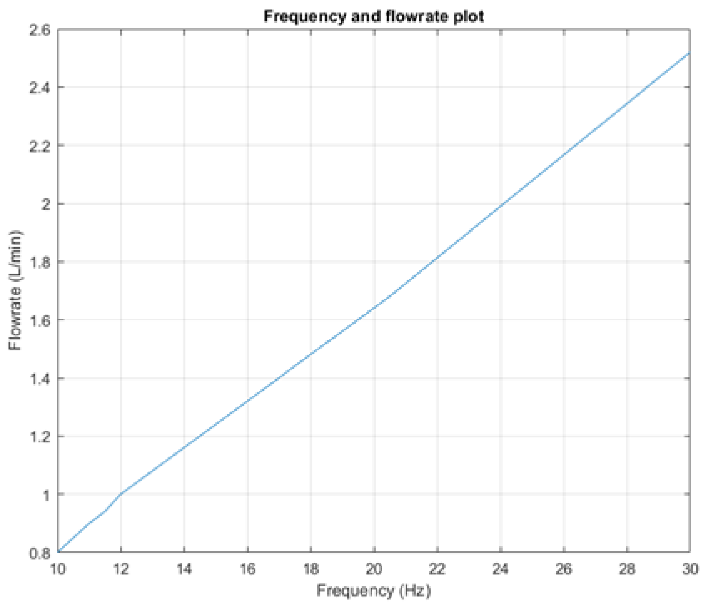

Figure. 5.17. Calibrated infeed pump flow rate and frequency.

From figure 5.17 above, calibrating the pump's flowrate ensures that when a frequency value is supplied either by the user or the controller the corresponding flowrate in L/min is achieved.

The second task is to calibrate the high voltage thyristor. The high voltage (HV) thyristor effectively controls the rms voltage delivered to the primary side of the HV transformer (1:10).

The input term to the thyristor is a dimensionless unit scaled from 0 to 100 while the output is the rms voltage (0 – 415V) from the thyristor which is scaled using the input terms. The effective control of the applied high voltage from the HV transformer is achieved by controlling and applying the appropriate input term to the thyristor. Figure 5.18 below shows the relationship between the input to the HV thyristor and the corresponding high voltage output from the HV transformer measured experimentally. The plot is produced from the HV sensor values recorded from the control panel and the thyristor set point entered by the user. The first 100 thyristor setpoints entered by the user are 0,1,2,3,4,5…100 and the corresponding HV values are recorded.

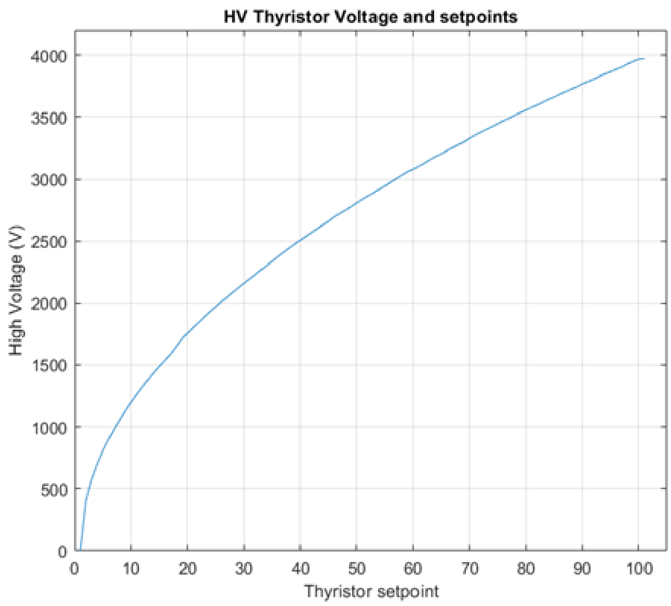

Figure. 5.18. Input/Output of the HV Thyristor

From figure 5.18, it is seen that the input-output relationship of the HV thyristor is not linear. Therefore, a polynomial function is developed to represent the relationship between the thyristor input setpoint and the HV transformer output. The developed polynomial function translates the controller action into corresponding dimensionless thyristor setpoint and voltage. Therefore, when a user or the controller presents a dimensionless thyristor input the corresponding HV can be determined in simulation.

The controller and plant architecture are represented in figure 5.19.

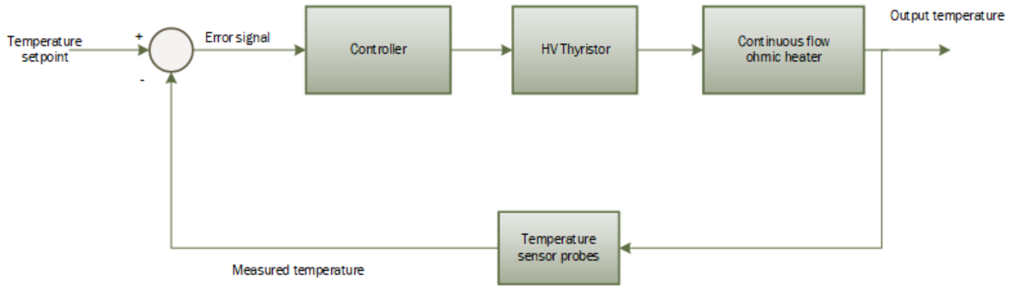

Fig. 5.19. Controller and plant architecture.

5.3 Implementation of PID Control

The closed loop control of the continuous flow ohmic heater using PID control technique is shown below in figure 5.20.

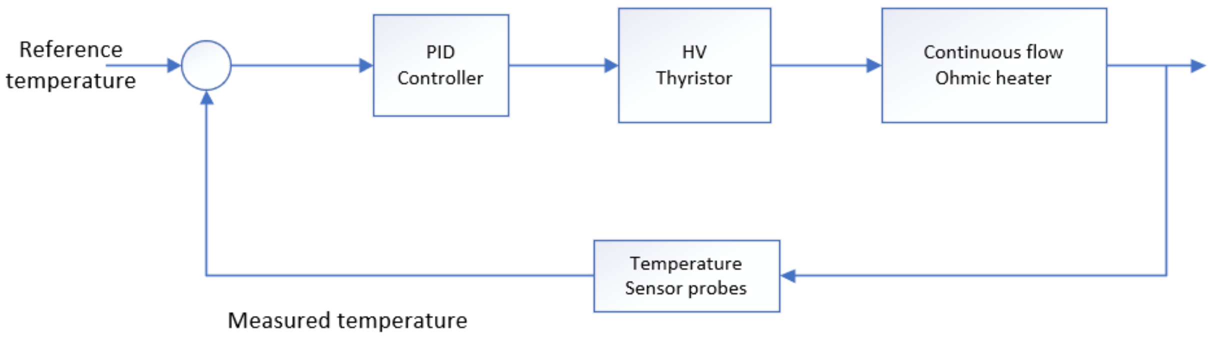

Figure 5.20. Closed loop PID control of the continuous flow ohmic heater

The product flow rate is kept constant throughout the heating process. The desired output temperature is given as a reference to the PID controller. The temperature at the output is measured by 2 optic fibre temperature probes at the outlet of the heater. A further thermocouple is placed outside the heating region to further validate the readings by the optic fibre probes. The measured temperature is compared to the reference temperature and the error generated feeds into the PID controller. The PID controller then gives the HV thyristor a dimensionless value ranging from 0 to 100. This dimensionless value received by the HV thyristor corresponds to a HV voltage reading which is applied to the electrodes.

The desired performance of the PID controller is ensured by proper tuning of the controller gains. An interesting feature this paper presents is that the controller can be tuned in simulation before deployment on the physical hardware.

The PID is tuned using the Ziegler-Nichols tunning method. The tunning method was performed in simulation before the tunned PID gains were deployed on the CFOH controller. This method begins by setting to zero the integral and derivative term while the proportional term is increased until the system is unstable. The proportional term when the system becomes unstable is called K_{max} and the frequency of oscillation is F_O.

Table 5.4 below describes how the PID gains are obtained using Ziegler-Nichols tunning method.

Table 5.4. Ziegler-Nichols tunning method

Controller	Proportional term K_p	Integral term K_i	Derivative term K_d
P controller	0.5 K_{max}	0	0
PI controller	0.45 K_{max}	1.2 F_o	0
PID controller	0.6 K_{max}	2.0 F_o	$0.125/F_o$

5.3.1 PID in simulation vs implementation

This section compares the developed controllers in simulation and there corresponding performance in implementation on the physical ohmic heater. The comparison can also serve as the closed loop validation of the continuous flow ohmic heater TF model developed.

The comparison of the simulation result to the real-life implementation of the PID controller on the continuous flow ohmic heater is shown in this section.

In figure 5.21 below, the electrical conductivity at room temperature is measured to be 0.33S/m. During this test the product flow rate is kept constant at 0.78L/min. A general fixed temperature setpoint is set to 90°C. The PID controller is tuned setting the proportional (P) term to 2.5, Integral (I) term to 0.2 and the Derivative (D) term to 0.

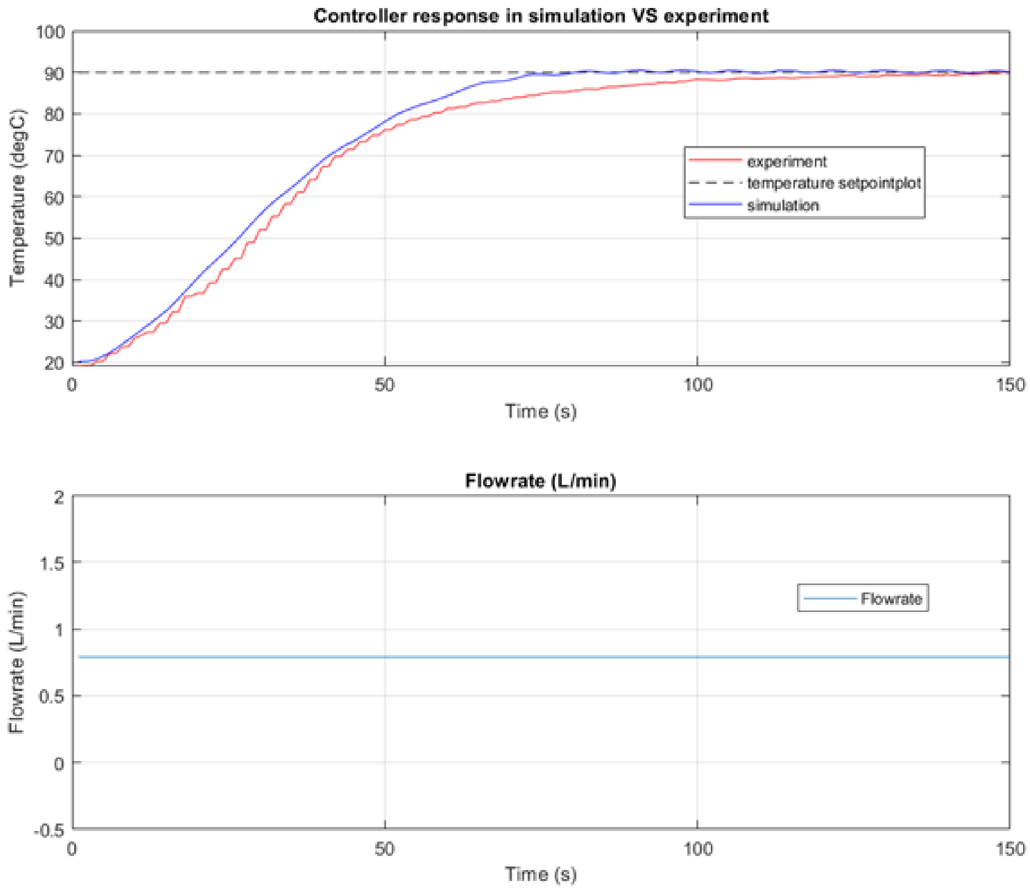

Figure 5.21. PID comparison between the simulated and deployed controller.

In figure 5.21 above, the PID controller in simulation is compared to the implemented PID controller. It was observed that given the same conditions, the PID controller in simulation has a shorter rise time and settling time of 70s. The deployed controller has a longer settling time of 105s. The performance of the PID in simulation can represent the 'ideal' condition when a constant flowrate of saline solution of 0.33S/m is heated to 90°C. This combination represents a low electrical conductivity and constant flowrate of the saline solution heated.

In figure 5.22 below, the PID controller is simulated at changing flowrates. The initial electrical conductivity measured at room temperature is 0.7S/m.

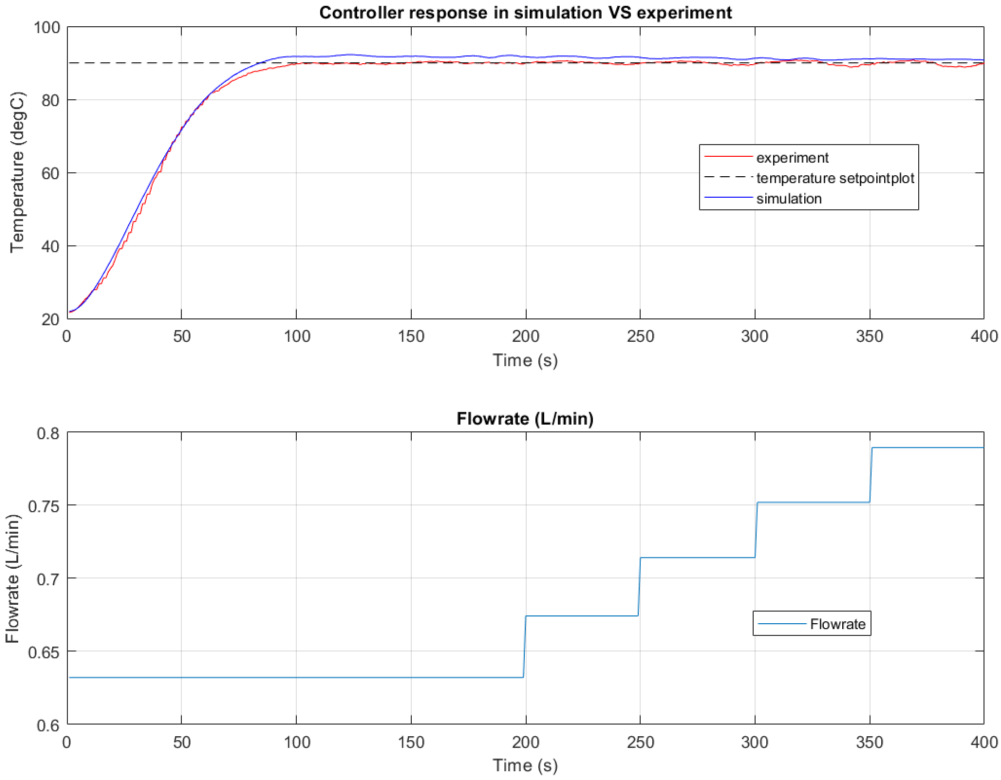

Figure 5.22. PID simulated and experimental response for changing flowrates. 0.7S/m

In figure 5.22 above, the combination used is the high electrical conductivity and variable flow rate of the saline solution. This combination is chosen to represent possible scenarios in which the CFOH plant would operate in. It was observed that with the simulated controller, a steady state error of 3°C was observed till about 250s. Compared to the real-life controller implementation, reduced steady state error was observed until 300s. Fluctuations in the output temperature became significant after 300s when the controller was implemented on the CFOH plant. These fluctuations are due to the accumulated error due to the rapidly changing flowrate on the CFOH from time 200s to 400s.

5.4 Implementation of MPC and AMPC

Model-based predictive control (MPC) refers to a class of sophisticated control techniques that use a process model to predict the future behaviour of the controlled system. (Schwenzer, Ay, Bergs, & Abel, 2021). At each time step, the MPC determines an optimal solution for the control output using the prediction model by solving a constrained optimization problem using predictions of future costs, disturbances, and constraints over a moving time horizon. Hence, the MPC is referred to as a “receding horizon” control (Mattingley, Wang, & Boyd, 2011). In essence, the idea is that a short-term (predictive) optimization achieves optimality over a long time.

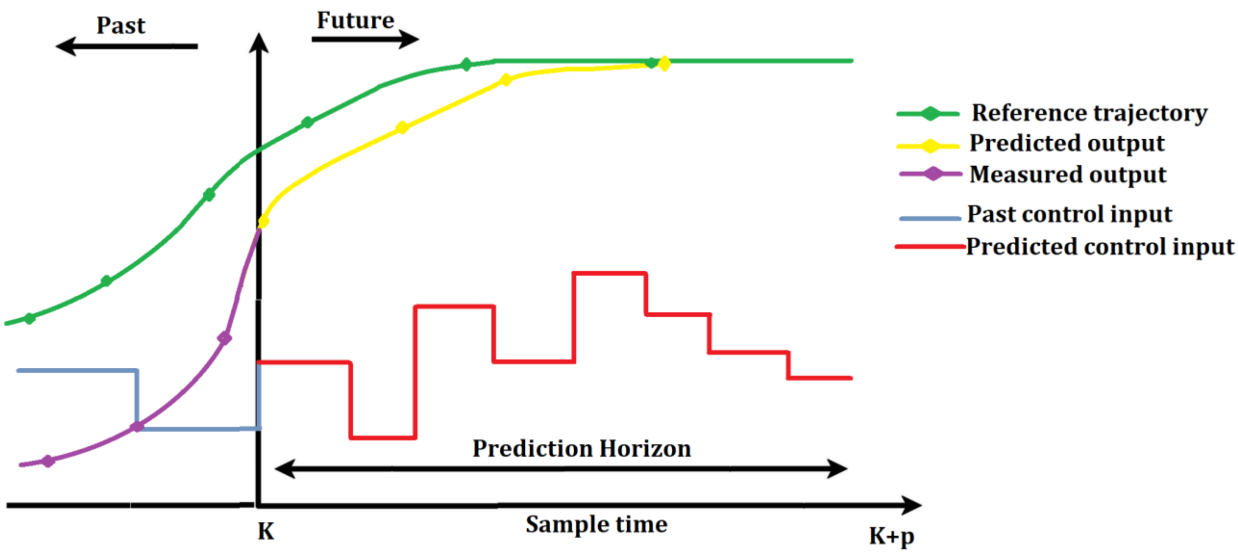

Figure 5.23 The principle of the model based predictive control (Schwenzer, Ay, Bergs, & Abel, 2021).

Short-term prediction over a long time achieves optimal results since the error forecast is small compared to a distant prediction. The short term control action over the prediction horizon is referred to as the control horizon. The combination of prediction and optimization (control horizon) is the main difference from conventional control approaches, which use precomputed control laws (Mayne, Rawlings, Rao, & Scokaert, 2000). The main disadvantage of MPC is that the optimization problem must be solved at each time step, which lead control engineers to think that it can only be used for systems with slow sampling typically less than one Hz (Mattingley, Wang, & Boyd, 2011). Several techniques have recently been developed to get around this problem. In one approach, called explicit MPC, the optimization problem is solved analytically and explicitly, so evaluating the control policy requires only a lookup table search (Bemporad & Filippi, 2003).

The MPC is represented by the form:

$$x(k+1) = Ax(\mathrm{k}) + B_u u(\mathrm{k}) + B_v v(\mathrm{k}) + \ B_d d(\mathrm{k}), \tag{5.9}$$

$$y(k) = Cx(\mathrm{k}) + D_v v(\mathrm{k}) + D_d d(\mathrm{k}), \tag{5.10}$$

where A, B_u, B_v, B_d, C, D_v andD_d are matrices parameters that can vary with time. k is the time index, x is the plant model states, u is the control input (manipulated variable (MV)), v, is measured disturbance, d is the unmeasured disturbance and y is the plant output.

A traditional MPC controller includes a linearised and fixed nominal operating point (x) at which the plant model applies the optimal control solution (u). For the MPC used in this work, the properties are given below:

$A = \begin{bmatrix} 0.999 & 0.295 \\ -7.2 * 10^{-4} & 0.970 \end{bmatrix}$, $B_u = \begin{bmatrix} 8.27 * 10^{-5} \\ 5.48 * 10^{-4} \end{bmatrix}$, $B_v = 0$, $B_d = 0$, $C = [1\ 0]$,

$D_v = 0$, $D_d = 3.3 * 10^{-4}$. Sampling time = 0.3s, Prediction Horizon = 30, Control Horizon = 3. The control horizon of 3 is chosen as the controller inputs short term prediction over a prediction horizon of 30. The higher the control horizon the control action of the controller diminishes. The prediction horizon is chosen to compensate for time for food product to flow from the inlet to the outlet of the CFOH. Also, the prediction horizon was chosen to allow sufficient time for temperature build up within the heating chamber.

The Manipulated variable rate (Δu) = $2.78 * 10^{-4}$. Output variable weight = 0.0011. The reasons for selecting the manipulated variable rate and output variable weights are explained subsequently.

In AMPC, as time evolves the nominal operating point will be updated and time varying to be consistent with the updated plant model. AMPC can be written in the form:

$$x(k+1) = x_n + A(x(\mathrm{k}) - \ x_n) + B(u(\mathrm{k}) - u_n) + \Delta x_n \tag{5.11}$$

$$y(k) = y_n + C(x(\mathrm{k}) - \ x_n) + D(u(\mathrm{k}) - u_n) \tag{5.12}$$

where A, B, C and D are the parameter matrices to be updated, x_n is the nominal operating point of the AMPC. Δx_n is the nominal state increments, u_n is the nominal input and y_n is the nominal output. For the AMPC used in this research, the same properties of the MPC were used the only additional variables are the nominal state increase $\Delta x_n = 0.000278$, $y_n = 0.0010, u_n = 20$

The constraints and cost function of the MPC and AMPC are the same. The main difference is that the AMPC uses an online model running in real-time to determine the solution to the optimisation problem. The following cost functions and their effect on the controller are when developed in MATLAB:

1. Y.wt (Output variable (OV) weight)
2. U.wt (Manipulated variable (MV) weight)
3. dU.wt (Manipulated variable rate weight)

The effects of the cost functions on the performance of the controller are highlighted in the tables below. The effects of the cost function are the same for both the MPC and AMPC.

Table 5.5 below shows the cost function evaluation and effect on the controller for the OV weight. The OV weight is a function of the output of the plant. For the CFOH, the OV is the measured temperature.

Table 5.5. Effect of the magnitude of the OV cost function on the MPC and AMPC.

Y.wt <= 0	**Y.wt >=1**
• The controller is sluggish to correct steady state error (SSE). • Temperature overshoot and SSE increases progressively	• No significant improvement/effect is seen.

It can be seen from table 5.5 above that the influence of the OV cost function is between 0 and 1. From simulation it was observed that a low value of OV magnitude close to zero results in large SSE while a value close to 0.0011 results in reduced SSE. Hence a value of 0.05 for the OV was chosen. Furthermore, it was observed that when a value between 0.05 to 1 is used the influence of the OV diminishes and no significant improvement on the controller is seen.

Table 5.6 below shows the effect of the magnitude of the MV rate weight on the MPC and AMPC. The MV variable for the CFOH is the applied voltage.

Table 5.6. The effect of the MV weight cost function on the MPC and AMPC

U.wt < 0	**U.wt = 0**	**U.wt > 0**
• No effect on the SSE is seen. • No effect on the applied power is seen.	• Very aggressive controller performance • Increased power dissipation.	• Increased settling time • As U.wt >0, controller becomes less aggressive.

From table 5.6 above, an MV value less than zero as no effect on the SSE. A value of zero makes the controller very aggressive, this feature might be useful if the response time (rise time) of the overall system if of priority over steady state error (SSE). The advantage of having MV equal to zero is faster rise time but at the detriment of increased power demand which may not be practical in real life scenarios. When MV is greater than zero, the power dissipation is more efficient, practical, and realistic. For MV > 0, the controller becomes less aggressive but results in heating rate of food product can be steady and uniform. It was also observed that the reduction in the aggressiveness of the controller diminishes as the value approaches number 1. The MV chosen in the development of the MPC and AMPC is 0.

Below in table 5.7 the effects of the MV rate weights are presented. The MV rate weight DU.wt is the rate of change of the MV from the controller. Therefore, DU.wt is the rate at which the applied voltage varies.

Table 5.7. The effect of DU.wt on the MPC and AMPC

DU.wt <= 0	**DU.wt > 0**
• No effect seen	• SSE increases with increasing DU.wt • The controller reacts slowly to changes.

From table 5.7 above, it was observed that when DU.wt <= 0 no effect on the controller is seen but the controller is penalised when DU.wt is greater than 0. A value of 0 was chosen for the DU.wt variable in both MPC and AMPC. The DU.wt value chosen in the development of the MPC and AMPC is 0.000278.

When all the cost functions and their effects on the controller are compared, the MV cost function has the most significant effect on the controller. The MV cost function adjusts the controller's aggressiveness. The magnitude of MV cost function relates to the magnitude of the applied voltage to the CFOH.

5.4.1 MPC in simulation vs implementation

Similar to the comparison of the simulated PID controller to the deployed controller. The same comparison template and conditions are employed. The MPC in simulation is compared to the deployed version for a fixed flowrate of 0.78L/min and in another case the same pattern of changing flowrate used for the PID controller. All parameters such as the temperature setpoint and electrical conductivity are kept uniform.

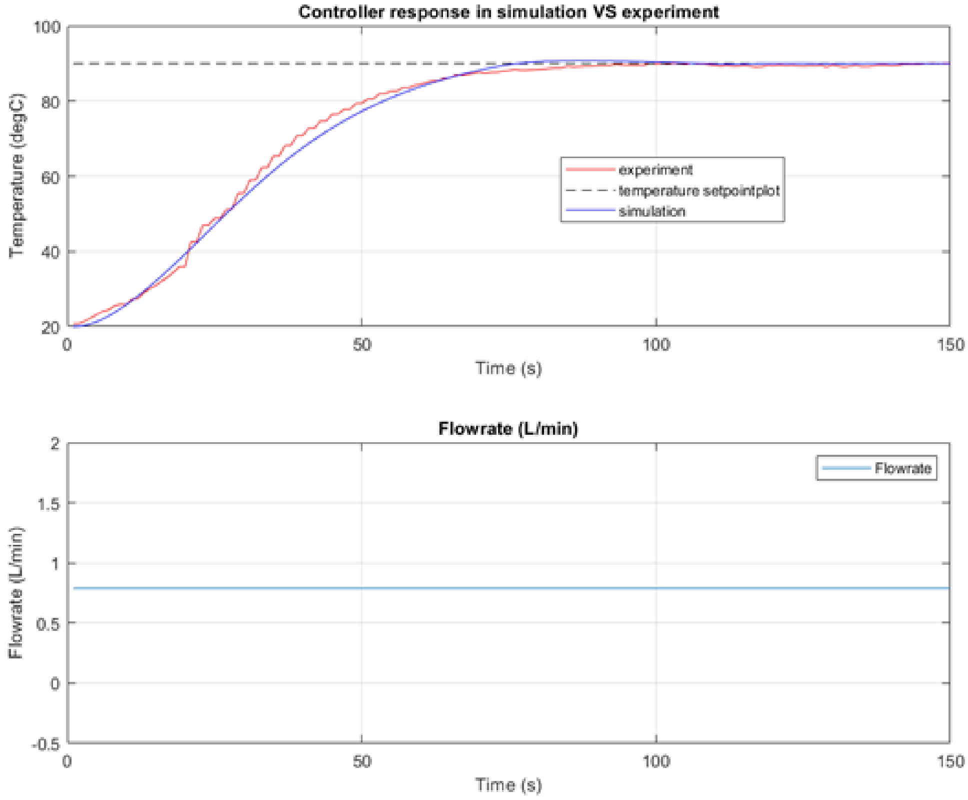

Figure 5.24. MPC in simulation compared to the deployed version 0.78L/m, 0.33S/m

From figure 5.24 above, the temperature response of the simulated controller and the deployed controller have a similar rise time profile and settling time of about 70s. Compared to the settling time of the deployed PID controller which was 105s both the simulated and deployed MPC performs better. For both the simulated and deployed MPC controller, little or no steady state error was observed. This implies that the CFOH model and the MPC in simulation gives an accurate closed loop model when compared to experimental data.

Figure 5.25 below shows the comparison under changing flowrates.

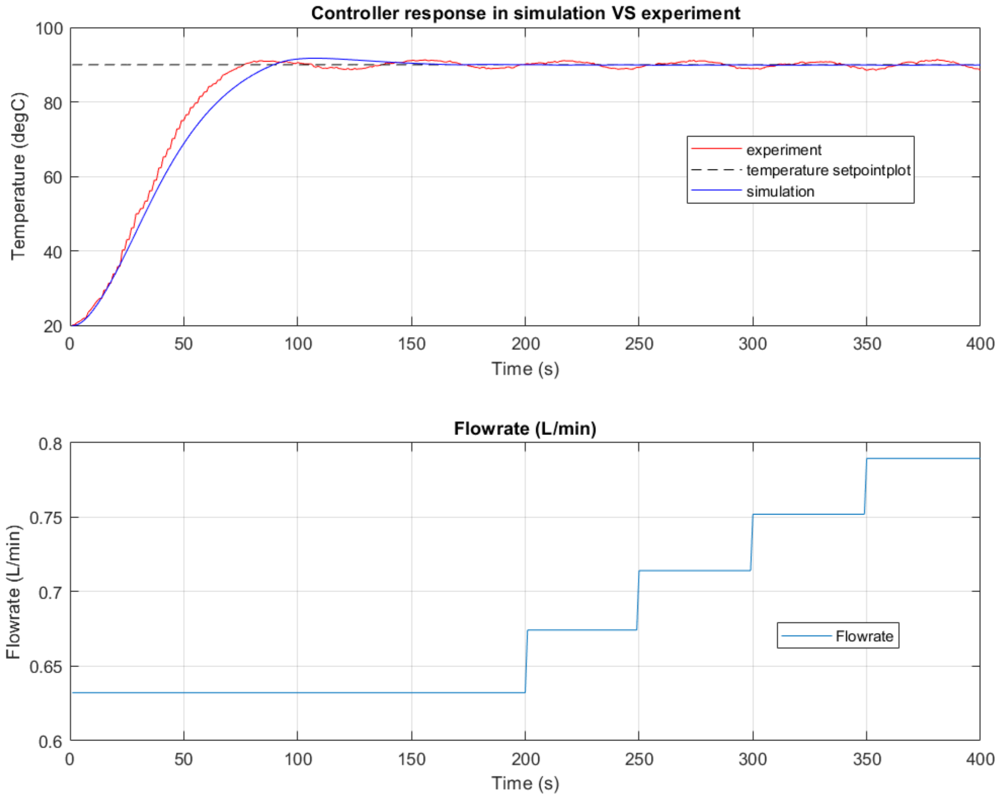

Figure 5.25. MPC in simulation compared to deployment for changing flowrates. 0.7S/m

When a combination of high electrical conductivity of saline solution is used, a faster heating rate and shorter settling time of 70s was observed with the deployed MPC controller. While in simulation, a slower heating rate and a longer settling time of 80s was observed. The MPC appears to struggle at higher electrical conductivity because the MPC optimisation model was linearised at an infeed electrical conductivity of 0.3S/m at 1L/m. Therefore, when the conditions at linearisation vary the performance of the MPC diminishes. This diminishing performance can be correct if the optimisation model is constantly changing with the infeed parameters. AMPC which is discussed in the next section addresses this issue.

5.4.2 AMPC in simulation vs implementation

Like the previous controllers compared in simulation and deployment, the same comparison basis is used for the AMPC.

Figure 5.26 below shows the comparison between the simulated AMPC and the deployed AMPC for a fixed flowrate of 0.78L/min at 0.33S/m.

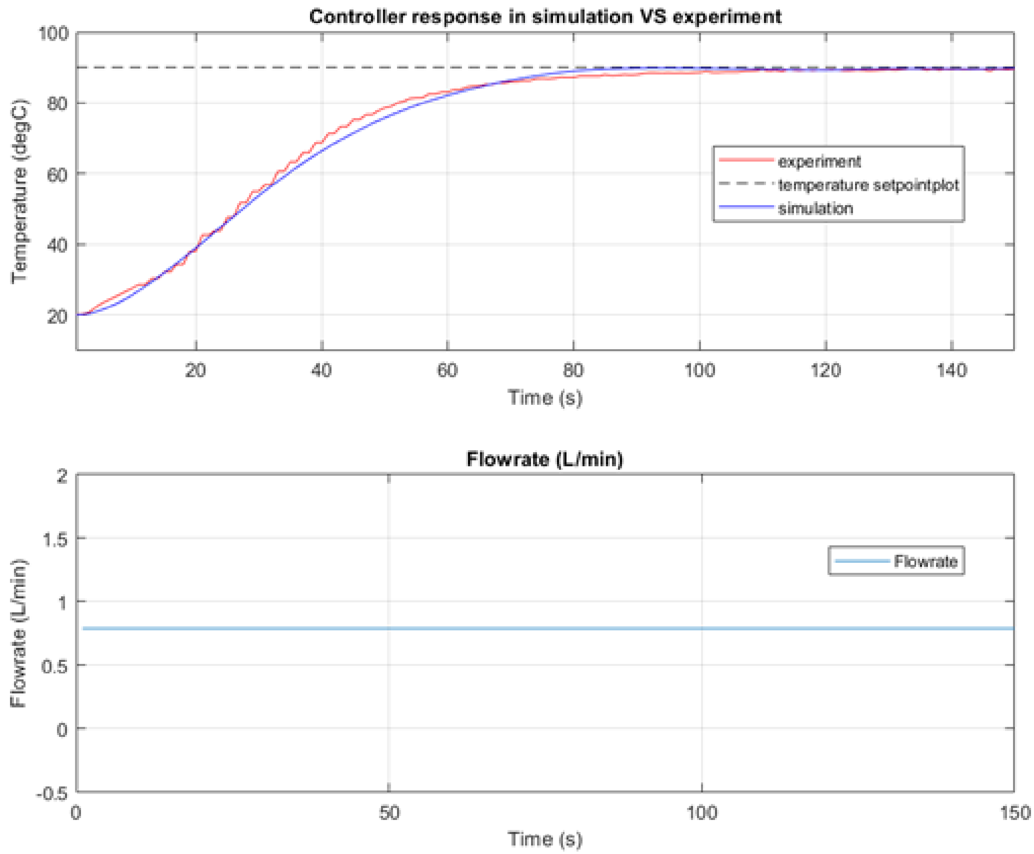

Figure 5.26. Simulated AMPC compared to the deployed version for a fixed flowrate at 0.33S/m

From figure 5.26 above, the temperature response from the simulated AMPC and the deployed AMPC are close in terms of the temperature rise and the settling time. The settling time of about 80s was observed. No steady state error was recorded. When compared to the response of the PID controller both the MPC and AMPC outperforms the PID controller when a combination of low electrical conductivity and fixed flowrate of saline solution was used.

In figure 5.27 below, the AMPC is compared in simulation and deployment using the same parameter basis for the previous controllers.

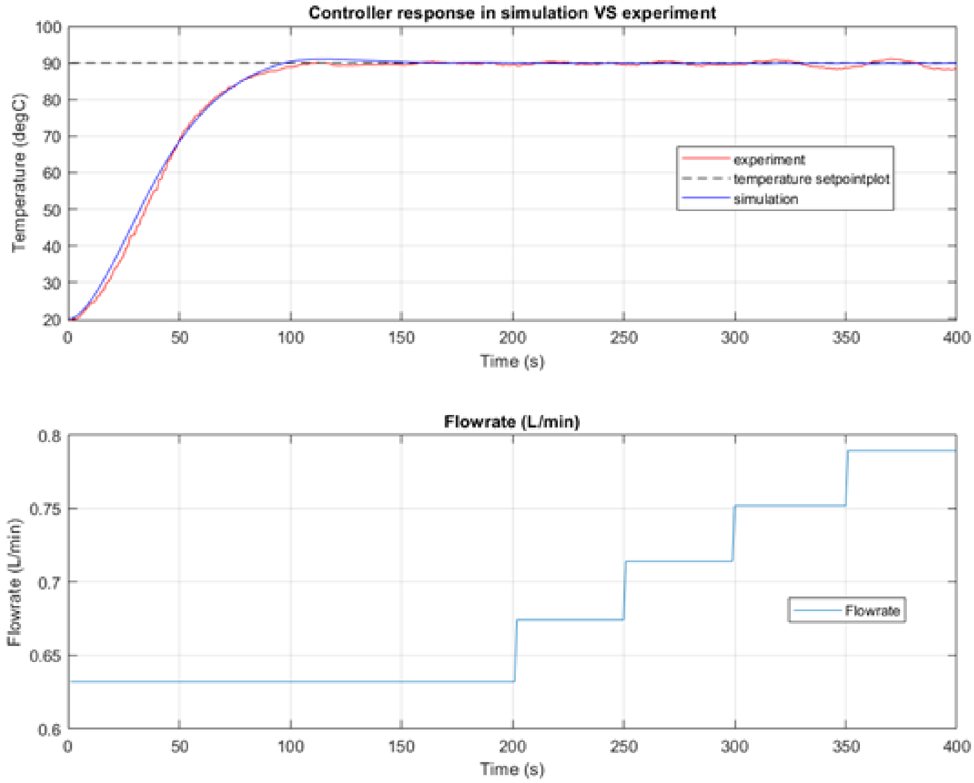

Figure 5.27. AMPC comparison in simulation and deployment for changing flowrates at 0.7S/m

From the figure above, the rise in output temperature of the simulated and deployed AMPC from time 0s to 100s are uniform. Compared to the MPC controller in simulation where the rise in output temperature lagged the experimental output. The AMPC addresses the disadvantage of the MPC where the initial conditions are used to linearise the MPC optimisation model. For this combination of high electrical conductivity and varying flowrate the optimisation function of the AMPC is not linearised, it varies with the varying process parameters. A general trend is seen from 300s to 400s where the accumulated error due to varying flowrates presents oscillations in the output temperature of the experiment. The oscillation due to varying flowrates was observed to be more with the MPC and less with the PID and AMPC.

5.5 General comparison of the deployed controllers

In this section, the deployed controllers are compared, and their corresponding temperature response are plotted. The plotted response of the deployed controller is the same experimental data previously compared to the simulated controller response in section 5.4 and section 5.5.

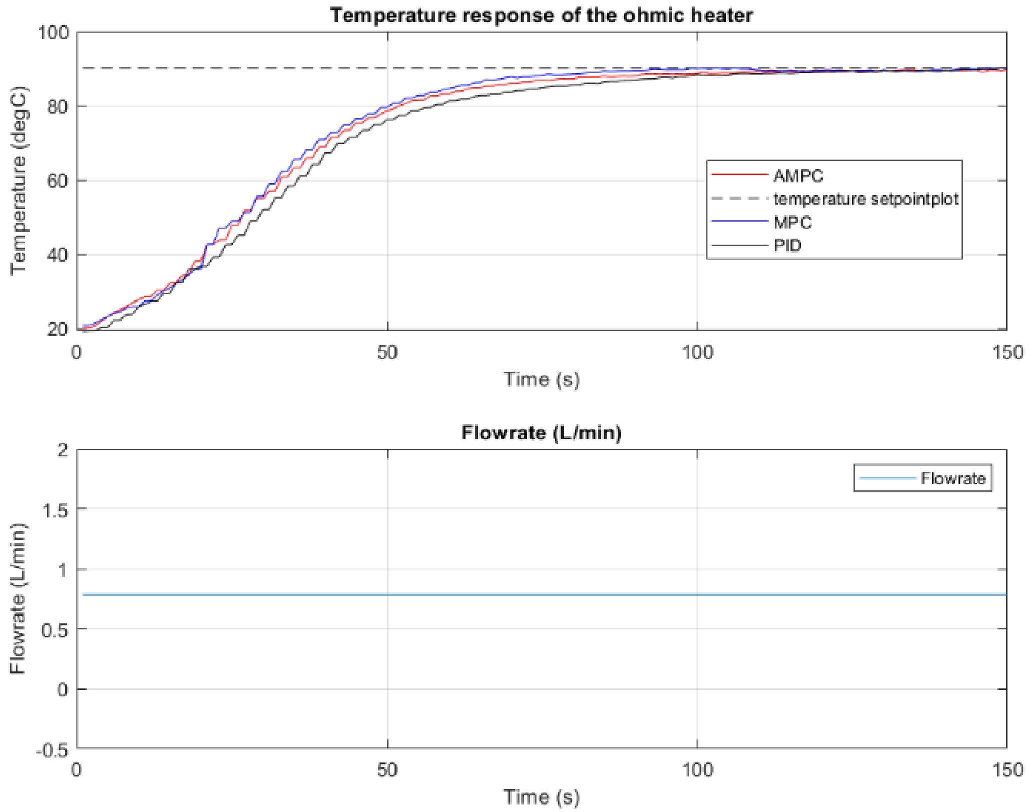

Figure 5.28. A general comparison of the deployed controllers at 0.78L/min and 0.33S/m.

Figure 5.28 above gives the experimental responses of MPC, AMPC and PID plotted together under the same conditions of flowrate and electrical conductivity.

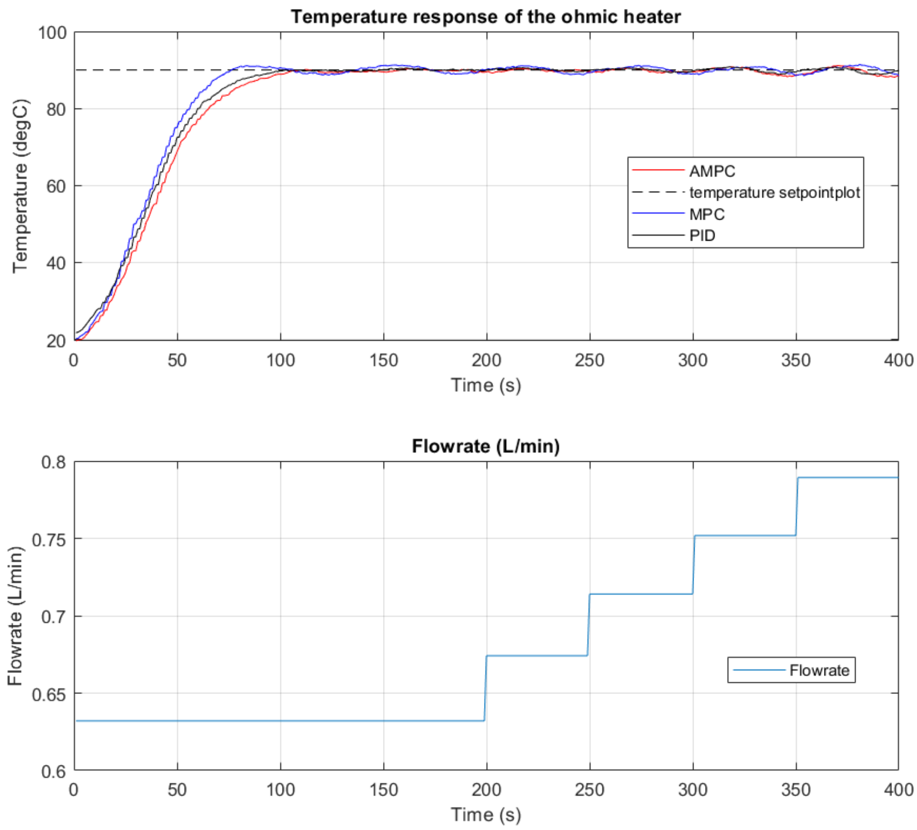

Figure 5.29. AMPC, MPC and PID experimental response for changing flowrates at 0.7S/m.

From figure 5.29 above, the continuous flow ohmic heater is subjected to changing flowrates and increased input electrical conductivity.

From the results of the modelling and applying classical and advanced controllers the following points are noted:

i. The transfer function model of the continuous flow ohmic heater to a high degree represents the physical plant.

ii. For various input parameters and operating conditions, the developed model can represent the plant.

iii. The MPC and AMPC performs better than the PID in simulation and deployment.

iv. Under varying flowrates, the AMPC performs better than MPC and PID. This indicates that under changing conditions, the AMPC is the ideal controller.

Table 5.8. A general performance comparison of PID, MPC and AMPC in simulation with constant flow rates from figure 5.28

Controller	Steady state error	Rise time	Settling time (s)
PID	0.7	90	120
MPC	0.3	80	90
AMPC	0.2	80	100

5.6 Energy comparison of the deployed controllers

The electrical power delivered by the ohmic heater is recorded by an on-board power meter in real-time in the MATLAB environment. For temperature measurements, within the electrodes, two pairs of optic fibre temperature probes are placed side by side at the midpoint of the heating chamber between the first and second electrode and just before the third electrode. Two sets of thermocouples are used. The first thermocouple is placed at the infeed into the ohmic heating chamber just before the first electrode to measure the product inlet temperature. At the outlet a second thermocouple is placed after the third electrode to further validate and measure the outlet temperature. Special care was taken to avoid placing unshielded thermocouples between the electric field. The steps taken are described below:

I. Ensure a minimum of 20L of product is in the infeed tank (e.g., saline or orange juice)
II. An appropriate flow rate of 60L/hr was set.
III. The desired process controller is chosen (e.g., PID, MPC or AMPC)
IV. Target temperature of 90 °C was set.
V. Heating commences and the process runs for 200s.
VI. Data are being recorded in real-time.
VII. The process can be repeated.

The energy balance equation can be expressed as the total energy input to total energy output given as below:

$$\sum Energy_{in} = \sum Energy_{out} \tag{5.13}$$

$$\sum Energy_{in} = (\dot{m}C_p(T_{in} - T_{room}))_{in} + E_{electrical} \tag{5.14}$$

$$\sum Energy_{out} = (\dot{m}C_p(T_{out} - T_{in}))_{out} + E_{loss}, \tag{5.15}$$

where $\sum Energy_{in}$ is the sum of the energy into the CFOH, $\sum Energy_{out}$ is the sum of energy as a result of the ohmic heating effect and thermophysical properties. $E_{electrical}$ is the electrical energy into the ohmic heater, $\dot{m}$ is the mass flowrate, C_p is the heat capacity of the heated food product. T_{in} is the inlet temperature of the food product from the infeed tank. T_{room} is the room temperature and T_{out} is the outlet temperature recorded.

The energy losses considered are due to thermal conduction to the applicators and heat loss at the titanium electrodes. Therefore, the heat loss (E_{loss}) is given by:

$$E_{loss} = \nabla\cdot(\mathrm{k}\cdot\nabla\mathrm{T}) + (\dot{m}C_{Ti}(T_{out} - T_{electrode}))_{loss}, \tag{5.16}$$

where C_{Ti} is the heat capacity of Titanium while $T_{electrode}$ is the initial temperature of the electrodes. The latent heat of vaporisation is not considered because the only opening is from the applicator outlet. The energy efficiency ɳ has described by Darvishi, Hosainpour, Nargesi, & Fadavi, (2015) and is given by:

$$ɳ = \frac{\sum Energy_{out}}{\sum Energy_{in}} \text{ X } 100. \tag{5.17}$$

5.6.1 Heating rate of saline and energy efficiency with PID, MPC and AMPC

In the figures below, the product temperature as a function of the applied voltage is presented at a constant flowrate of 60L/hr (1L/min). The performance of the choice of advanced process control is also shown by the deviation of the outfeed temperature from the setpoint heating temperature of 90 °C. The energy efficiency of heating saline to 90 °C in the ohmic heater is also presented. The energy efficiency is derived from the application of equation (4.17).

In Figure 5.30, the plot shows the overlapped temperature output profiles from the CFOH and the voltage profiles when PID, MPC and AMPC controllers are used in heating saline solution independently. The plot is zoomed in between 40s and 100s to show the performance of the various controllers.

In Figure 5.31 below, the plot shows the controller voltage output to the CFOH. The plot is zoomed between 20s and 100s to show the performance of the controllers in terms of the voltage applied.

As can be seen from Figure 5.30, the rapid heating is an advantage of ohmic heating. The outlet temperature reached the setpoint temperature from 18°C to 90°C and settled within 2 minutes of heating. Steady state error of about 2°C is observed from the PID temperature profile. The use of the MPC controller gives a better desirable outfeed temperature comparing to the use of the PID controller. A reduced steady state error of about 0.8 °C is observed comparing to 2°C when a PID controller was used.

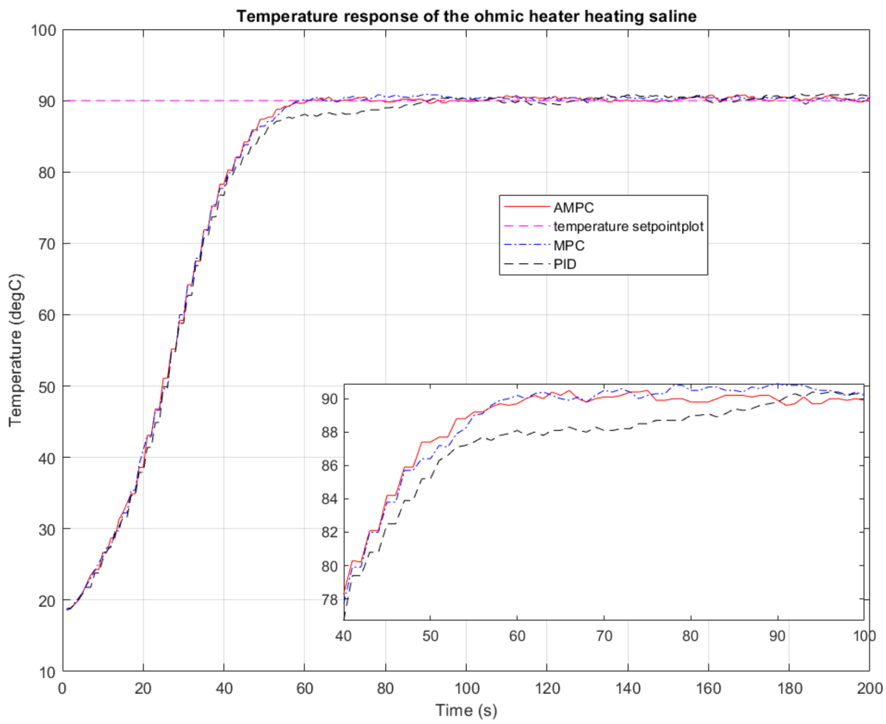

Figure 5.30 Temperature response heating saline using PID, MPC and AMPC controller. Zoomed in between 40s and 100s.

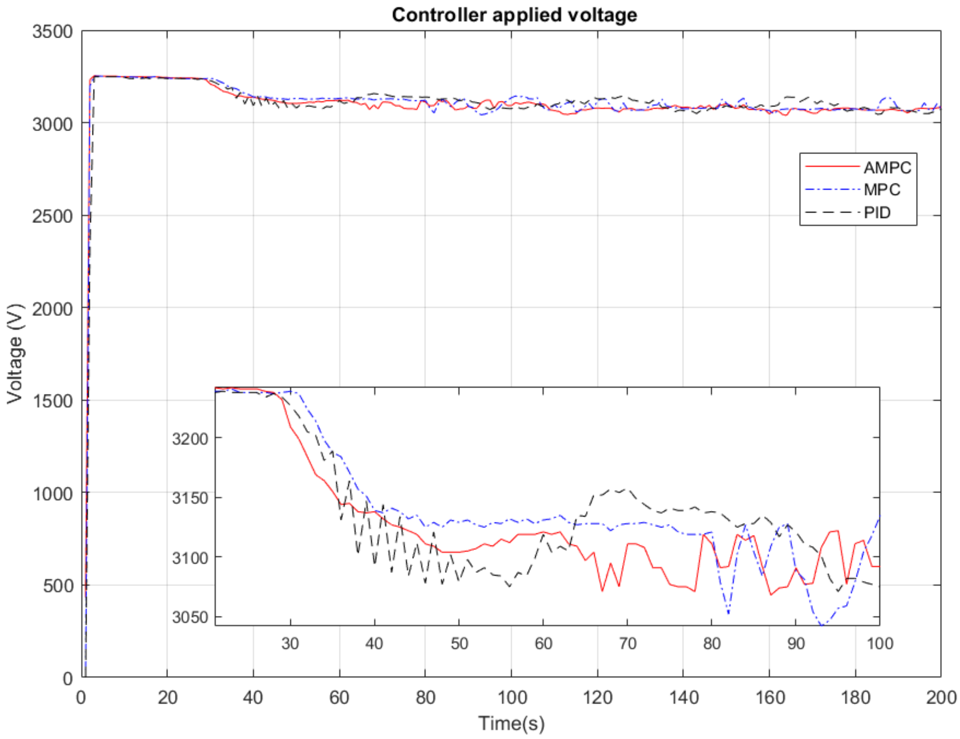

Figure 5.31 The voltage response heating saline using PID, MPC and AMPC controller. Zoomed in between 20s and 100s.

When the AMPC controller is used, the steady state error observed is about 0.6 °C. This demonstrates that the AMPC controller has a better performance in terms of tracking reference temperature setpoints than both the PID and MPC controllers. Comparing the voltage response of the AMPC controller to the PID controller, a smoother voltage profile is seen compared to an oscillatory pattern with the PID seen in Fig 5.31 from 35s onwards. When the AMPC controller voltage response is compared to the MPC controller, aggressive short steps in voltage was observed as seen in Fig 5.31 from 80s onwards. These aggressive short steps in controller voltage by the MPC in contrast to the dynamic AMPC voltage correction shows that the MPC is less robust in correcting errors.

The real-time recorded electrical power consumption and energy efficiency are shown in Figure 5.32 below.

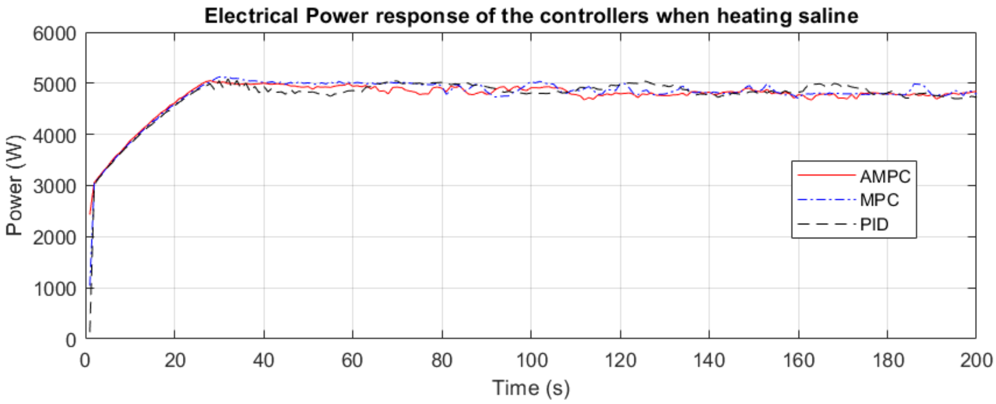

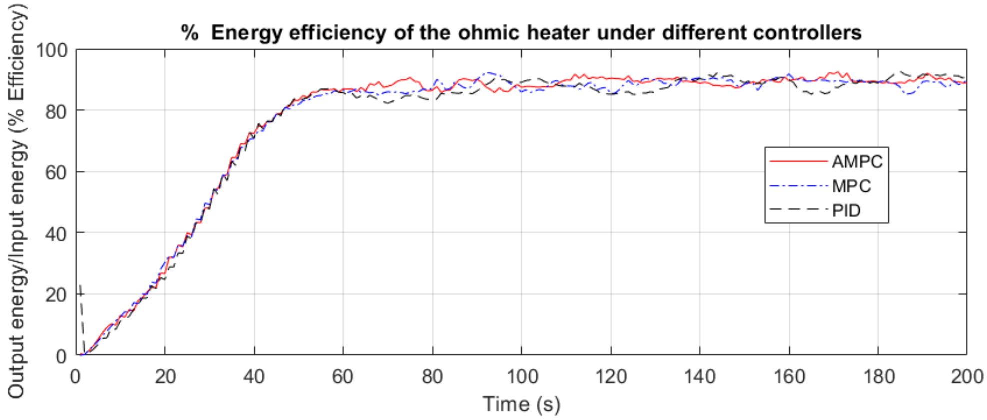

Figure 5.32. Electrical power and energy efficiency of the ohmic heater while heating saline.

In figure 5.32, the electrical power input to the CFOH is the smoothest when AMPC is used compared to PID and MPC. The PID electrical power input is observed to oscillate when the desired setpoint temperature was reached from 60s to 200s. The absence of oscillation on the electrical power input in Figure 5.32 when MPC and AMPC are used suggests that they are a more robust controller than the PID controller. Even though there is no significant change in the applied electrical power the energy efficiency when a PID controller is used is the lowest. The AMPC is observed to have the highest energy efficiency.

Table 5.8 shows the electrical power consumed and the energy efficiency of the ohmic heater between 1-60s and 60s to 200s. The efficiency is evaluated from 0 to 60s and from 60s to 200s. This is because 0 to 60s represents the temperature build up within the heating chamber.

Table 5.9 Energy consumption and energy efficiency of heated saline using PID, MPC and AMPC controller.

Time (s)	PID Power (KWh)	MPC Power (KWh)	AMPC Power (KWh)	PID Energy efficiency (%)	MPC Energy efficiency (%)	AMPC Energy efficiency (%)
1-60s	4.46	4.57	4.5	86.39	87.50	88.3
60-200s	26.5	26.4	26.2	87.91	88.40	89.1

From the table above, the use of the MPC controller increases the energy efficiency of the ohmic heater. This can be seen from the temperature plot in Figure 5.31 The conversion of input energy to heat for the continuous flow ohmic heater is more efficient using a MPC controller than a PID controller. However, there is no significant change in the electrical energy consumed by both controllers. The energy efficiency is the highest when compared to PID and MPC controller. This means that using AMPC to the ohmic heater gives a higher temperature conversion rate from the applied power.

5.6.2 Heating rate of orange juice and energy efficiency with PID, MPC and AMPC

A similar procedure to section 5.6.1 is repeated for orange juice at infeed temperature of 9-10 °C. In Figure 5.33, the temperature response while heating orange juice to 90 °C when a PID, MPC and AMPC controller is used is shown. The orange juice in the infeed tank is 10 °C, the initial temperature recorded from the outfeed temperature probes due to heating as seen in figure 5.33 below is 18 °C.

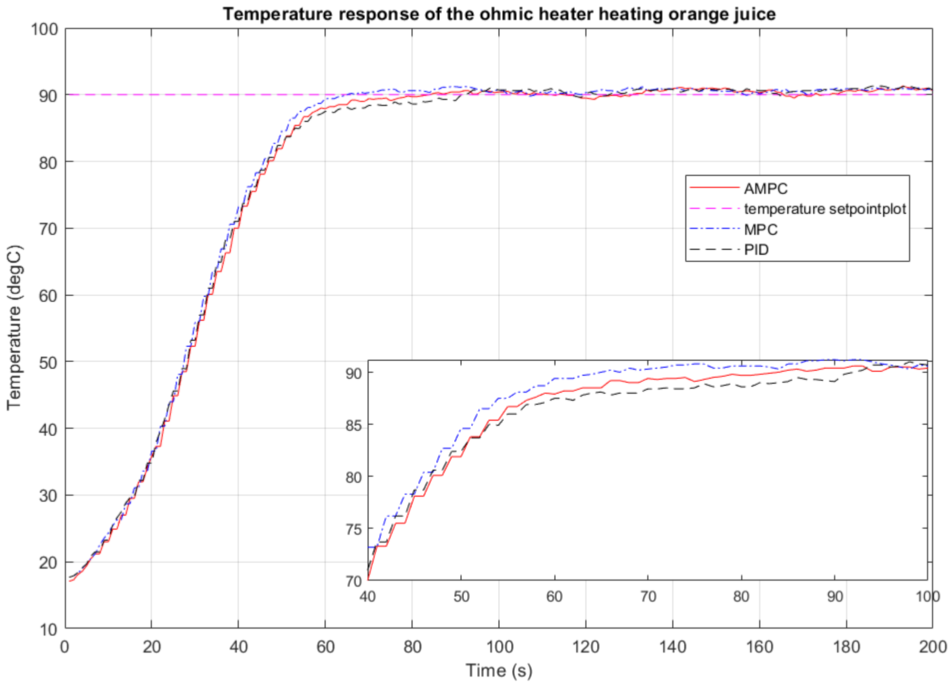

Figure 5.33. Temperature response heating orange juice using PID, MPC and AMPC controller.

In Figure 5.33, the rapid heating of the CFOH is seen as the temperature rises from 10°C to 90°C and settles in just over 70s. When the MPC control is used, the temperature response of the CFOH is desired, steady state error is less than 0.8°C and the output temperature settles within 60 seconds. The settling time when AMPC is used to heat orange juice to 90°C is about 65s. From figure 5.33, the PID controller exhibited the least performance due to its large settling time of 95s.

In figure 5.34 below, the controller voltage response to the CFOH during heating is presented. The controller voltage response shows how the HV is applied to the CFOH by the controllers to obtain the desired output temperature.

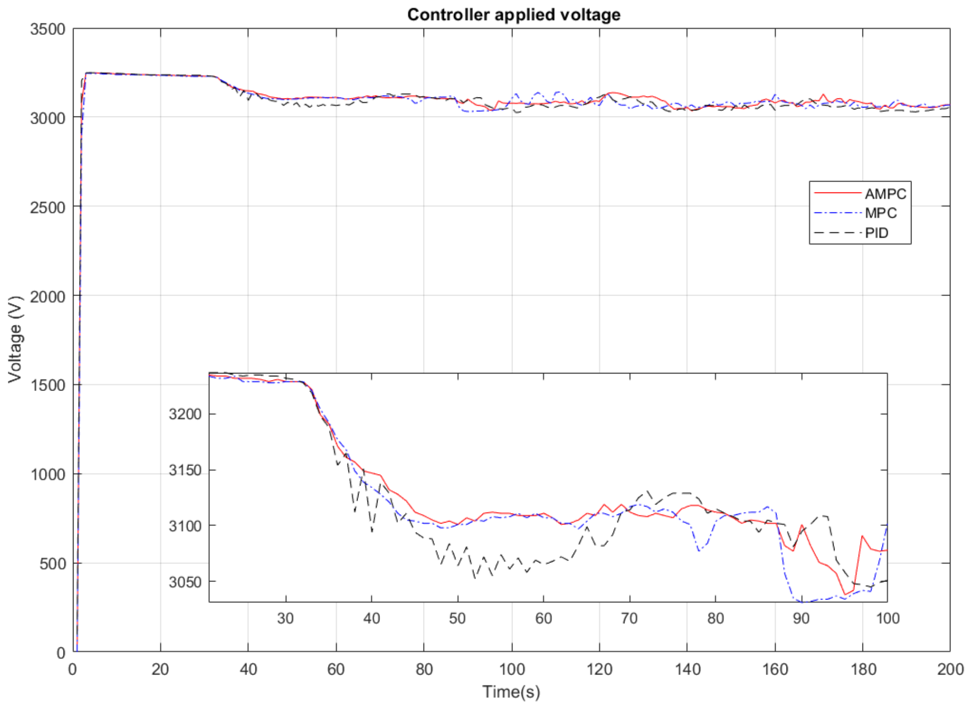

Figure 5.34 The voltage response heating orange juice using PID, MPC and AMPC controller. Zoomed in between 20s and 100s.

From Figure 5.34, voltage oscillation is observed between 20s and 100s this is because the PID controller struggles to keep the output temperature at the desired setpoint of 90°C (as shown in fig 5.33). The voltage profile of the AMPC is less aggressive compared to the response of the MPC and reduced voltage oscillation is seen when compared to PID response.

In Figure 5.35, the electrical power response profiles and energy efficiency of the CFOH when PID, MPC and AMPC controller is used to heat orange juice is shown.

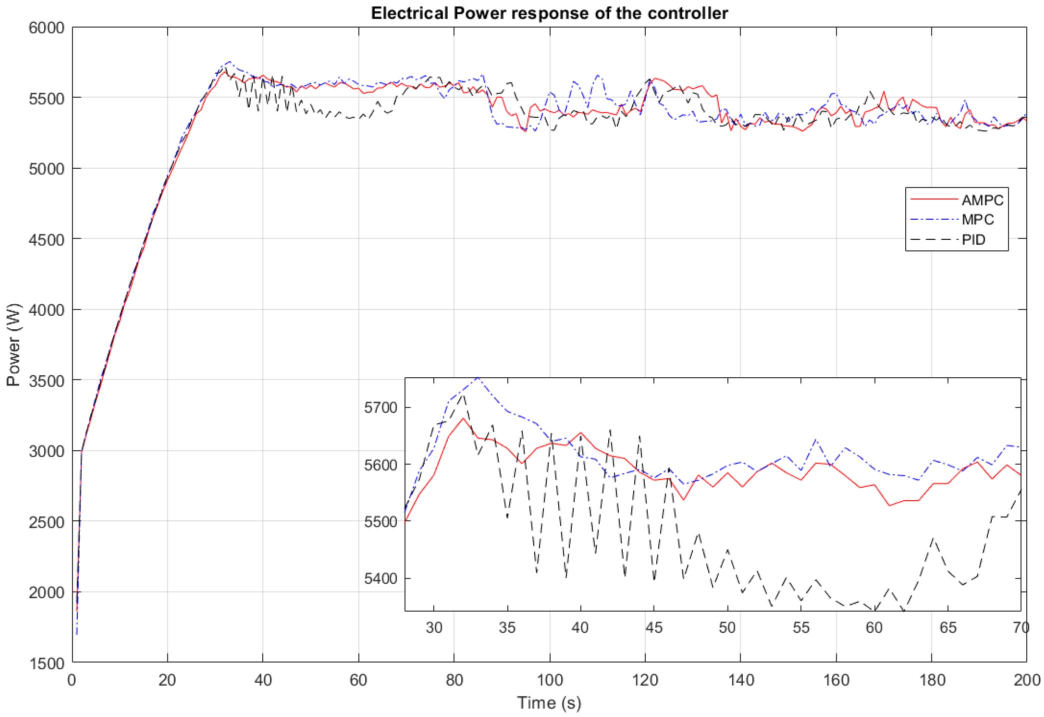

Figure 5.35. Electrical power and energy efficiency of the ohmic heater

From Figure 5.35, undesired sustained oscillation is observed for the electrical power input when the PID controller is used. This sustained oscillation is as a result of the PID performance. Between 30s to 70s the PID controller struggles to keep the output temperature close to the desired setpoint temperature. This resulted in large steady state error and large settling time as shown in figure 5.33 above.

It can be seen in Figure 5.35 from the electrical power input that the MPC takes aggressive control actions to keep the output temperature close to the desired temperature of 90°C. In Figure 5.35, the electrical power input to the CFOH when AMPC controller is used appears to be aggressive albeit not as aggressive as the MPC.

Figure 5.36 below shows the energy efficiency of the ohmic heater while heating orange juice. The efficiency is derived from the equations presented in section 5.6.

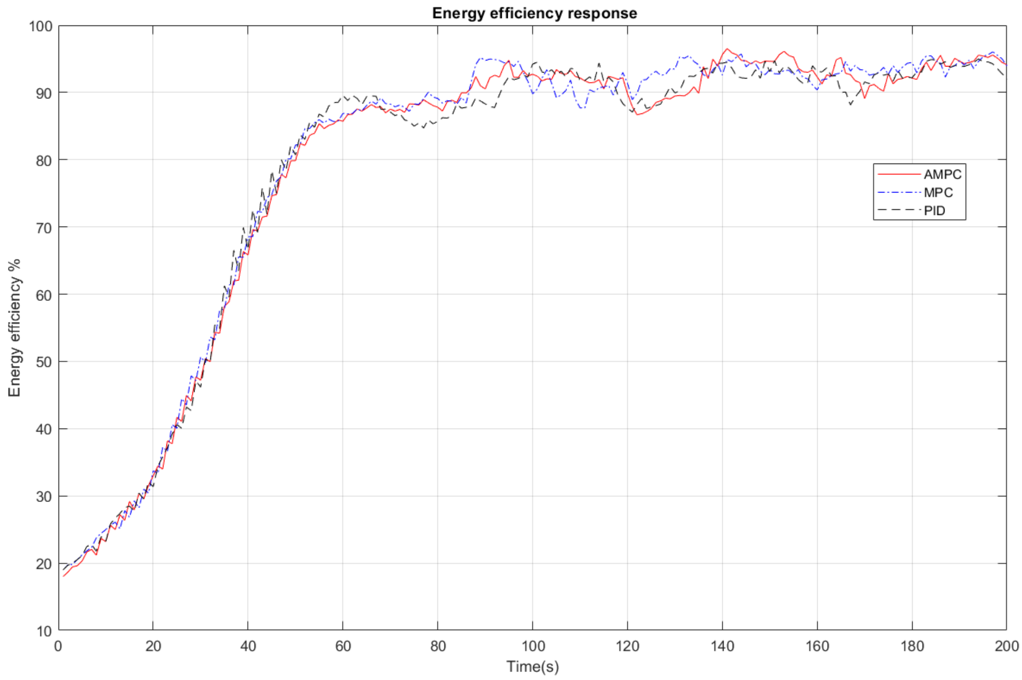

Figure 5.36. Energy efficiency of the ohmic heater heating orange juice

The energy efficiency of the CFOH when AMPC is used decreases just after 120s and then increases. This trend is consistent with both the PID and MPC and can be attributed to product mixing within the heating chamber. This is because heat builds up within the two heating sections of the ohmic cell and food products in each section are at different temperatures.

Table 5.10 gives the energy consumption and energy efficiency of the CFOH when the PID controller is used.

Table 5.10 Energy consumption and energy efficiency of heated orange juice using PID, MPC and AMPC controller.

Time (s)	**PID Power (KWh)**	**MPC Power (KWh)**	**AMPC Power (KWh)**	**PID Energy efficiency (%)**	**MPC Energy efficiency (%)**	**AMPC Energy efficiency (%)**
1-60s	4.9	5.0	4.9	52.5	52.6	51.6
60-200s	29.5	29.6	29.5	91.0	92.1	91.8

From Table 5.10, reduced energy efficiency is observed in the first 60 seconds of operation. The reduced energy efficiency which is the conversion of electrical energy to heat can be attributed to the low inlet product temperature of 9-10 °C. In table 5.9, the MPC has a higher energy efficiency when compared to the PID controller. This can be attributed to the aggressive nature of the controller action to keep the output temperature close to the desired setpoint temperature. From Table 5.10, no significant change in the electrical power consumed during heating is seen when compared to PID and MPC. A general trend of lower energy efficiency is observed from 0 to 60 seconds. Comparing to PID, the AMPC has a higher energy efficiency but not to the MPC.

5.7 Discussion

From the results above, it was observed that while heating saline solution using PID, MPC, and AMPC, there is no significant change in the electrical power consumed during heating. However, the energy efficiency conversion from electrical power to heat improves when an AMPC controller is used. While heating saline, the tuned PID controlled system has the lowest energy efficiency (87.9%), MPC has an energy efficiency of 88.40%, and AMPC has an energy efficiency of 89.1%

For the heating of orange juice, a low energy efficiency of less than 53% was observed in the first 60 s of operation. This is due to the low input product temperature of 9 °C. After the first 60 s of operation, the temperature built up within the heating chamber significantly increased, hence the increased energy efficiency of 91.0%, 92.2%, and 91.8% for PID, MPC, and AMPC, respectively. Also, no significant difference in the electrical power is observed. In Figure 5.37, the energy efficiency comparison chart of the controllers when applied to saline and orange juice is shown.

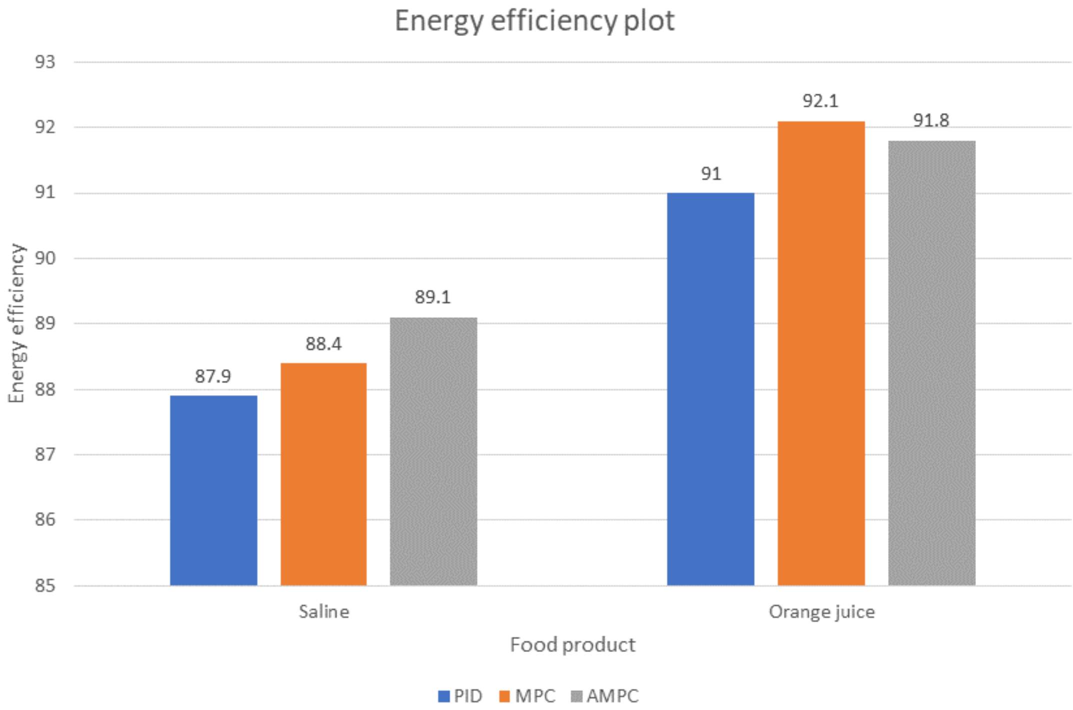

Figure 5.37. Energy efficiency plot of the ohmic heater for different controllers

It was observed that the MPC has a higher energy efficiency than PID and AMPC when heating from a much lower temperature of 9 °C. However, the AMPC has a higher energy efficiency than the PID and MPC when heating starts from a higher temperature of 18 °C. The author is tempted to attribute this characteristic to the very aggressive control of the MPC to keep the output temperature close to the desired setpoint value, but future studies will be conducted to fully answer this question.

In this study, the food products used were a saline solution and orange juice, which are uniform and homogenous in nature. When the CFOH is used, the heating times are drastically reduced to less than 1 min for a flow rate of 1 L/min with a minimum efficiency of 87.9% for saline and 91% for orange juice. The energy efficiency achieved is very similar to the work reported in Aydin, Kurt, & Kaya, (2020), where a non-homogenous food product consisting of fish samples was heated using a smaller scale batch OH (2.5 kW), and a similar trend of fast heating time and energy efficiency of 89.89% were recorded. Due to the lack of published work using CFOH, it is not possible to directly compare with other results in the literature. However, Atuonwu et al. (2018) produced a detailed analysis of energy performance for several innovative and conventional food preservation technologies including high-pressure processing (HPP), microwave volumetric heating (MVH), batch ohmic heating (OH), and conventional thermal treatment (UHT) where orange juice was heated from ambient temperature (approx. 20 °C) to 76 °C. For a fair comparison, the best results from each of the heating methods with different set-ups were selected to compare with the results produced in this paper. In Atuonwu et al. (2018), a hypothetical continuous OH (Cont. OH) was also used in the comparison where the continuous OH process, without voltage switching temperature control, was expected to achieve an energy efficiency of 95%, in theory. The comparison chart can be seen in Figure 5.38.

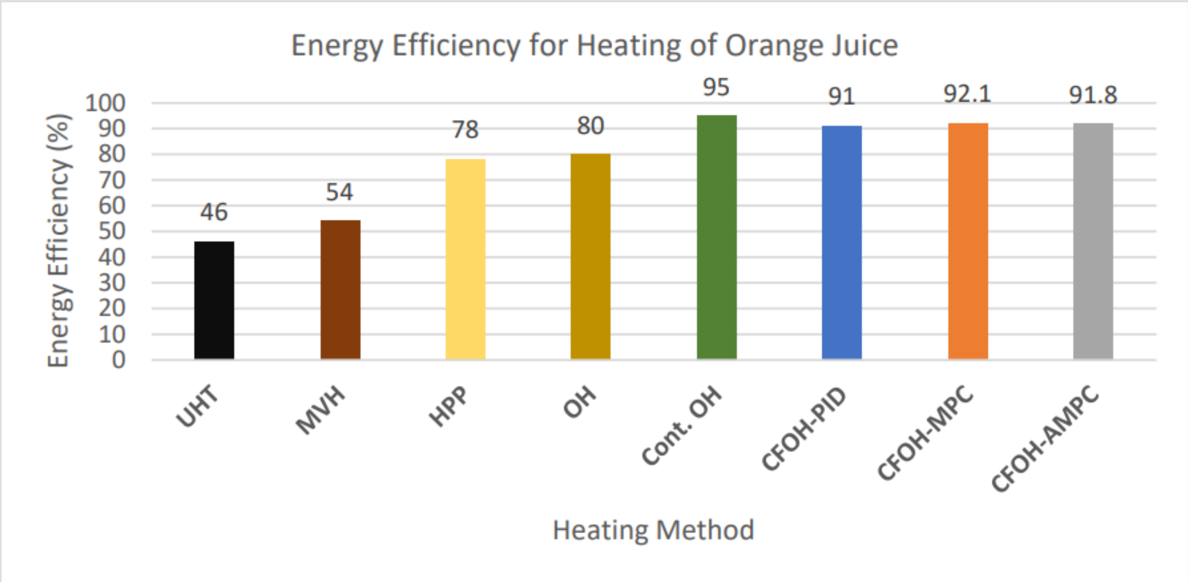

Figure 5.38. Energy efficiency comparison with different heating methods. Note: the first 5 data were quoted from Atuonwu et al. (2018).

As shown in Figure 5.38, not surprisingly, the conventional technology UHT—which was represented by an electrically powered hot water-to-orange juice heat exchanger—had the lowest energy efficiency of 46% because of the heat loss during heat transfer. The MVH system, even when the magnetron cooling energy was discounted, could only achieve 54% of energy efficiency. As a non-thermal method, HPP could produce 78% of energy efficiency at a 95% filling ratio, which was a huge improvement from 31% of energy efficiency at a 36% filling ratio. The batch OH process had the highest energy efficiency of 80% among all the thermal processes. It is clear that the CFOH process in this work compares favourably with all the heating technologies from Atuonwu et al. (2018), even when the starting temperature was much lower at 10 °C. The average energy efficiency of 91.6% for all three controllers is not far off from the 95% claimed in the hypothetical continuous OH process.

5.8 Summary

In this chapter, the development of the CFOH model using state space and transfer function approach was presented. The modelling technique combines the energy balance equation, electrical conductivity as a function of temperature and the physical dimensions of the built CFOH plant to develop the model. The model was built in MATLAB/Simulink environment using a combination of block diagrams and function blocks.

The developed model was validated in open loop with experimental data. In the open loop model validation, real-time data passed to the model and the output temperature is compared to the experimental temperature. Saline solution was the test solution used in the validation experiment.

The implementation of advanced process control from a lab-based PC unto the PLC hardware using OPC server/client protocol was described. The process parameters which form the input and output tags from the PLC were described. The tags transmit the data values from the temperature sensors, voltage sensor, current sensor, power sensor, motor speed control and the HV thyristor (which is the controller output).

The development of the PID, MPC and AMPC controllers were discussed. Before the controllers were deployed on the CFOH, the controllers were evaluated in simulation first. Before the controllers were deployed, a safety system was developed to automatically set the HV thyristor values to safe operating regions to prevent overheating and high electrical current values. The performances of the controllers in simulation were evaluated and compared to the performances when deployed physically on the CFOH. This presented a hardware in the loop (HIL) system whereby the controllers can be fine-tuned in simulation instead of running multiple physical trials.

Heating trials were conducted on saline solution and orange juice. The performance of PID, MPC and AMPC controller in terms of the rise time and steady state error was evaluated. Further comparison was presented to evaluate the energy efficiencies of the controllers. It was found that the AMPC is the most energy efficient controller followed by MPC and PID.

Chapter 6. Industrial heating of tomato basil sauces

In this section, the Proportional, Integral and Derivative (PID) controller, Model Predictive Controller (MPC) and Adaptive Model Predictive Control (AMPC) were implemented on the designed continuous flow ohmic heater (CFOH) pilot plant to process tomato basil sauce. The tomato basil sauce before being heated is made up of tomato puree, basil, spices, and other ingredients. In this section, a case study for the pilot scale heating of tomato basil sauce with advanced process control with applications in the food industry is presented. The performances and energy efficiencies of the different control techniques implemented are compared. The author presents the quantitative results which demonstrate significant improvements in controlling the CFOH process regarding food materials and the industrial practicality of using the CFOH.

The gaps in literature which this research addresses are:

- Energy efficiency analysis of a CFOH pilot plant
- The industrial practicality of applying advanced process control to a CFOH pilot plant.

6.1 Material and methods

6.1.1 Materials

50L of Tomato sauce was prepared from commercially available pure tomato puree purchased from a local market which is then mixed with basil, spices, and other ingredients.

Figure. 6.1. Pure tomato puree before the addition of spices and ingredients.

Figure. 6.2. The tomato basil sauce is prepared after the addition of spices and other ingredients.

The tomato basil sauce was heated in the continuous flow ohmic heater (CFOH). In the heating process, the initial mixing of the sauce is conducted in the infeed tank to ensure that the product is uniformly mixed. The tomato basil sauce was prepared at room temperature and heated to 90°C at a constant flowrate of 1L/min in the CFOH. The heated sauce is collected in the outfeed tank (see Figure 4.1.).

Even though some quantity of olive oil and sunflower oil which was about 4% of the total volume was added as part of the ingredients, the presence of salt and ionic spices was sufficient to significantly raise the electrical conductivity of the sauce. During the heating process, the temperature of the product was measured using optic fibre temperature sensors positioned along the heating chamber. A further set of two thermocouples were used to measure the product infeed temperature and to validate the outfeed temperature. The steps taken in the analysis of the energy efficiency of the CFOH are as described in section 5.7.

6.2. Results

During the ohmic heating of the tomato basil sauce, the controller objectives are:

- Desired transient response to user temperature input. This ensures that the temperature rise within the heating chamber is not too fast or too slow. This goal also places emphases on eliminating temperature over-shoots in order to prevent boiling and pressure build up within the heating chamber.
- Desired steady state response. This objective eliminates steady state error at the setpoint temperature.
- Robustness. This ensures that the CFOH has a stable and controllable response.

Figure 6.3 below shows the temperature response of the CFOH when the tomato basil sauce is heated to a setpoint temperature of 90°C using a PID controller. The electrical power supplied by the controller during heating is also shown as recorded by an onboard power meter in the control panel. The performance of the PID controller is shown by the deviation of the output temperature from the setpoint temperature. The trend of the energy efficiency derived from equation (5.7.5) is also shown.

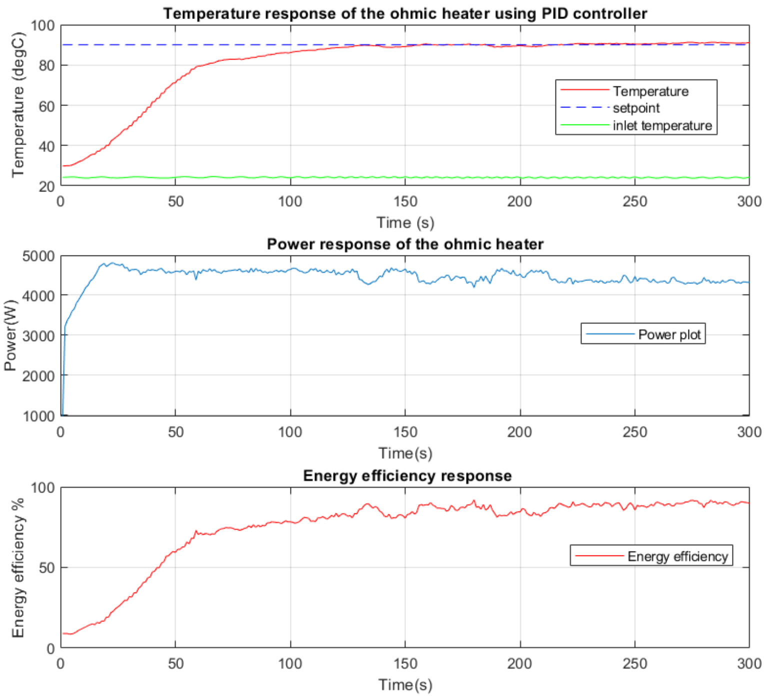

Figure. 6.3. Temperature response heating tomato basil sauce with PID controller.

As seen in Figure 6.3, the rapid heating derived from OH is an advantage as the outfeed temperature is close to the setpoint of 90°C in less than 2 minutes of run time.

In Figure 6.4 below, the temperature response is presented when the MPC controller is used in heating. The MPC controller has a shorter settling time of 90s compared to that of the PID controller of 117s as shown in table 6.1.

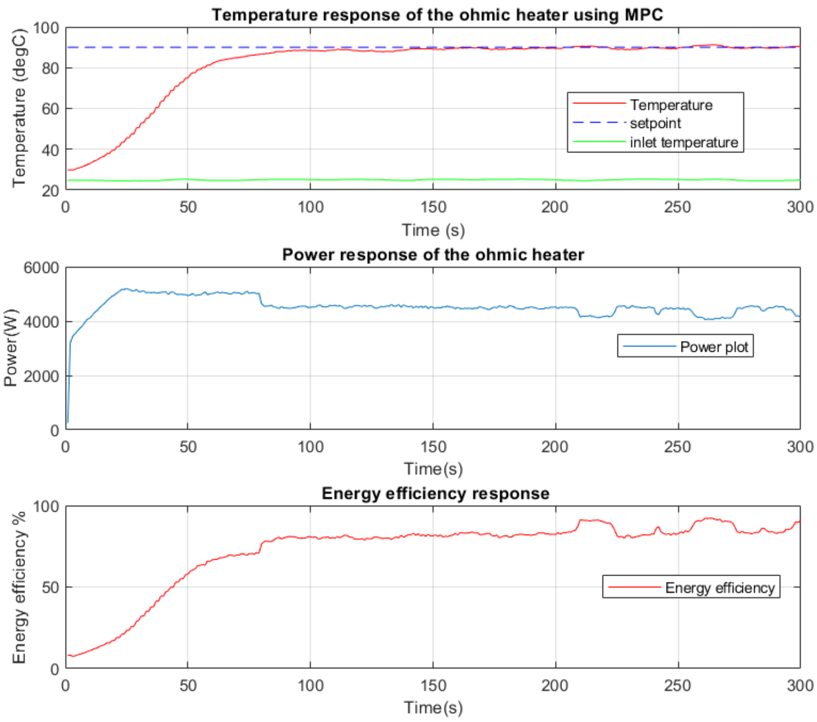

Figure. 6.4. Temperature response heating tomato basil sauce with MPC controller.

The response from applying AMPC controller is shown in Figure 6.5. The performance of the AMPC controller in terms of temperature transient time, steady state error, temperature overshoots, temperature undershoots and settling time exceed both the PID and MPC controller. The settling time of the AMPC was observed to be 76s, a much shorter time compared to 117s and 90s of PID and MPC respectively.

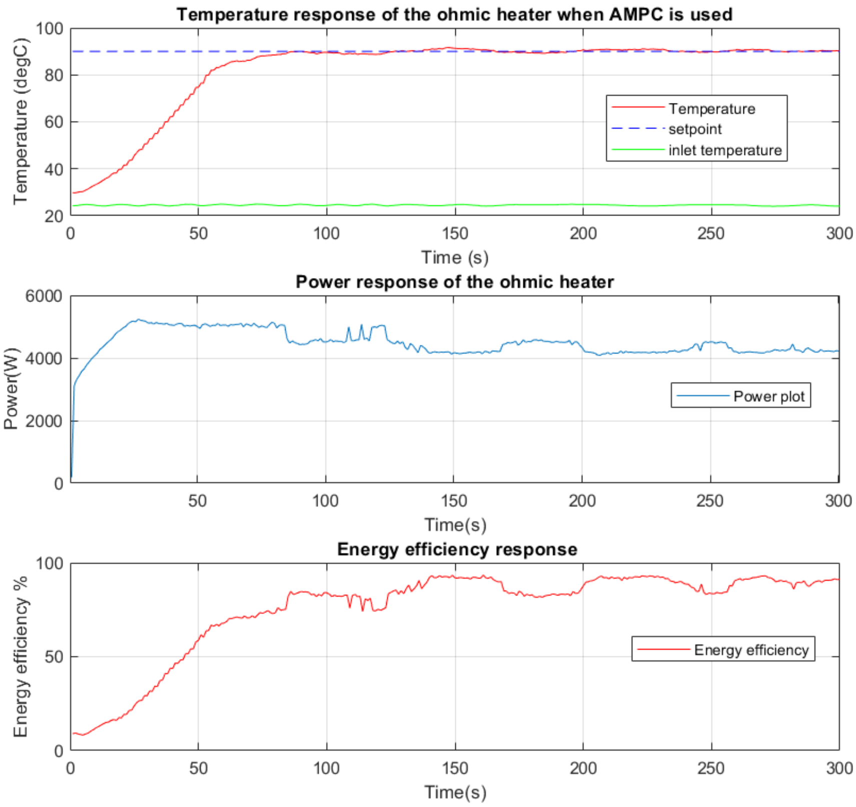

Figure. 6.5. Temperature response heating tomato basil sauce with AMPC controller

The performances of the PID, MPC and AMPC are further evaluated in table 5.1 below based on the objectives of the controller.

Table 6.1 Performance comparison of PID, MPC and AMPC controllers.

Controller	**Settling time (2% criteria)**	**Max overshoot**	**Max undershoots**
PID	117s	91.2°C	88.8°C
MPC	90s	91.2°C	88.8°C
AMPC	76s	91.6°C	89.7°C

According to Table 6.1, the AMPC controller gives the shortest settling time of 76s which indicates that the final and set-point temperature of 90°C is reached (with a 2% criterion) the quickest. The PID controller is the slowest to reach the setpoint, at 117s. The performance of the PID and MPC controllers are similar in terms of the maximum overshoot and maximum undershoot temperature observed. With the AMPC, the maximum overshoot observed was 91.6°C which is higher than both MPC and PID. However, the AMPC has a higher maximum temperature undershoot of 89.7°C which indicates that the deviation from the setpoint temperature is the lowest compared to other controllers.

Table 6.2 below shows the root mean square error (RMSE) of the temperature response of the PID, MPC and AMPC controllers when compared to the temperature setpoint of 90°C. The RMSE comparison is taken after the first 60s of heating.

Table 6.2 RMSE values of the PID, MPC and AMPC controllers.

Controller	**Setpoint Temperature (°C)**	**RMSE value**
PID	90	2.99
MPC	90	1.83
AMPC	90	1.18

From table 6.2, the weighted average error between the setpoint temperature and actual temperature for the AMPC is 1.18 which is the lowest compared to the PID and MPC controllers. A low RMSE value of 1.18 indicates a good value when compared to 90°C indicates less than 2% deviation from the setpoint temperature. In terms of performance comparison between the controllers, the AMPC gives the least RMSE.

Table 6.3 below shows the mean energy comparison of the different controllers in Figure 6.3, Figure 6.4, and Figure 6.5. The mean efficiency of the controller is recorded from 60s to 300s. The mean efficiency is taken after 60s to ensure appropriate temperature build up within the heating chamber.

Table 6.3 Energy consumption and energy efficiency of the implemented controllers

Time (s)	PID Power (KWh)	MPC Power (KWh)	AMPC Power (KWh)	PID Energy efficiency (%)	MPC Energy efficiency (%)	AMPC Energy efficiency (%)
0-60s	4.41	4.70	4.70	35.14	33.57	33.98
60-300s	71.47	71.89	70.76	88.72	88.96	89.81

From Table 6.3 above, the conversion of electrical energy to heat with the CFOH is highest when AMPC controller is adopted, compared to PID and MPC. This indicates that the rate of conversion of electrical energy to heat is highest with AMPC. When heating up the tomato sauce (in the first 60s), low energy efficiencies were observed for all 3 different controllers. This is due to the initial temperature building up within the heating chamber and the viscosity of the tomato sauce. The heating rate and energy efficiency conversion is generally low in the initial build up for product with higher viscosity (Marcotte, 1999).

6.3 Discussion

Faster heating rate of the CFOH comes with detrimental effects such as temperature overshoots, uneven heating, boiling and large steady state errors. Hence, a steady rise in temperature is preferred. This steady rise in temperature is seen in Figures 6.3-6.5 and ensures uniform heating of the tomato sauce and the tomato sauce does not boil within the heating chamber. Therefore, the PID, MPC and AMPC controllers are tuned to remove temperature overshoots for achieving desired temperature profiles. The efficiency seen from the results does not take into consideration the energy loss in the positive displacement infeed pump. The energy dissipated in the pump is assumed to be isolated from the heating process.

The results demonstrated in this section suggest that the practical industrial application of continuous flow ohmic heating of tomato basil sauce can be an alternative to conventional heating. The heating experiments were carried out using tomato basil sauce prepared using pure tomato puree, basil, spices and other ingredients. The advanced MPC and AMPC controllers were designed based on a validated mathematical model and innovatively implemented using an OPC server through MATLAB/Simulink for real-time control. This is the first time such experimental results have been obtained and reported. From the experimental results, it was established that the CFOH has an energy efficiency conversion percentage of at least 88.72%. The analysis has also shown that the energy conversion percentage can be increased by applying advanced controllers such as MPC and AMPC. It was also observed that during the heating process, there are no significant electrical power differences when PID, MPC and AMPC controllers were used, and that the energy efficiency observed was a function of the controller performance.

6.4 Summary

In this chapter, the industrial pilot scale heating trial of tomato basil sauce was discussed. The trial was conducted in collaboration with a local manufacturer of food sauces in Sheffield. The aim of this trial was to test the practicality of the CFOH and advanced process control to the heat treatment of tomato sauce. During the trial 50L of tomato basil sauce was heated to 90°C at a flow rate of 1L/min. Each heating batch was left to run for at least 6minutes. When the heated tomato sauce was collected, the taste test conducted on the spot was adjudged to be very satisfactory.

The use of advanced process controllers in the heating process was shown to be very advantageous. With the use of MPC and AMPC, better desired temperature response was observed compared to the PID controller. With AMPC and MPC, the desired steady state response while heating the sauce at 90°C was observed to be very satisfactory as the largest temperature deviation was less than 1°C from the setpoint of 90°C.

Finally, the energy efficiencies of the MPC, AMPC and PID controllers were compared. The comparison was done during the temperature transient stage (0-60s) and when the temperature has reached steady state (60 – 300s).

Chapter 7. Conclusions and future work

At the outset of this thesis, the author's research aimed to apply ohmic heating and advanced process control to industrial food processing, driven by the motivation to improve food process sustainability and create an energy efficient heating process. This concluding chapter presents the significance of the findings, their contribution to knowledge, the achievement of the aims and objective, and new questions to be considered following these discoveries. Section 7.1 presents the main conclusions drawn from the research work presented in Chapters 3, 4, 5 and 6. Meanwhile, Section 7.2 introduces remaining questions yet to be explored and future works that would complement the research findings.

7.1 Main conclusions

Chapter 3 demonstrated the modelling and validation of a batch ohmic heater using several modelling techniques. The first principle PDE model of the batch ohmic heater was developed using COMSOL, while MATLAB/SIMULINK was employed for the mathematical model and system identification model. The approach to developing the batch ohmic heater model ranged from the first principle (mathematical model using block diagram) to data-driven approach (system identification model). The developed models used a simple algorithm based on the energy balance equation, thus making them less computationally intensive. The CFOH model results were compared and evaluated against real life experimental data. The minimum normalised root mean squared error (NRMSE) observed was 0.00895 and the maximum NRMSE was 0.0165. The maximum deviation of temperature between real-life experiment and the simulation was about 3°C.

In Chapter 4, the design and development of the CFOH plant were discussed. The design specifications of the CFOH, including the power capacity, the maximum infeed electrical conductivity, the maximum operational current, maximum product flow rates, and maximum outfeed temperature were presented. This chapter also provided general operating procedures to ensure safe usage of the CFOH. All components used in the development of the CFOH were described.

Chapter 5 took a holistic approach to the modelling, design and performance analysis of a CFOH. A novel approach to design and validate a CFOH model based using the state space model and relationship between the energy balance equation and other process parameters was presented in chapter 5. In collaboration with industry partners and technicians, a CFOH pilot plant with a capacity of 1L/m and power of 10kW was designed and constructed. The developed state-space model of the CFOH was validated using experimental data. This model was validated first in open-loop without a controller and then a controller was deployed in a closed-loop configuration. During the operation of the CFOH, the energy efficiency analysis of the plant when different controllers were deployed to the plant was conducted. The work done with the CFOH presented a novel approach to modelling the CFOH and deploying advanced process control from the MATLAB environment to a PLC-based hardware using OPC servers. The PID, MPC and AMPC controllers were deployed on the CFOH, and the performance of these controllers in terms of energy efficiency, heating rate and steady state errors were evaluated. It was observed that the AMPC and MPC are more energy efficient than the PID controller in heating operations. However, it was observed that while heating product from a colder input temperature the MPC had a better efficiency than the AMPC (as seen in fig 5.37). To obtain a desired transient heating response, the AMPC, MPC and PID controllers can be tuned accordingly to the operator's choice. In tuning these controllers, the PID is the simplest to tune because only three terms are varied. The AMPC is complex to tune and improve, HIL technique is required to tune the AMPC controller. This makes the AMPC cumbersome to fine tune. The AMPC gives the least steady state error while the largest steady state error was observed with the PID controller. It was also observed that transient oscillations about the setpoint temperature is more prominent with the PID controller.

In chapter 6, the industrial pilot scale application of the CFOH for heating tomato basil sauces was presented. The performance and energy efficiencies of the PID, MPC and AMPC controllers were compared. The work undertaken at NCEFE with respect to OH, advanced process control and pilot plant scale implementation represented another step towards creating a robust CFOH pilot plant system. The envisioned robust CFOH pilot plant would be energy efficient, and the advanced process control method used would accommodate different foods with various chemical and thermophysical properties. Ultimately, this would enable the CFOH pilot plant to be autonomous, energy efficient and more accurate in heating food products to desired temperature setpoints.

7.2 Future work

This work focused on the modelling, control, and analysis of MEF in food processing. The contributions presented represent only a fraction of the true potential of MEF in food processing. In this section, potential questions and areas of interests are suggested for further investigation regarding the CFOH.

7.2.1 Addition of insulated holding tubes

The current design of the CFOH only includes an outfeed tank (see figure 4.1) that collects heated food products. Incorporating insulated holding tubes into the CFOH design would ensure that even the slowest-heating food particle flowing through the heating chamber gets commercially sterilised (Kamonpatana, 2012). These holding tubes would also promote uniformity in the exit temperature of the food products if the residence time were short. (Varghese, Pandey, Radhakrishna, & Bawa, 2014). Ultimately, the inclusion of insulated holding tubes could extend the functional capability of the CFOH, enabling it not only to heat food particles, but also to pasteurise and sterilise food products.

7.2.2 Microbial lethality test

Based on the analysis of existing literature, Escherichia coli is found to be the most frequently analysed microbial species in microbial lethality tests. However, studies focusing on fungi are relatively less numerous compared to other bacteria species (Müller, Ferreira Marczak, & Sarkis, 2020). It is necessary to investigate the effect of MEF using the CFOH on other species of bacteria and fungi and compare the outcomes to those obtained with conventional methods. The parameter in conventional heating methods that ensure the desired degree of lethality and microbial reduction is the duration for which the food must be kept at a specific temperature (Raso & Barbosa-Cánovas, 2003). The effect of variables such as electric field, frequency and residence time needs to be studied further to attain a desirable level of microbial lethality and inactivation. For example, the effect of frequency on microbial lethality needs to be further studied because there is scarce experimental data to explain the real impact on the microbial inactivation rate (Müller, Ferreira Marczak, & Sarkis, 2020. The exploration of additional technological functionality such as pressure-assisted sterilisation could further enhance the capability of the CFOH, especially when temperatures reach the boiling point of the heated food.

References

Airikka, P. (2004). Advanced control methods for industrial process control. Computing & Control Engineering Journal. 15. 18- 23. 10.1049/cce:20040303 Applied mathematics for science and engineering (2014). . Beaverton: Copyright Clearance Centre.

Assiry, A. M., Gaily, M. H., Alsamee, M., & Sarifudin, A. (2010). Electrical conductivity of seawater during ohmic heating. Desalination, 260(1), 9-17. doi: 10.1016/j.desal.2010.05.015

Atuonwu, J. C., Leadley, C., Bosman, A., Tassou, S. A., Lopez-Quiroga, E., & Fryer, P. J. (2018). Comparative assessment of innovative and conventional food preservation technologies: Process energy performance and greenhouse gas emissions. Innovative Food Science & Emerging Technologies, 50, 174-187. doi: 10.1016/j.ifset.2018.09.008

Aydin, C., Kurt, Ü, & Kaya, Y. (2020). Comparison of the effects of ohmic and conventional heating methods on some quality parameters of the hot-smoked fish pâté. Journal of Aquatic Food Product Technology, 29(4), 407-416. doi:10.1080/10498850.2020.1741752

Bemporad, A., & Filippi, C. (2003). Suboptimal explicit receding horizon control via approximate multiparametric quadratic programming. Journal of Optimization Theory and Applications, 117(1), 9-38. doi:10.1023/A:1023696221899

Bogner, S., & Colburn, M. (2011). Rapid liquid heating

Cappato, L. P., Ferreira, M. V. S., Guimaraes, J. T., Portela, J. B., Costa, A. L. R., Freitas, M. Q., et al. (2017). Ohmic heating in dairy processing: Relevant aspects for safety and quality. Trends in Food Science & Technology, 62, 104-112. doi:10.1016/j.tifs.2017.01.010

Chandarana, D. I., & Unverferth, J. A. (1996). Residence time distribution of particulate foods at aseptic processing temperatures. Journal of Food Engineering, 28(3), 349-360. doi:10.1016/0260-8774(95)00046-1

Chandra, U. (Ed.). (2011). Microwave Heating. InTech. doi: 10.5772/825

Chávez-Campos, G.M., Téllez-Anguiano, A. d.C., Salazar-Torres, J., Vergara-Hernandez, H., & Vázquez-Gómez, O. (2019). An ohmic heating model based on the thermal circuit method, case of study for parameter determination. Journal of Thermal Science and Engineering Applications, 12(2), 1-9. doi:10.1115/1.4043897

Chen, S. (1992). Intelligent control of semiconductor manufacturing processes IEEE. doi:10.1109/FUZZY.1992.258602

Choi, W., Kim, S., Park, S., Ahn, J., & Kang, D. (2020). Numerical analysis of rectangular type batch ohmic heater to identify the cold point. Food Science & Nutrition; Food Sci Nutr, 8(1), 648-658. doi:10.1002/fsn3.1353

Darvishi, H., Hosainpour, A., Nargesi, F., & Fadavi, A. (2015). Exergy and energy analyses of liquid food in an ohmic heating process: A case study of tomato production. Innovative Food Science & Emerging Technologies, 31, 73-82. doi:10.1016/j.ifset.2015.06.012

De Alwis, A., & Fryer, P. J. (1990). A finite-element analysis of heat generation and transfer during ohmic heating of food. Oxford] : Pergamon Press. doi:10.1016/0009-2509(90)80006-Z

Elliott, S. J., & Sutton, T. J. (1996). Performance of feedforward and feedback systems for active control. IEEE Transactions on Speech and Audio Processing, 4(3), 214-223. doi:10.1109/89.496217

El-Mashad, H., & Pan, Z. (2017). Application of induction heating in food processing and cooking. Food Engineering Reviews, 9(2), 82-90. doi:10.1007/s12393-016-9156-0

Food and drink Federation (2021). Achieving Net Zero: A Handbook for the Food and Drink Sector. https://www.fdf.org.uk/fdf/resources/publications/guidance/net-zero-handbook/net-zero-handbook/

Gavahian, M., & Farahnaky, A. (2018). Ohmic-assisted hydrodistillation technology: A review. Trends in Food Science & Technology, 72, 153-161. doi:10.1016/j.tifs.2017.12.014

Ghosh, D., Hermonat, E., Mhaskar, P., Snowling, S., & Goel, R. (2019). Hybrid modeling approach integrating first-principles models with subspace identification. Industrial & Engineering Chemistry Research; Ind.Eng.Chem.Res, 58(30), 13533-13543. doi:10.1021/acs.iecr.9b00900

Glasgow, L. A. (2014). Applied mathematics for science and engineering. Hoboken, New Jersey: Wiley.

Goeltenboth, F., Baecher, W., Startz, A., & Gussmann, J. (2010). Continuous flow heater and method for the open-loop and closed-loop control of such a continuous flow heater

Goullieux, A., Pain, J.P. (2005). Ohmic heating. In Emerging Technologies for Food Processing; Sun, D.W., Ed.; Elsevier Academic Press: Cambridge, UK; Chapter 18, pp. 469–506.

Guo, W., Llave, Y., Jin, Y., Fukuoka, M., & Sakai, N. (2017). Mathematical modelling of ohmic heating of two-component foods with non-uniform electric properties at high frequencies. Innovative Food Science & Emerging Technologies, 39, 63-78. doi:10.1016/j.ifset.2016.11.005

Hisashi, I., Wenling, W., Goro, T., & Shoichi, K. (2008). Heat processing apparatus, method of automatically tuning control constants, and storage medium

Icier, F. (2009). Influence of ohmic heating on rheological and electrical properties of reconstituted whey solutions. Food and Bioproducts Processing, 87(4), 308-316. doi:10.1016/j.fbp.2009.01.002

Icier, F., & Ilicali, C. (2004). Electrical conductivity of apple and sour cherry juice concentrates during ohmic heating. Journal of Food Process Engineering, 27(3), 159-180. doi:10.1111/j.1745-4530.2004.tb00628.x

Icier, F., & Ilicali, C. (2005a). The effects of concentration on electrical conductivity of orange juice concentrates during ohmic heating. European Food Research and Technology, 220(3), 406-414. doi:10.1007/s00217-004-1043-x

Icier, F., & Ilicali, C. (2005b). Temperature dependent electrical conductivities of fruit purees during ohmic heating. Food Research International, 38(10), 1135-1142. doi:10.1016/j.foodres.2005.04.003

Jaeger, H., Roth, A., Toepfl, S., Holzhauser, T., Engel, K., Knorr, D., et al. (2016). Opinion on the use of ohmic heating for the treatment of foods. Trends in Food Science & Technology, 55, 84-97. doi:10.1016/j.tifs.2016.07.007

Kamonpatana, P. (2012). Mathematical modeling and microbiological verification of ohmic heating of solid-liquid mixures in continuous flow ohmic heater systems. ProQuest Dissertations Publishing).

Kamonpatana, P., Mohamed, H. M. H., Shynkaryk, M., Heskitt, B., Yousef, A. E., & Sastry, S. K. (2013). Mathematical modeling and microbiological verification of ohmic heating of a multicomponent mixture of particles in a continuous flow ohmic heater system with electric field parallel to flow. Journal of Food Science; J Food Sci, 78(11), E1721-E1734. doi:10.1111/1750-3841.12287

Kanogchaipramot, K., Tongkhao, K., Sajjaanantakul, T., & Kamonpatana, P. (2016). Ohmic heating of an electrically conductive food package. Journal of Food Science; J Food Sci, 81(12), E2966-E2976. doi:10.1111/1750-3841.13542

Kaur, N., & Singh, A. K. (2015). Ohmic heating: Concept and Applications—A review. Critical Reviews in Food Science and Nutrition; Crit Rev Food Sci Nutr, 56(14), 2338-2351. doi:10.1080/10408398.2013.835303

Kumar, T. (2018). A review on ohmic heating technology: Principle, applications and scope. International Journal of Agriculture Environment & Biotechnology, 11(4), 679-687. doi:10.30954/0974-1712.08.2018.10

Lawson, D. I., & McGuire, J. H. (1953). The solution of transient heat-flow problems by analogous electrical networks. Proceedings / Institution of Mechanical Engineers, 167(1), 275-290. doi:10.1243/PIME_PROC_1953_167_034_02

Li, J., & Li, F. (2019). Active control of thermal buckling for plates using a temperature feedback control method. Smart Materials and Structures; Smart Mater.Struct, 28(4), 45001. doi:10.1088/1361-665X/ab04e6

Li, M. A. N., Likun, P., Leigang, H., Zan, W. E. I., & Chunyan, L. I. (2013). Feedforward temperature control method for cleaning liquid

Liberzon, D., & Trenn, S. (2013). The bang-bang funnel controller: Time delays and case study EUCA. doi:10.23919/ECC.2013.6669120

Lima, M., & Sastry, S. K. (1999). The effects of ohmic heating frequency on hot-air drying rate and juice yield. Journal of Food Engineering, 41(2), 115-119. doi:10.1016/S0260-8774(99)00080-1

Liu, L., Liu, L., Tian, S., Tian, S., Xue, D., Xue, D., et al. (2019). Industrial feedforward control technology: A review. Journal of Intelligent Manufacturing, 30(8), 2819-2833. doi:10.1007/s10845-018-1399-6

Maloney, N., & Harrison, M. (2016). Advanced heating technologies for food processing. (pp. 203-256) doi:10.1016/B978-1-78242-447-5.00008-3

Marcotte, M. (1999). Ohmic heating of viscous liquid foods. ProQuest Dissertations Publishing.

Manson, J.E. and Cullen, J.F. (1974), Thermal process simulation for aseptic processing of foods containing discrete particulate matter. Journal of Food Science, 39: 1084-1089. https://doi.org/10.1111/j.1365-2621.1974.tb07324.x

Mattingley, J., Wang, Y., & Boyd, S. (2011). Receding horizon control: Automatic generation of high-speed solvers. IEEE Control Systems, 31(3), 52-65. doi:10.1109/MCS.2011.940571

Mayne, D. Q., Rawlings, J. B., Rao, C. V., & Scokaert, P. O. M. (2000). Constrained model predictive control: Stability and optimality. Automatica (Oxford), 36(6), 789-814. doi:10.1016/S0005-1098(99)00214-9

Mizrahi, S., Kopelman, I. J., & Perlman, J. (1975). Blanching by electro-conductive heating. Oxford]: Blackwell Science Ltd. doi:10.1111%2Fj.1365-2621.1975.tb00031.x

Müller, W. A., Ferreira Marczak, L. D., & Sarkis, J. R. (2020). Microbial inactivation by ohmic heating: Literature review and influence of different process variables. Trends in Food Science & Technology, 99, 650-659. doi:10.1016/j.tifs.2020.03.021

Ohmic heating in food processing (2014). . Beaverton: Ringgold Inc.

Oluwole-Ojo, O.N, Zhang, H., Howarth, M., & Xu, X. (2021). Model based design and validation of a batch ohmic heating system. Modelling, 2 (4), 641-658. http://doi.org/10.3390/modelling2040034

Oluwole-Ojo, O.N., Zhang, H., Howarth, M., & Xu, X. (2023). Energy Consumption Analysis of a Continuous Flow Ohmic Heater with Advanced Process Controls. Energies, 16 (2). http://doi.org/10.3390/en16020868

Skudder, P. J., & Stirling, R. (1992). The commercial development of ohmic heating processes. Paper presented at the - IEE Colloquium on Advanced Food Technology, pp. 3/1-3/2.

Paul Singh, R., & Heldman, D. R. (2009). Introduction to food engineering (4th ed.). US: Academic Press.

Palaniappan, S., Sastry, S.K. (1991) Electrical conductivities of selected foods during ohmic heating. J Food Process Eng 14:221–236

Palaniappan, S. & Sastry, S.K. (1991). Electrical conductivities of selected solid foods during ohmic heating. Journal of Food Process Engineering, 14, 221-136

Palaniappan, S., and Sastry, S.K. (1991) Electrical Conductivities of Selected Solid Foods during Ohmic Heating. Journal of Food Process Engineering, 14, 221-236. https://doi.org/10.1111/j.1745-4530.1991.tb00093.x

Pesso, T., & Piva, S. (2017). Laminar forced convection in a cylindrical collinear ohmic sterilizer. Thermal Science, 21(5), 2217-2226. doi:10.2298/TSCI151105124P

Pidhayny, D. (1972). The origins of feedback control. IEEE Transactions on Automatic Control, 17(2), 283-284. doi:10.1109/TAC.1972.1099919

Raso, J., & Barbosa-Cánovas, G. V. (2003). Nonthermal preservation of foods using combined processing techniques. Critical Reviews in Food Science and Nutrition; Crit Rev Food Sci Nutr, 43(3), 265-285. doi:10.1080/10408690390826527

Richardson, P. (. S.). (2001). Thermal technologies in food processing. Cambridge: Woodhead.

Robertson, A. F., & Gross, D. (1958). An electrical-analog method for transient heat-flow analysis. Journal of Research of the National Bureau of Standards (1934), 61(2), 105. doi:10.6028/jres.061.016

Ruan, R., Ye, X., Chen, P., Doona, C. J., & Taub, I. (2001). 13 - ohmic heating. (pp. 241-265) Elsevier Ltd. doi:10.1533/9781855736610.3.241

Sagita, D., Darmajana, D. A., Hidayat, D. D., Novrinaldi, & Sitorus, A. (2020). Design and performance of ohmic-based fermentor model for controlling fermentation process IOP Publishing. doi:10.1088/1755-1315/542/1/012033

Sakr, M., & Liu, S. (2014). A comprehensive review on applications of ohmic heating (OH). Renewable & Sustainable Energy Reviews, 39, 262-269. doi:10.1016/j.rser.2014.07.061

Salengke, S., & Sastry, S. K. (2007). Models for ohmic heating of solid–liquid mixtures under worst-case heating scenarios. Journal of Food Engineering, 83(3), 337-355. doi:10.1016/j.jfoodeng.2007.03.026

Sarang, S., Heskitt, B., Tulsiyan, P., & Sastry, S. K. (2009). Residence time distribution (RTD) of particulate foods in a continuous flow pilot-scale ohmic heater. Journal of Food Science; J Food Sci, 74(6), E322-E327. doi:10.1111/j.1750-3841.2009.01248.x

Sastry, S.K. (1992) A model for heating of liquid-particle mixtures in a continuous flow ohmic heater. J Food Process Eng 15:263–278

Sastry, S.K. (2008). Ohmic heating and moderate electric field processing. Food Science and Technology International, 14(5), 419-422. doi:10.1177/1082013208098813

Sastry, S.K & Palaniappan, S. (1992a). Mathematical modelling and experimental studies on ohmic heating of liquid-particle mixtures in a static heater. Journal of Food Process Engineering, 241-261.

Sastry, S. K. & Palaniappan, S. (1992). Ohmic heating of liquid-particle mixtures. Food Technology, 46 (12), 64-67.

Sastry, S. K. & Palaniappan, S. (1992). Influence of particle orientation on the effective electrical resistance and ohmic heating rate of a liquid-particle mixture Journal of Food Process Engineering, 15, 213-227.

Sastry, S.K & Cornelius B.D. (2002) Aseptic Processing of Foods Containing Solid Particulates. Wiley, ISBN:9780471363590

Sastry, S.K., Jun, S., Somavat, R., Samaranayake, C., Yousef, A., & Pandit, R.B. (2009). “Heating and sterilization technology for long duration space missions”. Interdisciplinary Transport Phenomena: Annals of NY Academy of Sciences, 1161, pp.562-569

Schwenzer, M., Ay, M., Bergs, T., & Abel, D. (2021). Review on model predictive control: An engineering perspective. International Journal of Advanced Manufacturing Technology, 117(5-6), 1327-1349. doi:10.1007/s00170-021-07682-3

Seborg, D. E. (2011). Process dynamics and control (3rd ed.). Hoboken, N.J: John Wiley & Sons.

Sellers, D. (2007). An Overview of Proportional plus Integral plus Derivative Control and Suggestions for Its Successful Application and Implementation.

Silva, V. L. M., Santos, L. M. N. B. F., & Silva, A. M. S. (2017). Ohmic heating: An emerging concept in organic synthesis. Chemistry : A European Journal; Chemistry, 23(33), 7853-7865. doi:10.1002/chem.201700307

Sofi’i, I., Arifin, Z., & Oktafrina. (2022). Energy consumption for patchouli oil extraction using ohmic heating. IOP Conference Series. Earth and Environmental Science; IOP Conf.Ser.: Earth Environ.Sci, 1012(1), 12062. doi:10.1088/1755-1315/1012/1/012062

Solomatine, D., See, L., & Abrahart, R. J. (2008). Data-driven modelling: Concepts, approaches and experiences. (pp. 17-30) doi:10.1007/978-3-540-79881-1_2

Somavat, R., Kamonpatana, P., Mohamed, H. M. H., & Sastry, S. K. (2012). Ohmic sterilization inside a multi-layered laminate pouch for long-duration space missions. Journal of Food Engineering, 112(3), 134-143. doi:10.1016/j.jfoodeng.2012.03.019

Steere, R. C. (1971). Solution of two-dimensional transient heat flow problems by electrical analogue. Physics Education, 6(6), 443-447. doi:10.1088/0031-9120/6/6/006

Stirling, R. (1987). Ohmic heating—a new process for the food industry. Power Engineering Journal, 1(6), 365. doi:10.1049/pe:19870065

Stirling, & Robert. (1993). Ohmic heating apparatus using electrodes formed of closed microporosity material

Tao, K. M., Kosut, R. L., Ekblad, M., & Aral, G. (1994). Feedforward learning applied to RTP of semiconductor wafers IEEE. doi:10.1109/CDC.1994.410927

TATEM, J. A. (1955). Temperature control apparatus for electrode type boilers

Thamkaew, G., & Gómez Galindo, F. (2020). Influence of pulsed and moderate electric field protocols on the reversible permeabilization and drying of thai basil leaves. Innovative Food Science & Emerging Technologies, 64, 102430. doi:10.1016/j.ifset.2020.102430

Therdthai, N., & Zhou, W. (2001). Artificial neural network modelling of the electrical conductivity property of recombined milk. Journal of Food Engineering, 50(2), 107-111. doi:10.1016/S0260-8774(00)00202-8

Tulsiyan, P., Sarang, S., & Sastry, S. K. (2009). Measurement of residence time distribution of a multicomponent system inside an ohmic heater using radio frequency identification. Journal of Food Engineering, 93(3), 313-317. doi:10.1016/j.jfoodeng.2009.01.032

Vandoren, V. J. (1998). Open-loop control offers some advantages. Control Engineering, 45(13)

Varghese, K. S., Varghese, K. S., Pandey, M. C., Pandey, M. C., Radhakrishna, K., Radhakrishna, K. (2014). Technology, applications and modelling of ohmic heating: A review. Journal of Food Science and Technology; J Food Sci Technol, 51(10), 2304-2317. doi:10.1007/s13197-012-0710-3

Wang, W. C. & Sastry, S. K. (1997). Changes in electrical conductivity of selected vegetables during multiple thermal treatments. Journal of Food Process Engineering, 20(6), 499-516. doi:10.1111/j.1745-4530.1997.tb00435.x

Yildiz, H., Bozkurt, H., & Icier, F. (2009). Ohmic and conventional heating of pomegranate juice: Effects on rheology, color, and total phenolics. Food Science and Technology International, 15(5), 503-512. doi:10.1177/1082013209350352

Zell, M., Lyng, J. G., Cronin, D. A., & Morgan, D. J. (2010). Ohmic cooking of whole beef muscle — evaluation of the impact of a novel rapid ohmic cooking method on product quality. Meat Science; Meat Sci, 86(2), 258-263. doi:10.1016/j.meatsci.2010.04.007

Zhang, L., & Fryer, P. J. (1993). Models for the electrical heating of solid-liquid food mixtures. Chemical Engineering Science, 48(4), 633-642. doi:10.1016/0009-2509(93)80132-A

Zhang, L., Zeng, A., & Zhang, Y. (2007). On remote real-time communication between MATLAB and PLC based on OPC technology. Paper presented at the pp. 545-548. doi:10.1109/CHICC.2006.4346760

Zhao, Y., Flugstad, B., Kolbe, E., Park, J. W., & Wells, J. H. (2000). Using capacitive (radio frequency) dielectric heating in food processing and preservation – a review. Journal of Food Process Engineering, 23(1), 25-55. doi:10.1111/j.1745-4530.2000.tb00502.x

List of figures

σ	Electrical conductivity (S/m)
T	Temperature (°C)
V	Voltage (Volts)
ρ	Density (kg/m^3)
k	Thermal conductivity (W/mK)
c	Specific heat capacity (J/kgK)
T_o	Initial temperature (°C)
$\mathrm{Q_h}$	Volumetric heat (W/m^3)
$\mathrm{q_r}$	Radiation heat transfer (J/s · m^{2}K^4)
E	Applied electric field (V/m)
$\mathrm{Q_h}$	Volumetric heat (W/m^3)
K_p	proportional term
K_i	Integral term
K_d	Derivative term
$\dot{\mathrm{m}}_{\mathrm{in}}$	Input flowrate (Kg/s)
$\mathrm{H_{in}}$	Inlet enthalpy
$\mathrm{H_{out}}$	Outlet enthalpy
$\dot{\mathrm{m}}_{\mathrm{out}}$	Output flowrate (Kg/s)
Q	rate of electrical heating
v	Volume (m^3)
T_{ref}	Reference temperature
$\dot{\mathrm{m}}$	Flowrate
$\mathrm{V_e}$	Applied voltage
A	Area of the heating section
L	Gap between the electrodes

Appendix A. MATLAB codes

A. Code describing the state space realization.

The following code describes the MATLAB function block for state space realisation in Simulink.

```
function xdot = fcn(mdot,x,u)

%y =0;
%x = ones(2,1);
%u = ones (1,1);

% Model parameters
rho = 1050;  %density
v1 = 1.8e-4;   %v1, volume in first chamber
v2 = 2.5e-4;   %v2, volume in second chamber


% Continuous-time model
A = [0  1; -(1/(((rho*v1)/mdot)*((rho*v2)/mdot))) -
(((rho*v1)/mdot)+((rho*v2)/mdot))/(((rho*v1)/mdot)*((rho*v2)/mdot))];

B = [0; 1/(((rho*v1)/mdot)*((rho*v2)/mdot))];
C = [1 0];
D = 0;

xdot =A*x + B*u;
```

B. Code describing the auto-level control.

The following code is the pseudo code explaining the block diagram designed in Simulink.

```
% Pseudo code of the thyristor level safety controller
T_in      %Measured input temperature
T_out     %Desired referenced temperature
C         % Heat capacity
m_dot     %mass flowrate
k         %Thermal conductivity
```

```
L         %gap between the electrodes
A         %Area of the heating chamber
I         %measured electrical current.
P         %Measured electrical power.
E_cond    % Electrical conductivity
V         %High voltage
Thy       %Thyristor setpoint
% Calculate the temperature difference
Delta_T = T_out-T_in;
%Theoretical Heat gained plus conduction
H_gained = ((Delta_T*L*m_dot*C) + (Delta_T*(1/k)));
%Estimate the online electrical conductivity from measured current and power
E_cond = ((I*I)/P)*A;
%Determine V^2
V_squared = H_gained/E_cond;
%Determine V
V = sqrt(V_squared);
%Saturate V from 0 to 4200V
V = saturate(0,4200,V);
%Convert the V to equivalent thyristor value.
Thy = convert(V);
```

C. Values for the design of the voltage converter.

```
%thyristor HV voltage with corresponding thy setpoint. e.g value 1 = 418V
Thyristor = [0 407 572 698 805 897 982 1059 1131 1198 1262 1322 1381 1437 1488
1537 1585 ...
    1645 1707 1757 1801 1844 1888 1929 1969 2009 2047 2085 ...
      2122 2158 2194 2228 2265 2301 2338 2374 2408 2442 2474 2507 2538 2569 2599
2629 ...
      2659 2694 2724 2749 2777 2808 2837 2864 2888 2919 2944 2975 ...
      3002 3029 3058 3078 3104 3129 3157 3182 3202 3228 3254 3278 3299 3329 3355
3379 ...
      3399 3424 3447 3471 3489 3514 3535 3557 3578 3599 3621 3642 3662 3684 3704
3725 ...
      3745 3767 3787 3804 3827 3849 3867 3887 3904 3929 3949 3967 3972];
```

```
  number_of_set = 0:100;             %Number of thyristor points corresponding to
Voltage
  no = number_of_set';

  THY=Thyristor';

  %%
p = polyfit(no,THY,10);
f = polyval(p,no);
T = table(no,THY,f,THY-f,'VariableNames',{'X','Y','Fit','FitError'});
plot(no,f);
hold
plot(no,THY, 'r')
```

Appendix B. Data plotting and analysis code

Code to analyse the data from the PLC in real time.

A. Code to plot only the temperature probe.

```
%only the temperature probe

t41 =tf4';
plot(t41(:,2))            %Fibre probe 1
hold

t31 =tf3';
plot(t31(:,2))            %Fibre probe 2

t21 =tf2';
plot(t21(:,2))            %Fibre probe 3

t11 =tf1';
plot(t11(:,2))            %Fibre probe 4

tc11 =tc1';
plot(tc11(:,2))           %Inlet thermocouple probe

tc22 =tc2';
plot(tc22(:,2))           %Outlet thermocouple probe

legend('Fibre_B1','Fibre_A2','Fibre_A1', 'Fibre_B2','T_inlet', 'T_outlet')
grid on
xlabel('Time (s)')
ylabel('Temperature (degC)')
```

B. Code to plot the HV

```
Hv =HV';
plot(Hv(:,2))
legend('Voltage plot')
grid on;
xlabel('Time(s)')
```

```
ylabel('Voltage(V)')
title(' Applied Voltage')
```

C. Code to plot the temperature, voltage, current, setpoint, power, flowrate and electrical conductivity.

```
%%
Vplot = Hv(min:max,2);
Tplot = tc22(min:max,2);
Tplot2 = t41(min:max,2);
Tplot3 = t11(min:max,2);
Tinit = tc11(min:max,2);
thypoint =thysetpoint';
Thyplot = thypoint(min:max,2);
Irms =irms';
Irmsplot = Irms(min:max,2);
Vms =Vrms';
Vrmsplot = Vms(min:max,2);
Power =power';
Powerplot = Power(min:max,2);
setpoint =setpointb';
setpointplot = setpoint(min:max,2);
 econd =econd';
 econdplot = econd(min:max,2);
  %econd2 =econd2';
 %econdplot2 = econd2(min:max,2);
% Ct1 =ct1';
% Ct1plot = Ct1(min:max,2);
% Ct2 =ct2';
% Ct2plot = Ct2(min:max,2);
Ct3 =ct3';
Ct3plot = Ct3(min:max,2);
 flw =flowrate';
 flwplot = flw(min:max,2);
Lpm =Lpermin';
Lpmplot = Lpm(min:max,2);
```

D. Plot to save process variable data.

```
save  plot1.mat Tplot Tplot2 Tplot3 Tinit Vplot  Vrmsplot Powerplot Irmsplot
Ct3plot  setpointplot  Lpmplot flwplot econdplot %econdplot2 %Ct1plot Ct2plot
Thyplot
```

E. Sample code to plot zoomed in plots.

```
% ------Temp and voltage------------------------------
%test
subplot(2,1,1);
t = 1:200;
%--------------------------
plot(ampctemp, '-r')
hold
plot(setpointplot, '--m')
plot(mpctemp, '-.b')
plot(pidtemp, '--k')
title ('Temperature response of the ohmic heater heating orange juice');
axis([0 200 10 100])
xlabel('Time (s)')
ylabel('Temperature (degC)')
legend('AMPC','temperature setpointplot', 'MPC','PID')
grid on;
grid on;
% create a new pair of axes inside current figure
axes('position',[.40 .175 .50 .30])
box on % put box around new pair of axes
indexOfInterest = (t < 101) & (t > 39); % range of t near perturbation
plot(t(indexOfInterest),ampctemp(indexOfInterest), '-
r',t(indexOfInterest),mpctemp(indexOfInterest), '-
.b',t(indexOfInterest),pidtemp(indexOfInterest), '--k') % plot on new axes
axis tight


subplot(2,1,2);
plot(ampcV, '-r')
hold
plot(mpcV, '-.b')
```

```
plot(pidV, '--k')
xlabel('Time(s)')
ylabel('Voltage (V)')
title(' Controller applied voltage')
legend('AMPC', 'MPC','PID')
grid on;
grid on;
% create a new pair of axes inside current figure
axes('position',[.25 .175 .60 .30])
box on % put box around new pair of axes
indexOfInterest = (t < 101) & (t > 20); % range of t near perturbation
plot(t(indexOfInterest),ampcV(indexOfInterest), '-
r',t(indexOfInterest),mpcV(indexOfInterest), '-
.b',t(indexOfInterest),pidV(indexOfInterest), '--k') % plot on new axes
axis tight
```

Appendix C. PLC IP configuration

Code describing the IP configuration.

IP Address Summary

==================

192.168.1.10   PLC (FX5UC)

192.168.1.11   HMI (GS2107)

192.168.1.12   EPACK

192.168.1.13   Inverter (FR-E720)

Connect using fixed IP on your PC/Mac of:-

192.168.1.250

255.255.255.0

(gateway not required, but can be 192.168.1.1 or similar...)

Process variables available on PLC (192.168.1.10:5001)

==

HV Readings

HV(V)   x 1   D130

CT1(A) x 1000   D132

CT2(A) x 1000   D133

Thyristor Readings

P(W)   x 1   D74

Vrms(V) x 10   D64

Irms(A) x 100   D61

CT3(A) x 100   D134

Transformer Temperatures

TX1(°C) x 10 D117

TX2(°C) x 10 D118

Process Temperatures

TC1(°C) x 10 D111

TC2(°C) x 10 D112

FT1(°C) x 10 D135

FT2(°C) x 10 D136

FT3(°C) x 10 D137

FT4(°C) x 10 D138

Process Control

===============

Drive Mode D2010 (0 for continuous, 1 for MEF)

Setpoint x 100 D2011

On/Off M10 (boolean)

MEF Repeat Time x 1000 : D2012 (32-bit)

MEF Pulse Width x 1000 : D2014 (32-bit)

Pump(Hz) x 100 D2020

On/Off Y200 (boolean)

Appendix D. Health and safety

First risk assessment case.

Risk Assessment Case

Case Id:	62807658	**User:**	OLUWALOBA OLUWOLE-OJO
Case Status:	Closed	**Email:**	[redacted]
Date Opened:	29/10/2021	**Phone:**	
Date Closed:	29/10/2021 13:30:03	**Open Items:**	0

Activity Details

Risk Assessment Title:

Operating a continuous flow ohmic heater

Location / Area:

NCEFE, Attercliffe

Activity / Task Being Undertaken:

This activity is part of the research on the use of moderate electric field (MEF) in food processing.
The equipment used is a custom built continuous flow MEF system.
Different liquid food substance will be heated.
The internal mechanism of the MEF system is sealed off from the outside during operation.
The only access to the device during operation is through the use of a laptop based monitoring control system.
The MEF system is situated in the laboratory workspace at NCEFE
The project is overseen by Dr. Hongwei Zhang.
Risk of exposure is limited to research student, NCEFE technician and permitted visitors.

Date of Assessment:

28/10/2021

Assessor Name:

OLUWALOBA OLUWOLE-OJO

Assessment Review Date:

28/10/2022

How will this risk assessment be communicated to those affected by its activities?:

- [x] Email

Date	Added By	Severity	Likelihood	Assigned To	Closed Date	Status
No records to display.						

Who might be harmed? (Tick all that apply)

- [x] Students

How could they be harmed?

Electrocution and burns when in contact bare parts

What are you already doing?

- [x] Undertake a visual inspection of electrical equipment before use.
- [x] Internal component is sealed off during operation
- [x] Ensure dry operating environment

Any additional controls required?

(Left empty)

Please provide details of all controls

Ensure signs are clear
Only the technician can access restricted parts of the equipment

Additional risks for special groups? (Tick all that apply)

(Left empty)

What are the additional risks?

(Left empty)

What are you already doing?

(Left empty)

Any additional controls required?

(Left empty)

Likelihood (The possibility that something could happen)

Remote

Consequence (The probable outcome of the potential incident)

Serious

Risk Level

			Consequence/Severity				
			Minor	Moderate	Serious	Major	Critical/Fatal
Probability	Likelihood	Rating	1	2	**3**	4	5
0.8 - 1	Almost Certain	5	5	10	15	20	25
0.6 - 0.8	Very Likely	4	4	8	12	16	20
0.4 - 0.6	Likely	3	3	6	9	12	15
0.2 - 0.4	Occasional	2	2	4	6	8	10
0 - 0.2	Remote	**1**	1	2	**3**	4	5

Item Review Date

01/11/2021

Hot liquid food

Risk Level: 2 (Low)

Updated On: 29/10/2021

Date	Added By	Severity	Likelihood	Assigned To	Closed Date	Status
No records to display.						

Who might be harmed? (Tick all that apply)

☑ Students

How could they be harmed?

contact with hot liquid

What are you already doing?

Ensure the use of PPE

Any additional controls required?

(Left empty)

Additional risks for special groups? (Tick all that apply)

(Left empty)

What are the additional risks?

(Left empty)

What are you already doing?

(Left empty)

Any additional controls required?

(Left empty)

Likelihood (The possibility that something could happen)

Remote

Consequence (The probable outcome of the potential incident)

Moderate

Risk Level

			Consequence/Severity				
			Minor	Moderate	Serious	Major	Critical/Fatal
Probability	Likelihood	Rating	1	**2**	3	4	5
0.8 - 1	Almost Certain	5	5	10	15	20	25
0.6 - 0.8	Very Likely	4	4	8	12	16	20
0.4 - 0.6	Likely	3	3	6	9	12	15
0.2 - 0.4	Occasional	2	2	4	6	8	10
0 - 0.2	Remote	**1**	1	**2**	3	4	5

Item Review Date

28/10/2022

PPE

Risk Level: N/A

Updated On: 29/10/2021

Date	Added By	Severity	Likelihood	Assigned To	Closed Date	Status
No records to display.						

Personal Protective Equipment Required (Tick all that apply)

- [x] Hand protection

  Details & Standards

  Gloves for carrying food samples

- [x] Lab coat

  Details & Standards

  To protect from food spillage

- [x] Face mask

  Details & Standards

  Face mask for Covid-19 protection

Approval

CLOSED

Overall Risk Level: 2 (Low)

Updated On: 29/10/2021

Date	Added By	Severity	Likelihood	Assigned To	Closed Date	Status
29/10/2021 13:30	OLUWALOBA OLUWOLE-OJO	n/a	n/a	HONGWEI ZHANG	29/10/2021	Approved

Date	Noted By	Note
29/10/2021 13:30	HONGWEI ZHANG	Risk level signed off.
29/10/2021 13:26	OLUWALOBA OLUWOLE-OJO	Assessment resubmitted for review.
29/10/2021 12:01	HONGWEI ZHANG	Risk level rejected and risk assessment returned to the submitter.
29/10/2021 12:01	HONGWEI ZHANG	For 'Electricity', should the hazard be 'electric shock and burns from contact with live parts'?
29/10/2021 11:51	OLUWALOBA OLUWOLE-OJO	Sign-off required from All Staff

Risk assessment for heating tomato sauce

Risk Assessment Case

Case Id:	63397196	**User:**	OLUWALOBA NIFEMI OLUWOLE-OJO
Case Status:	Closed	**Email:**	l.oluwole-ojo@shu.ac.uk
Date Opened:	08/12/2022	**Phone:**	Unknown
Date Closed:	08/12/2022 16:52:27	**Open Items:**	0

Activity Details

Risk Assessment Title:

Ohmic heating of tomato sauces

Location / Area:

NCEFE, Attercliffe

Activity / Task Being Undertaken:

Task: Ohmic heating of tomato sauces.

The continuous flow ohmic heater will be used to heat tomato sauces
Location: NCEFE/ Low care

Date of Assessment:

08/12/2022

Assessor Name:

OLUWALOBA NIFEMI OLUWOLE-OJO

Assessment Review Date:

08/12/2023

How will this risk assessment be communicated to those affected by its activities?:

- [x] Email

Supporting Documentation:

(Left empty)

Temperature / Humidity / Climate

Risk Level: 1 (Low)

Updated On: 08/12/2022

Date	Added By	Severity	Likelihood	Assigned To	Closed Date	Status
No records to display.						

Who might be harmed? (Tick all that apply)

- [x] Students

How could they be harmed?

Burns due to hot tomato sauce

What are you already doing?

- [x] Position workstations away from radiant heat.
- [x] Provision of a sealed outfeed tank to collect hot product

Any additional controls required?

(Left empty)

Please provide details of all controls

Authorized assess is required in the Lab

Hot product is isolated in an outfeed tank

Additional risks for special groups? (Tick all that apply)

(Left empty)

What are the additional risks?

(Left empty)

What are you already doing?

(Left empty)

Any additional controls required?

(Left empty)

Likelihood (The possibility that something could happen)

Remote

Consequence (The probable outcome of the potential incident)

Minor

Risk Level

			Consequence/Severity				
			Minor	Moderate	Serious	Major	Critical/Fatal
Probability	Likelihood	Rating	**1**	2	3	4	5
0.8 - 1	Almost Certain	5	5	10	15	20	25
0.6 - 0.8	Very Likely	4	4	8	12	16	20
0.4 - 0.6	Likely	3	3	6	9	12	15
0.2 - 0.4	Occasional	2	2	4	6	8	10
0 - 0.2	Remote	**1**	**1**	2	3	4	5

Item Review Date

08/12/2023

PPE

Risk Level: N/A

Updated On: 08/12/2022

Date	Added By	Severity	Likelihood	Assigned To	Closed Date	Status
No records to display.						

Personal Protective Equipment Required (Tick all that apply)

(Left empty)

Approval

CLOSED

Overall Risk Level: 1 (Low)

Updated On: 08/12/2022

Date	Added By	Severity	Likelihood	Assigned To	Closed Date	Status
08/12/2022 16:52	OLUWALOBA NIFEMI OLUWOLE-OJO	n/a	n/a	HONGWEI ZHANG	08/12/2022	Approved

Date	Noted By	Note
08/12/2022 16:52	HONGWEI ZHANG	Risk level signed off.
08/12/2022 16:52	HONGWEI ZHANG	Happy to approve as this is an addition to the exisiting Risk Assessment for Ohmic Heating.
08/12/2022 12:47	OLUWALOBA NIFEMI OLUWOLE-	Sign-off required from All Staff